Leibniz Institute of Virology

Inhibition of the AIM2 inflammasome and pyroptosis by murine cytomegalovirus

Dissertation

Submitted to the

Department of Chemistry

Faculty of Mathematics, Informatics and Natural Sciences

University of Hamburg

In fulfillment of the requirements for the degree of

Doctor of Natural Sciences (Dr. rer. nat.)

by

Yingqi Deng

Born in Jilin, China

2023 in Hamburg, Germany

Prof. Dr. Wolfram Brune (First Reviewer)

Prof. Dr. Nicole Fischer (Second Reviewer)

Date of oral defense: 25.08.2023

Publications, presentations and awards

Publication

A cytomegalovirus inflammasome inhibitor curbs proinflammatory cytokine release and pyroptosis.

Yingqi Deng, Eleonore Ostermann, Wolfram Brune.

Nature Communications (under review)

Oral and poster presentations

Parts of this thesis were presented at the following conferences:

HPI Scientific Retreat	October 2018
	Hamburg, Germany
	Poster presentation
20th GfV workshop "Immunobiology of viral infections"	September 2021
	Zoom
	Oral presentation
31st Annual Meeting of the Society for Virology (GfV)	April 2022
	Munich, Germany
	Oral presentation
LIV Scientific Retreat	May 2022
	Hamburg, Germany
	Oral presentation
32nd Annual Meeting of the Society for Virology (GfV)	March 2023
	Ulm, Germany
	Oral presentation
47th Annual International Herpesvirus Workshop (IHW)	July 2023
	Missoula, U.S.
	Both Oral and poster presentations

Award

32nd Annual Meeting of the Society for Virology (GfV)   Travel award

Table of Contents

List of abbreviations

ActD	actinomycin D
AIM2	absent in melanoma 2
ALR	absent in melanoma 2 like receptor
Amp	ampicillin
ASC	apoptosis-associated speck-like protein containing a CARD
BAC	bacterial artificial chromosome
BAX	BCL-2-associated X protein
BAK	BCL-2 antagonist or killer
BCL-2	B-cell lymphoma 2
BMDM	bone marrow derived macrophages
CARD	Caspase-Recruitment Domain
CHX	cycloheximide
CHIKV	chikungunya virus
CpG	cytosine-phosphate-guanine
DAI	DNA-dependent activator of IFN regulatory factors
DCs	dendritic cells
DD	death domain
dsDNA	double-stranded DNA
dpi.	day(s) post infection
EBV	Epstein-Barr virus
ER	endoplasmic reticulum
FasL	Fas ligand
FL	full length
FADD	Fas-associated death domain-containing protein
GSDMD	Gasdermin D
HA	hemagglutinin
HCMV	human cytomegalovirus
HIN	hematopoietic expression, interferon-inducible nature, and nuclear localization
HIV	human immunodeficiency virus
hpi.	hour(s) post infection
HSV-1	herpes simplex virus 1

IE	immediate-early
IFI16	IFN-inducible protein 16
IFN	interferon
IKK	IκB kinase
IL	interleukin
IRF	interferon regulatory factor
KSHV	kaposi sarcoma-associated herpesvirus
LPS	lipopolysaccharides
MAVS	mitochondrial antiviral-signaling
MCMV	murine cytomegalovirus
MHC	major histocompatibility complex
MLKL	mixed lineage kinase domain like pseudokinase
MOI	multiplicity of infection
mRNA	messenger RNA
MyD88	myeloid differentiation primary response 88
NEMO	NF-κB essential modulator
NF-κB	nuclear factor 'kappa-light-chain-enhancer' of activated B-cells
NK	natural killer
NLR	Nod-like receptor
NLRP3	nucleotide-binding domain, leucine rich repeat containing receptor family Pyrin domain containing 3
ORFs	open reading frames
PAMP	pathogen-associated molecular pattern
PCD	programmed cell death
PCR	polymerase chain reaction
PEI	polyethylenimine
PI	propidium iodide
PIDD	p53-induced protein with a death domain
PRR	pathogen recognition receptor
PYD	Pyrin domain
RAIDD/CRADD	an adaptor protein containing a CARD and death domain
RHIM	RIP homotypic interacting motif
RIG-I	Retinoic acid-inducible gene I
RIPK	receptor interacting protein kinase

RLR	Retinoic acid-inducible gene I like receptor
RNA Poly III	RNA polymerase III
SDS-PAGE	sodium dodecyl sulfate polyacrylamide gel electrophoresis
STING	Stimulator of interferon genes
TBK1	TANK-binding kinase 1
TCID50	tissue culture infectious dose 50 %
TLR	Toll-like receptor
TNF-a	tumor necrosis factor alpha
TRAF	TNF receptor associated factor
UL	unique long
VACV	vaccinia virus
vICA	viral inhibitor of Caspase-8-induced apoptosis
vMIA	viral mitochondrion-localized inhibitor of apoptosis
vIRA	viral inhibitor of RIP activation
VSV	vesicular stomatitis virus
WB	western blot
WT	wild type
ZBP1/DAI	Z-DNA-binding protein 1

1 Zusammenfassung

Der programmierte Zelltod (PCD) spielt eine wichtige Rolle bei der Wirtsabwehr gegen Viren. Cytomegaloviren (CMV) besitzen die Fähigkeit, die zelluläre Abwehr geschickt zu manipulieren und verfügen über potente Inhibitoren der Apoptose und Nekroptose. Es ist jedoch noch kein CMV-Inhibitor für die Pyroptose bekannt, die die dritte Hauptform des PCD darstellt. Das AIM2-Inflammasom ist ein Sensor für doppelsträngige DNA (dsDNA), der durch DNA-Viren wie das murine Cytomegalovirus (MCMV) aktiviert wird. Die Aktivierung des Inflammasoms führt zur proteolytischen Aktivierung der Caspase-1 und zur Aktivierung der proinflammatorischen Zytokine Interleukin 1β (IL-1β) und IL-18. Die aktivierte Caspase-1 kann außerdem Gasdermin D (GSDMD) spalten, was zur Pyroptose führt. Während die Inflammasom-Aktivierung und -Signalübertragung gut erforscht sind, ist über die viralen Gegenmaßnahmen und ihre Bedeutung für die virale Infektion *in vivo* viel weniger bekannt.

Im Rahmen meines Dissertationsprojekts suchte ich nach einem MCMV-Inhibitor für das AIM2-Inflammasom. Ich identifizierte das virale Protein M84 als einen Inhibitor der Inflammasom-Signalübertragung, der mit dem DNA-Sensor AIM2 und dem Adaptorprotein ASC interagiert. Ich konnte zeigen, dass eine M84stop-MCMV-Mutante, die dieses Protein nicht exprimieren kann, eine erhöhte Caspase-1-Aktivierung sowie IL-1β- und IL-18-Sekretion in infizierten Makrophagen verursacht. Des Weiteren war M84*stop*-MCMV auch in der Lage, die Spaltung von GSDMD und den pyroptotischen Zelltod in Makrophagen zu verstärken. Diese Effekte führten zu einem signifikanten Wachstumsdefekt der M84stop-MCMV-Mutante in WT-Makrophagen, der durch Knockout von *Aim2* oder *Asc* oder durch Behandlung mit einem Caspase-1-Inhibitor behoben werden konnte. Dies deutet darauf hin, dass M84 das AIM2-Inflammasom moduliert, um die virale Replikation *in vitro* zu optimieren. Die biologischen Auswirkungen von M84 wurden durch *in-vivo*-Experimente weiter untersucht. Dabei zeigte sich, dass M84 die Freisetzung von IL-18 ins Serum modulierte und für eine effiziente Verbreitung des Virus in Milz und Leber erforderlich war. Die Abschwächung von M84*stop*-MCMV in infizierten WT-Mäusen konnte in *Asc*-Knockout-Mäusen nur teilweise wiederhergestellt werden, was darauf hindeutet, dass M84 weitere Funktionen haben könnte. Insgesamt zeigen diese Ergebnisse, dass die Hemmung

Zusammenfassung

des Inflammasom-Pyroptose-Wegs wichtig ist, um die MCMV-Replikation und -Verbreitung *in vivo* zu fördern.

Diese Studie liefert den ersten Beweis dafür, dass MCMV die AIM2-Inflammasom-abhängige Pyroptose unterdrückt, um die Erkennung viraler DNA durch das angeborene Immunsystem zu überwinden.

2 Abstract

Programmed cell death (PCD) plays an important role in the host defense against viruses. Cytomegaloviruses (CMVs) possess the ability to expertly manipulate cellular defenses and harbor potent inhibitors of apoptosis and necroptosis. However, there is no known CMV inhibitor for pyroptosis, which is the third major form of PCD. The AIM2 inflammasome is a sensor of double-stranded DNA (dsDNA) that is activated by DNA viruses such as murine cytomegalovirus (MCMV). Inflammasome assembly induces proteolytic activation of Caspase-1 and maturation of pro-inflammatory cytokines interleukin 1β (IL-1β) and IL-18. Activated Caspase-1 can also cleave Gasdermin D (GSDMD) leading to pyroptosis. While inflammasome activation and signaling are well studied, much less is known about viral countermeasures and their importance for viral infection *in vivo*.

In my thesis project, I searched for an MCMV inhibitor of the AIM2 inflammasome. I identified the viral M84 protein as an inhibitor of the inflammasome signaling that interacted with the DNA sensor AIM2 and the adaptor protein ASC. I could show that an M84*stop* MCMV mutant unable to express this protein caused increased Caspase-1 activation and IL-1β and IL-18 secretion in infected macrophages. Furthermore, M84*stop* MCMV was able to enhance GSDMD cleavage and pyroptotic cell death in macrophages. These effects resulted in a significant growth defect of the M84*stop* MCMV mutant in WT macrophages, which was rescued by knockout of either *Aim2* or *Asc* or by treatment with a Caspase-1 inhibitor, suggesting that M84 modulates AIM2 inflammasome to optimize viral replication *in vitro*. The biological impact of M84 was further investigated by *in vivo* experiments, showing that M84 modulated IL-18 release in the serum and was required for efficient viral dissemination to the spleen and liver. The attenuation of M84*stop* MCMV in infected WT mice was partially rescued in *Asc* knockout mice, indicating that M84 may have other functions. Altogether, these results demonstrate that the inhibition of the inflammasome-pyroptosis pathway is important to facilitate MCMV replication and dissemination *in vivo*.

This study provides the first evidence for MCMV suppressing AIM2-inflammasome-dependent pyroptosis to overcome innate immune sensing of viral DNA.

3 Introduction

3.1 Cytomegalovirus

3.1.1 Cytomegalovirus pathogenesis

Human cytomegalovirus (HCMV) infection was first observed in 1881 by Hugo Ribbert, who saw large cells in sections of the kidney from a luetic stillborn. In the 1950s, Weller, Smith and Rowe independently isolated HCMV from human patients and grew the virus in cell cultures. Weller finally named the virus "cytomegalovirus" (reviewed in [1]). In 1954, Margaret Smith isolated a murine cytomegalovirus (MCMV) strain from the salivary gland of infected laboratory mice, which was later named Smith strain [2]. CMVs are strictly species-specific and replicate only in the cells of their own or closely related species [3]. Therefore MCMV, the related mouse pathogen, is used to study viral pathogenesis *in vivo* [4].

HCMV can be transmitted from infected people by contact with body fluids including saliva, urine, stool, milk, and semen, as well as via genital secretions, solid-organ transplantation, blood transfusion and hematopoietic stem cell transplantation [5, 6]. After the primary infection, HCMV is never fully cleared from the host and remains in the body in a latent state, from which it can be reactivated later [7]. In immunocompetent individuals, the healthy immune system is able to efficiently keep HCMV infection under control with no or mild symptoms. Therefore, public awareness of HCMV infection is relatively low in spite of its high prevalence [8]. The seroprevalence of HCMV ranges from 35% to more than 95% worldwide with high incidence in both developed and developing countries (Figure 1) [9]. Of note, HCMV is one of the first viral infections to be identified diagnostically in transplant patients. The infection can occur as primary infection, reactivation from latent virus, as well as superinfection. The acute illness induced by HCMV infection commonly occurs in people with weakened immune systems, such as patients with congenital immunocompromised hosts, cancer patients undergoing chemotherapy, transplant recipients, and AIDS patients [10, 11]. In these weakened individuals, HCMV replicates rapidly which leads to viremia causing invasive diseases - for example, HCMV infection induces severe pneumonitis in organ transplant recipients, especially in allogenic bone marrow transplant patients [12]. There are other HCMV-associated diseases including

neutropenia, hepatitis, gastroenteritis, and retinitis [13, 14]. Moreover, the transmission from mother to child leads to congenital infection in newborns through three main routes: transplacental, peripartum, and via human milk [15-19]. The risk of HCMV vertical transmission from primary maternal infection during pregnancy can be as high as 40% [20]. Approximately 13.5% of newborns with congenital infection are symptomatic at birth [15], symptoms include microcephaly, cerebral palsy, mental retardation, hearing loss, neurological abnormalities, chorioretinitis, seizures, rash, hypotonia, and hepatosplenomegaly [21-23].
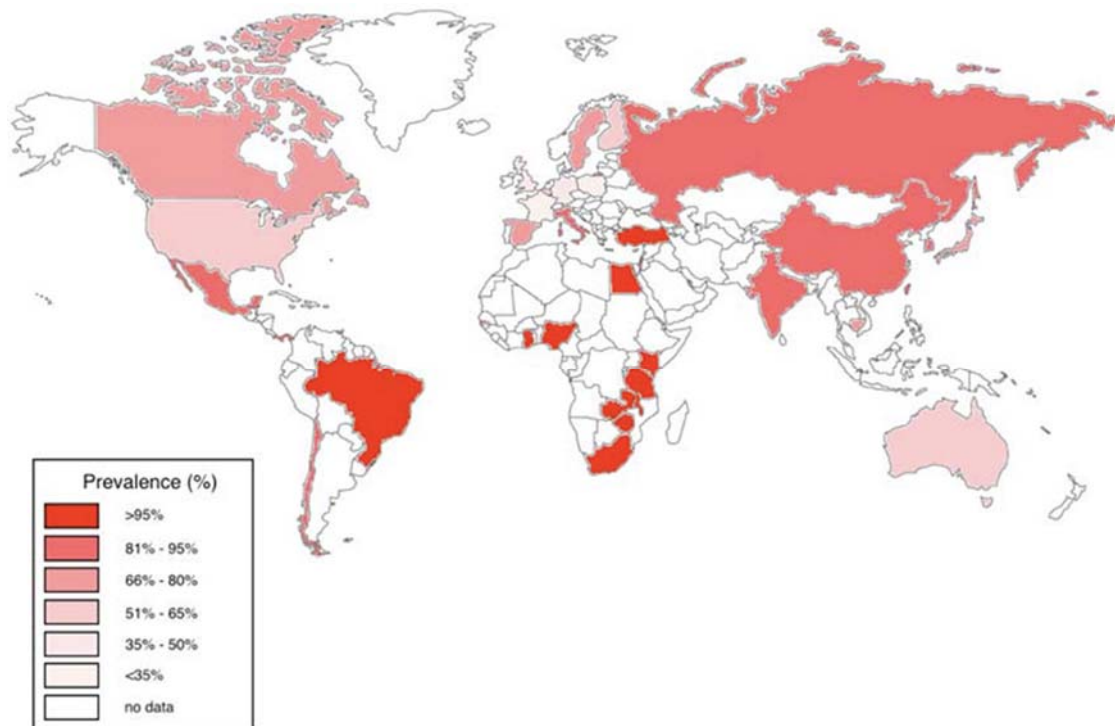
Figure 1. Worldwide HCMV seroprevalence rates in adults. Figure is acquired from [9].

3.1.2 Cytomegalovirus structure and life cycle

The HCMV genome, the largest among human herpesviruses, is a linear dsDNA of 230 to 240 kb encoding for 160-200 viral proteins [24]. The viral dsDNA core is encased in a highly ordered icosahedral nucleocapsid that is surrounded by a proteinaceous matrix containing the tegument proteins and viral RNA [25]. Tegument proteins are released into the cytosol as soon as the virus enters the cell and play important roles in immune evasion. Additionally, tegument proteins are crucial for viral gene expression and capsid migration to the nuclear pore for viral genome delivery. These tegument proteins are enclosed in a lipid bilayer envelope containing a number of viral

glycoproteins that are important for the viral attachment to enter into target cells and cell-cell fusion to spread to the neighbor cells. These components consist in the mature CMV virions (Figure 2) that have a diameter range of 200-300nm [26].
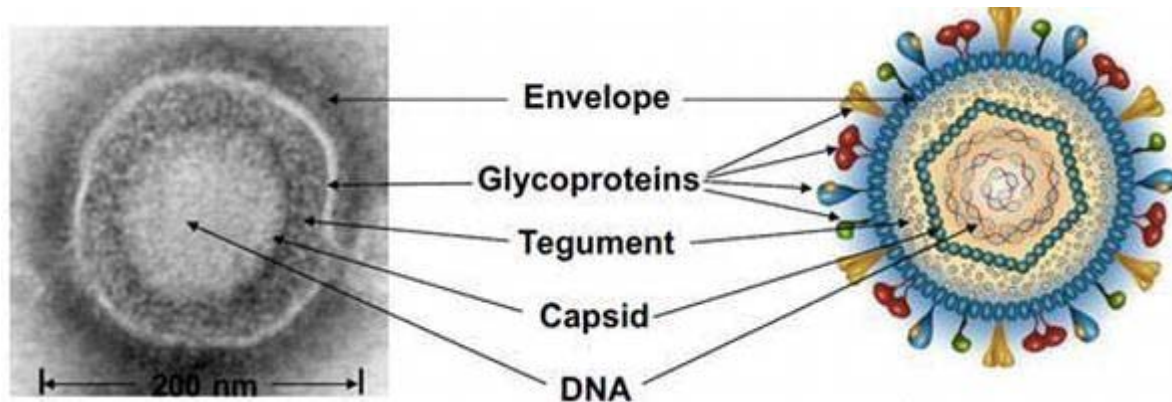
Figure 2. Structure of an HCMV virion.

The electron micrograph (left) and schematic representation (right) of an HCMV virion are shown. Figure is modified from [27].

HCMV has a broad tropism and is able to infect a wide variety of cell types, including fibroblasts, epithelial cells, endothelial cells, macrophages, dendritic cells, smooth muscle cells, and hepatocytes [28]. The broad cell-type tropism of HCMV is important for systemic spread in the host and between hosts. After primary infection, HCMV undergoes a latent state in myeloid cells of the bone marrow, allowing the virus to persist as a life-long infection [29-31].

The first step of HCMV life cycle is viral entry, which is the attachment and penetration of the host cells. During viral entry, the viral envelope glycoproteins, present on the surface of infectious virions, are able to interact with specific cell surface receptors to mediate fusion or endocytosis of the virion with the cell. Subsequently, the viral tegument proteins, virion mRNA and nucleocapsid are released into the cytoplasm. The viral capsid is transported to the nuclear membrane through interaction of specific tegument proteins with the host cell microtubules [32]. The viral genome is then injected into the host nucleus though the nuclear pores. Tegument proteins such as the most abundant tegument protein UL83, a member of the UL82-UL84 gene family in which proteins are thought to have evolved from a common ancestor by gene duplication [33], regulates the host immune responses to prevent clearance by the host [34]. The tegument proteins are also involved in the initiation of viral genes expression, such as UL82 protein that regulates viral immediate early (IE) gene expression. The

IE genes are expressed firstly which occur within 2 hours post infection, followed by the early (E) genes which occur starting from 4 hours post infection. The early proteins mediate viral genome replication through a rolling cycle mechanism. Some of the early proteins function essentially for counteracting cellular defense mechanisms. Furthermore, the early proteins also initiate the expression of late (L) genes, which encode proteins for structural components of the virion and promote viral capsid assembly in the nucleus [35]. After nuclear egress, the newly formed capsids are then transported to the viral assembly compartment in the cytosol. The viral capsids acquire the tegument and secondary envelope derived from the endoplasmic reticulum (ER), Golgi apparatus and endosomal machinery [36]. Finally, the mature infectious viral particles are transported by secretory vesicles to reach the plasma membrane and get released from the host cell (Figure 3) [37].
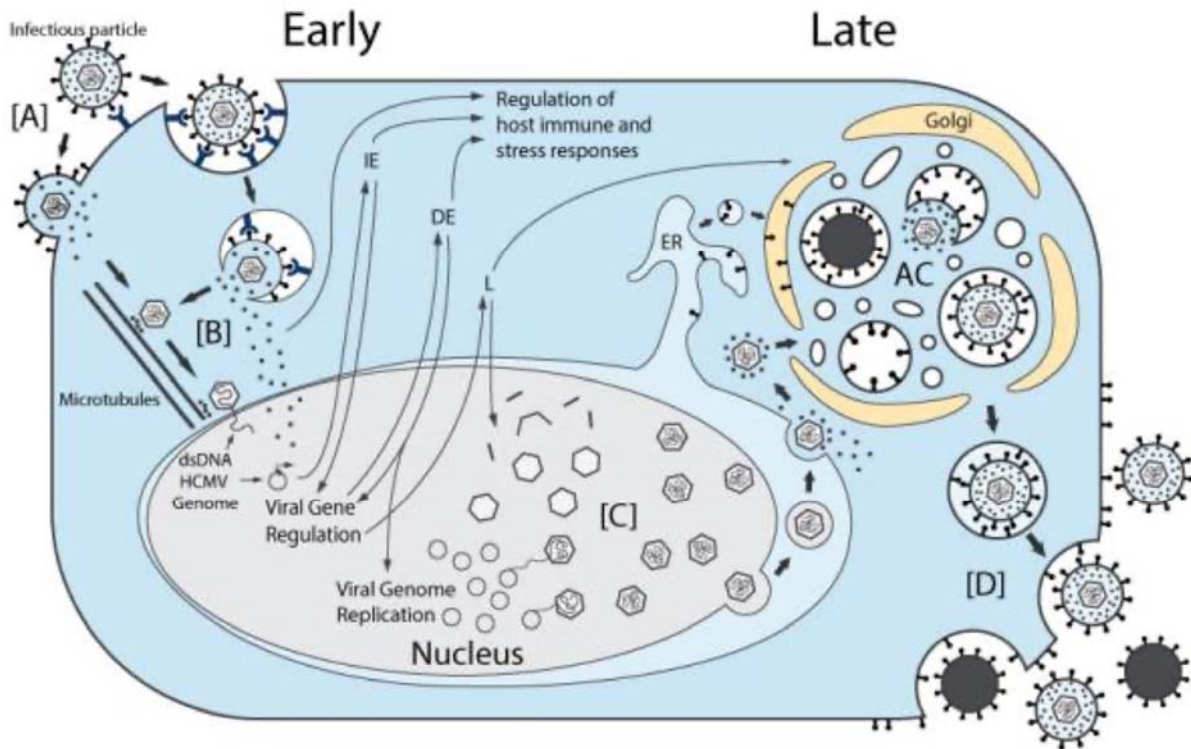
Figure 3. HCMV life cycle.

(A) Infectious viral particles enter into the host cell, the capsids and tegument proteins are released into the cytosol. (B) The capsids further translocate close to the nucleus. The viral genome is then injected into the nucleus and circularized. Viral gene expression and DNA replication are initiated: IE genes, E genes, viral DNA replication, and L genes. (C) Newly synthesized viral capsids assemble in the nucleus and egress to the cytosol. (D) Capsids migrate to the viral assembly compartments where they acquire tegument and viral envelope. The newly formed viral particles are finally released from the cell. Figure is modified from [37]**.**

3.2 Innate immune sensing of DNA

The innate immune system provides the first response against microbial pathogens by utilizing pattern recognition receptors (PRRs) to recognize pathogen-associated molecular patterns (PAMPs). PAMPs are produced by microbes but not host cells, which are specifically recognized by PRRs as non-self. The pathogen-derived DNA is a potent stimulator of innate immune DNA sensors. This immediate sensing activates the intracellular signaling cascades of the innate immune system resulting in the production of type I interferon (IFN) and induction of inflammatory responses (Figure 4).
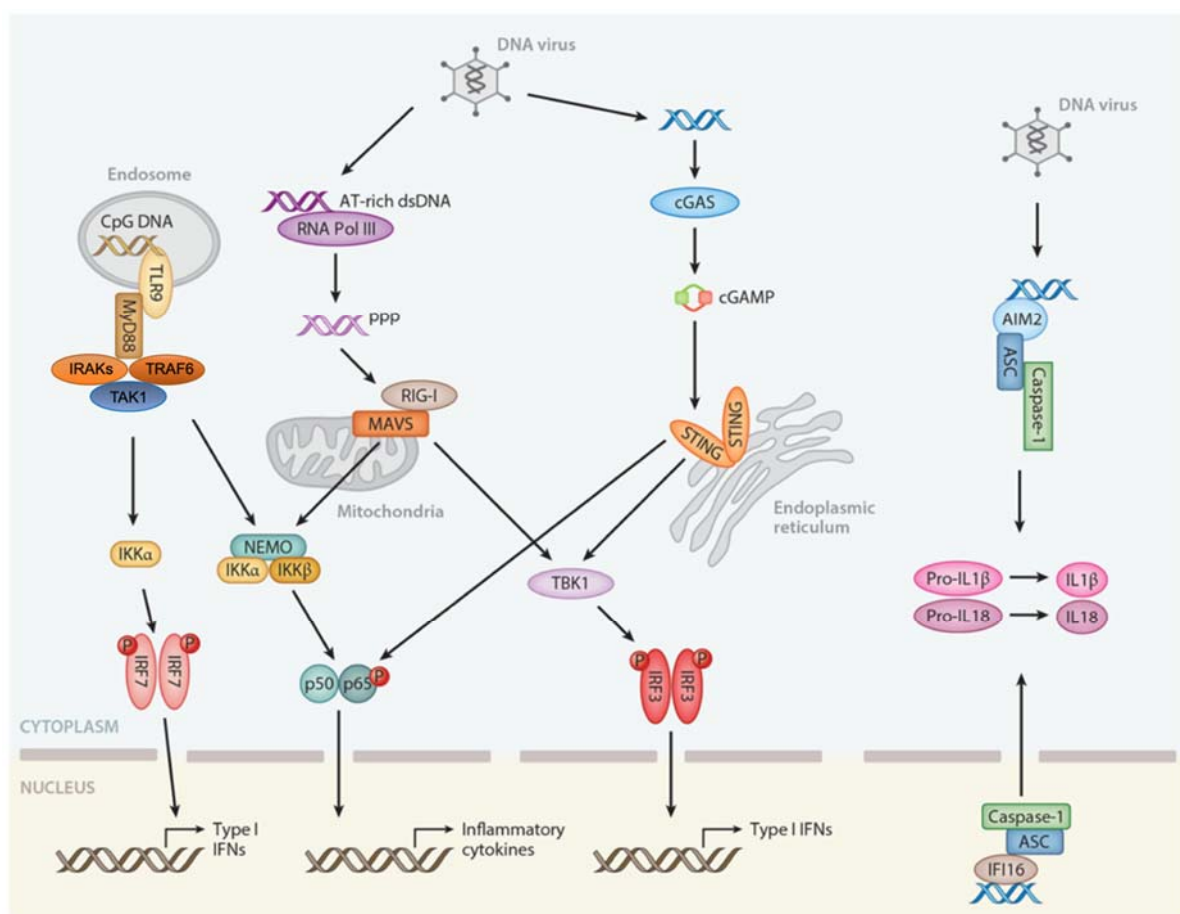
Figure 4. Main pathways of innate immune sensing of DNA in viral infection.

Toll-like receptor 9 (TLR9) senses CpG DNA in endosomes, recruiting MyD88 to activate NF-κB inducing inflammatory cytokines and IRF7-dependent type I interferons (IFNs). RNA polymerase III-RIG-I and cGAS-STING pathways sense pathogen-derived DNA and activate IRF3-dependent type I IFN responses through a common signaling kinase TBK1. Detection of microbial DNA by AIM2 and IFI16 activates the inflammasome, leading to cleavage of pro-IL-1β and pro-IL-18 by Caspase-1. Figure is modified from [38].

3.2.1 TLR9-dependent DNA sensing

The Toll like receptors (TLRs) include at least 10 proteins that recognize PAMPs and the TLR9 is the first well-described PRR for sensing DNA. TLR9 is not detectable on the cell surface [39, 40], but mainly observed in the intracellular components, including ER, lysosomes, and endosomes [41]. The sequestration of TLR9 in the ER is a mechanism of controlling TLR9 signaling. In addition, TLR9 is expressed in different cell types depending on the species. In mice, TLR9 is found in B cells, monocytes and almost all dendritic cells (DCs) subsets including classical DCs (cDCs) [42]. However, TLR9 expression is much more restricted in humans than in mice. In humans, TLR9 is predominantly expressed in plasmacytoid DCs (pDCs), which are professional type I IFN-producing DCs, and B cells among resting immune cells [42].

The unmethylated cytosine-phosphorothioate-guanosine (CpG) DNA motifs are the most well-known ligands of TLR9 [43]. CpG-DNA motifs are frequently present in viruses and bacteria but are rare in mammals. TLR9 is sequestered in the ER and initially translocating to the endosomes after CpG DNA stimulation [44, 45]. The early endosomes containing CpG DNA-TLR9 fuse with lysosomes, which thereby triggers TLR9-mediated signaling. Furthermore, these endosomal localizations are differentially sorted in different types of cells [46, 47]. The early endosomes are in fact containing two distinct populations: one is a dynamic population, which has high mobility on microtubules and rapid maturation toward late endosomes, and the other one is a static population, which has much more slower maturation [48]. TLR9 then recruits the TLR adaptor MyD88 (myeloid differentiation primary response 88) via TIR domain, which leads to the process of type I IFN response and pro-inflammatory cytokines through the activation of NF-κB (nuclear factor 'kappa-light-chain-enhancer' of activated B-cells). MyD88 contains a TIR domain and a death domain [49]. The association of TLR9 and MyD88 in turn activates the interleukin-1 receptor-associated kinase-1 and 4 (IRAK-1 and IRAK-4), which are essential for TLR9-mediated pro-inflammatory cytokine production, via the death domain of MyD88 [49, 50]. Activated IRAK-4 subsequently recruits tumor necrosis factor receptor associated factor 6 (TRAF6) [51], causing activation of transforming growth factor-β associated kinase 1 (TAK1). TAK1 then induces phosphorylation of IκB kinases (IKKs) complex leading to NF-κB activation, which is responsible for the transcription of pro-inflammatory cytokine genes, in non-pDCs such as cDCs [52]. Activation of TLR9 in pDCs is TLR9-

MyD88 dependent and associated with the interferon regulatory factor-7 (IRF7) signaling complex, which consists of IRF7, IRAK 4, IRAK1, TRAF6, resulting in the phosphorylation of IRF-7 and the induction of type I IFNs [53] (Figure 4).

3.2.2 The cGAS-STING-dependent DNA sensing

The cyclic guanosine monophosphate-adenosine monophosphate (cyclic GMP-AMP, cGAMP) synthase (cGAS) and the stimulator of interferon genes (STING) constitute the main signaling pathway of cGAS-STING that is triggered through interactions with DNA in the cytoplasm of mammalian cells (Figure 4) [54]. cGAS senses DNA and synthesizes cGAMP, a second messenger molecule that relays its signal to downstream innate immune responses through STING [54, 55].

During infection of cytosolic bacteria and some DNA viruses, the pathogen-derived DNA may be released into the cytoplasm of the host cell. Besides cytosolic DNA from bacterial or viral sources, cGAS has also been found to interact or at least to co-localize with endogenous self-DNA, including cytosolic DNA from nucleus and mitochondria [56]. The invading pathogens damage the host cell, causing the nuclear and mitochondrial DNA to be released into the cytoplasm. Both self- and non-self-cytoplasmic DNA can then be effectively recognized by cGAS. The C-terminal domain of cGAS contains positively charged DNA-binding sites, which bind the deoxyribose – phosphate backbone of DNA. The binding of DNA forms a 2:2 complex in the cytoplasm and leads to conformational changes of cGAS that rearrange the catalytic pocket of the enzyme allowing an optimal interaction with the substrates ATP and GTP [57]. The cGAS activation is DNA length-dependent, and it is possible that the N-terminal domain of cGAS dimers is stabilized by DNA protruding from the core binding sites [58]. As the secondary messenger, cGAMP binds to the adapter protein STING anchored to the ER inducing a conformational change and activation of STING [59]. The adaptor protein STING is expressed in distinct cell types including macrophages, dendritic cells (DCs) and lymphocytes, as well as endothelial and epithelial cells [60]. The cGAMP-bound STING subsequently migrates from ER to the Golgi [61-63]. In the process of migration, the oligomerized STING recruits and activates TANK-binding kinase 1 (TBK1) and IKK kinase as well as the downstream interferon regulatory factor 3 (IRF3) and NF-κB. TBK1 phosphorylates both STING and itself leading to the phosphorylation of IRF3, which induces its dimerization and translocation into the nucleus [64]. In the nucleus, IRF3 promotes the expression of type I IFNs, such as

interferon-beta (IFN-β). Therefore, a robust expression of type I IFN and a series of inflammatory factors are induced to enhance immune responses [65, 66].

3.2.3 Inflammasome-dependent DNA sensing

AIM2 (absent in melanoma 2) and IFI16 (interferon-inducible protein 16) are the most well-known dsDNA sensors inducing inflammasomes that belong to the same family of PYHIN (IFI200/HIN-200) proteins [67]. AIM2 is characterized by an N-terminal pyrin domain (PYD) and a C-terminal HIN (hematopoietic expression, interferon-inducible nature, and nuclear localization) domain. The HIN domain is responsible for recognizing and binding to dsDNA, and the PYD is responsible for engaging downstream adaptor protein ASC (apoptosis-associated speck-like protein containing a CARD) via homotypic interactions. In the absence of dsDNA, the PYD binds to the HIN domain keeping AIM2 in an auto-inhibited state [68]. The interaction between the HIN domain and the dsDNA is electrostatic interaction with the sugar-phosphate backbone, which is a sequence-independent response to cytosolic dsDNA [69]. Following this event, the AIM2^{PYD} helically assembles to generate a polymerized platform to nucleate downstream ASC^{PYD} filaments, initiating the assembly of AIM2 inflammasome [70, 71]. The adaptor protein ASC recruits downstream pro-Caspase-1 via homotypic interactions of CARD, resulting in proteolytic activation of Caspase-1 into cleaved forms p20 and p10. Active Caspase-1 cleaves pro-IL-1β and pro-IL-18 to their mature forms IL-1β and IL-18 as active inflammatory cytokines (Figure 4) [72], and leads to cleavage of gasdermin D (GSDMD), an executioner of pyroptosis. The N-terminal fragment of the cleaved GSDMD forms GSDMD-pores within the plasma membrane to trigger pyroptotic cell death [72]. In the quiescent state, AIM2 is mainly expressed in the spleen, peripheral blood and the intestine. AIM2 was shown to sense cytoplasmic bacterial, viral, and even host dsDNA, which plays an important role in the host defense against pathogens and is involved in autoimmune diseases [73].

IFI16, another AIM2-like receptor (ALR) family member, forms inflammasomes in both nucleus and cytoplasm whereas the AIM2 inflammasome is only present in the cytoplasm [74]. IFI16 contains a PYD and two HIN domains, a HIN-A and a HIN-B. In contrast to AIM2, the isolated IFI16 HIN domain displays a lower DNA-binding affinity [69]. The tandem HIN domains of both HIN-A and HIN-B are more effective in DNA binding than the single HIN-B domain or with the HIN-A domain alone [75]. The DNA binding affinity can be further strengthened by the presence of PYD in the full length

IFI16 protein. The non-DNA-binding PYD of IFI16 is necessary for the cooperation of IFI16 filaments assembly on dsDNA [76]. Interestingly, it has also been shown that IFI16 has a preference of binding cruciform structure DNA [77]. The PYD of IFI16 recruits ASC and subsequent downstream Caspase-1 in the same way as AIM2 PYD does (Figure 4). In this way, IFI16 contributes to the maturation and release of IL-1β and IL-18. However, the direct role of IFI16 in inducing pyroptosis, especially for the GSDMD cleavage and subsequent pyroptotic cell death, remains unclear.

Furthermore, RNA polymerase III (RNA Poly III) detects cytosolic dsDNA and induces type I IFN response depending on the retinoic acid inducible gene-I–mitochondrial antiviral signaling (RIG-I-MAVS) pathway (Figure 4). The underlying mechanism is that RNA Poly III transcribes dsDNA into dsRNA containing a 5'-triphosphate moiety, which is a known ligand of RIG-I [78, 79]. RIG-I is the founding member of the RIG-I-like receptor (RLR) family, which consists of two N-terminal CARDs, a central RNA helicase domain and a C-terminal regulatory domain (CTD). The CARDs are responsible for recruiting adaptor proteins to trigger the transmission of downstream signaling [80]. The central RNA helicase domain includes a conserved Asp–Glu–Ala–Asp motif, which is called DEAD box and has ATPase activity. The CTD binds to dsRNA leading to conformational changes inducing RIG-I oligomerization and subsequent association with MAVS via homotypic CARD-CARD interaction [81]. RIG-I was also shown to directly bind to ASC and Caspase-1 to form inflammasome complex [82].

3.3 Inflammasome activation in viral infection

Sensors involved in antiviral inflammasomes comprise NLRs (nucleotide-binding oligomerization domain and leucine-rich repeat-containing receptors), ALRs (AIM2-like receptors) and RLRs (RIG-I-like receptors). Although diverse inflammasomes function against a broad range of pathogens, the NLRP3, AIM2, and RIG-I inflammasomes have been identified to be highly specific and crucial in mediating the host responses to viral infection. The inflammasome activation initiates an inflammatory form of programmed cell death, named pyroptosis, accompanied by IL-1β and IL-18 release.

3.3.1 NLR inflammasomes

NLRs initiate host defense by recognizing microbial products or intracellular danger signals through inflammatory signaling complex [83]. The NLR family comprises 22

genes in humans and at least 34 genes in mice [84]. Structurally, the NLRs are multi-domain proteins that contain a common central NACHT (nucleotide- binding and oligomerization) domain, C-terminal leucine-rich repeats (LRRs), and N-terminal effector domain [85]. The N-terminal CARD or PYD are responsible for downstream signaling through homotypic interactions with other CARD- or PYD-containing proteins. The C-terminal LRRs play a crucial role in ligand sensing and autoregulation of NLR inflammasomes. The active multi-protein signaling platform is formed by the central NACHT oligomerization, which further recruits the adaptor protein and effector proteins, leading to an inflammatory response. Formation of the NLR inflammasomes trigger the activation of Caspases and the maturation of IL-1β and IL-18. Based on the diverse N-terminal effector domains, NLRs have been further classified into five subfamilies: the NLRAs (NLRs with acidic activation domain), NLRBs (NLRs with baculovirus IAP repeat (BIR) domain), NLRCs (NLRs with CARD domain), NLRPs (NLRs with PYD domain) and NLRXs (NLR family without strong homology to the N-terminal domain of any other NLR subfamily member) [86].

The NLRP3 inflammasome is the most studied inflammasome and comprises NLRP3, the adaptor protein ASC, and pro-Caspase-1. Activation of the NLRP3 inflammasome induces the activation of Caspase-1, the maturation of pro-inflammatory cytokines IL-1β and IL-18 and pyroptosis (Figure 5). The NLRP3 inflammasome responds to a wide variety of viral infections with both DNA and RNA viruses. The viral RNA of influenza virus and the viroporin M2 were found to activate the NLRP3 inflammasome in murine macrophages and the NLRP3 inflammasome has also been shown to play a crucial role in controlling viral infections *in vivo* [87, 88]. Furthermore, the viroporin of other RNA viruses such as human rhinovirus (HRV), encephalomyocarditis virus (EMCV) can activate the NLRP3 inflammasome as well (reviewed in [89]). The DNA viruses, such as adenovirus and leporipoxvirus myxoma virus can activate the NLRP3 inflammasome via cathepsin B release and reactive oxidative species (ROS) production [90]. Upon Herpes Simplex virus 1 (HSV-1) infection, the cGAS-STING-NLRP3 signaling facilitates the NLRP3 inflammasome activation and IL-1β secretion [91]. Another alpha-herpesvirus, varicella-zoster virus (VZV), activates the NLRP3 inflammasome but not AIM2 inflammasome [92]. NLRP6 is a tissue- and cell-type–specific pattern that functions as a viral RNA sensor and plays a prominent role in inhibiting EMCV intestinal replication *in vivo* [93]. Additionally, NLRP6 and its ability to form dsRNA-dependent liquid-liquid phase separation are important in inflammasome

activation and restriction of a coronavirus in a model of murine hepatitis virus (MHV) infection in the liver, *in vivo* [94]. The NLRP9b inflammasome was shown to restrict rotavirus infection in intestinal epithelial cells [95]. Influenza A virus (IAV) infection in the NLRC4 inflammasome-deficient mice significantly increased FasL expression on DCs, which led to cell death resulting in decreased viral clearance and survival [96, 97]. To date, numerous NLRs were shown to be activated in viral infection though some of them without a clear mechanism.
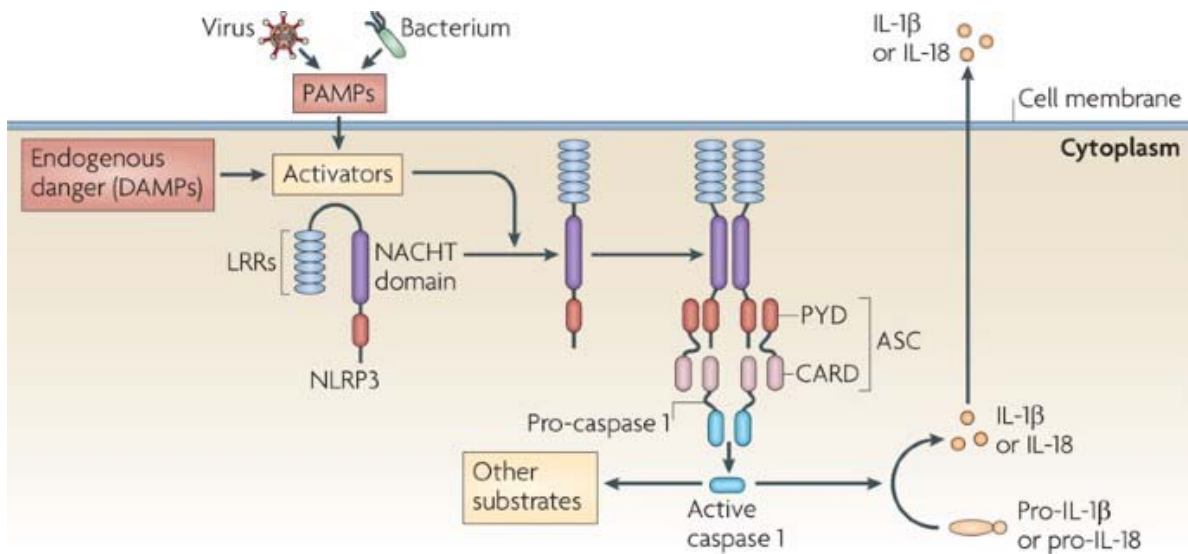
Figure 5. Mechanism of NLRP3 inflammasome complex formation.

The NLRP3 inflammasome, the best-studied NLR inflammasome, comprises NLRP3, the adaptor protein ASC, and pro-Caspase-1. NLRP3 senses ligands through LRRs, recruits ASC via PYD and further activates Caspase-1. The activated Caspas-1 induces the maturation of pro-inflammatory cytokines IL-1β and IL-18. Figure is taken from [98].

3.3.2 ALR inflammasomes

The ALRs AIM2 and IFI16 comprise an N-terminal pyrin domain (PYD) and C-terminal HIN domain(s) for dsDNA binding. The AIM2 inflammasome is the best described cytosolic dsDNA sensor whose activation induces pyroptosis and release of mature pro-inflammatory cytokines IL-1β and IL-18 (described in 3.2.3). The crucial role of the AIM2 inflammasome in antiviral infection against various DNA and RNA viruses has been identified. *Aim2* knockout cells and mice have been widely used to distinguish the AIM2 inflammasome from other inflammasomes. Activation of Caspase-1 in response to vaccinia virus (VACV)-derived dsDNA was identified as AIM2-dependent but NLRP3-independent [99]. Similarly, MCMV infection induced Caspase-1 activation

was detected in WT, *Nlrp3*^{-/-} and *Nlrc4*^{-/-} macrophages but not in *Asc*^{-/-} or *Aim2*^{-/-} macrophages from New Zealand Black mice [100]. In MCMV-infected *Aim2*^{-/-} or *Asc*^{-/-} mice, the viral titers in the spleen were elevated compared to those in WT mice, whereas the IL-18 levels in the serum were decreased [101]. AIM2 has been reported not only to sense dsDNA viral genome but also dsDNA products during the viral lifecycle. Chikungunya virus (CHIKV) and West Nile virus (WNV) (both RNA viruses) infection interfered with IL-1β production in the primary dermal fibroblasts treated with siRNA targeting AIM2 [102]. Furthermore, Zika virus (an ssRNA virus) was also found to be able to stimulate AIM2 expression and induce the secretion of IL-1β in infected primary human skin fibroblasts [103]. More studies are required to understand the mechanisms of AIM2 sensing RNA viruses, inducing inflammasome assembly and the subsequent activation of Caspase-1 as well as secretion of IL-1β.

Similar to AIM2, IFI16 belongs to the ALR family, whereas AIM2 is strictly cytosolic, IFI16 is mainly present in the nucleus due to its nuclear localization sequence. IFI16 has been shown to associate with the Kaposi sarcoma-associated herpesvirus (KSHV) viral dsDNA in the nucleus and it assembles inflammasome with ASC to trigger Caspase-1 activation in endothelial cells. Caspase-1 activation and subsequent cytosolic IL-1β processing were decreased in KSHV infection when IFI16 was knocked down [74]. IFI16-dependent Caspase-1 activation and inflammatory cytokine production also occurred in B-cell lines latently infected with KSHV or Epstein-Barr virus (EBV) and monocytes infected with EBV [104]. Another herpesvirus, HSV-1, activates both IFI16 and NLRP3 inflammasomes during infection [105], but the importance of the relative contributions of multiple inflammasomes has not been addressed. IFI16 was also shown to be a restriction factor against HCMV replication [106]. In contrast, the IFI204 protein, which is a putative homolog of IFI16 in the mouse, facilitates MCMV replication whereas the mechanism remains unclear [107, 108].

3.3.3 RLR inflammasome

RIG-I belongs to the RLR family and induces type I IFN production. The RIG-I signaling process is initiated by the interaction of RIG-I with MAVS through homotypic CARD interaction (described in 3.2.3). Numerous RNA viruses activate RIG-I during infection that triggers downstream IFN signaling and mediates the expression of proinflammatory cytokines via NF-κB [109]. Additionally, RIG-I has been shown to initiate inflammasome complex assembly by directly recruiting the adaptor ASC to form

oligomerization, subsequently inducing Caspase-1 activation and maturation of IL-1β and IL-18 [82, 110].

Upon IAV infection in epithelial cells, RIG-I was found to interact with ASC and Caspase-1 to assemble the RIG-I inflammasome, which then induces downstream IL-1β release [82]. Upon vesicular stomatitis virus (VSV) infection of murine DCs, it has been demonstrated that RIG-I induces the production of pro-IL-1β and release of IL-1β via NF-κB and Caspase-1 activation, in which RIG-I serves as an inflammasome activator. However, these activations are not detectable in VSV infected bone marrow-derived DCs (BMDCs) derived from RIG-I$^{-/-}$ mice [111]. The production of pro-IL-1β, release of IL-1β and the activation of NF-κB induced by RIG-I ligand 3pRNA are also blocked in BMDCs derived from MAVS$^{-/-}$ and CARD9$^{-/-}$ (NF-κB activator) mice whereas Caspse-1 activation was not affected. In the same report, RIG-I was co-immunoprecipitated with ASC in THP-1 cells during VSV infection. VSV and 3pRNA induced the activation of Caspase-1 and maturation of IL-1β that were blocked in ASC-deficient cells, but not in the NLRP3-deficient cells [111]. Conflictingly, another study showed that VSV is recognized by NLRP3 but not by RIG-I [112].The mechanism of VSV-induced inflammasome activation needs to be further investigated. These contrasting results suggest the possible existence of dual roles for RIG-I in viral infection.

3.4 Modulation of programmed cell death in cytomegalovirus infection

Programmed cell death (PCD) is an essential process that contributes to immune responses against viral infection by eliminating infected cells and restricting viral dissemination in hosts. There are three key pathways of PCD including apoptosis, necroptosis and pyroptosis (Figure 6). These distinct pathways involve different molecular mechanisms and triggers that regulate the self-destruction of cells. In order to counteract or evade PCD mechanisms, viruses have developed various strategies. CMVs are particularly sophisticated manipulators of cellular defenses and encode potent inhibitors of PCD.
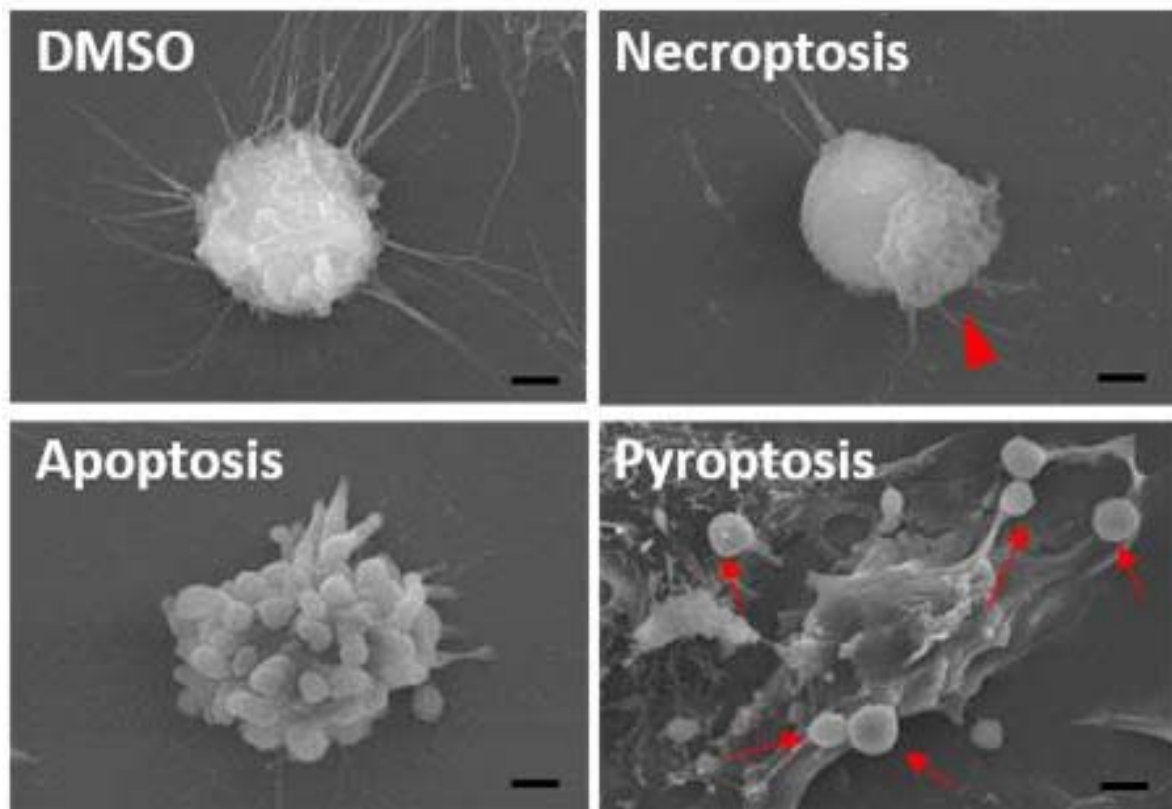
Figure 6. Three kinds of PCD have distinct morphological features.

Representative scanning electronic microscopy images of RAW-ASC macrophages stimulated for apoptosis, necroptosis and pyroptosis. DMSO treated cell is used as control. Arrowhead indicates explosion of necroptotic cells and arrow points to bubbling of pyroptotic cells. Scale bar 2 μm. Figure is modified from [113].

3.4.1 Manipulation of apoptosis by cytomegalovirus

During the past three decades, apoptosis has been the object of intense research, and for some time apoptosis was thought to be the only regulated form of cell death. The process of apoptosis regulates cell populations in development and aging, tissue homeostasis, and immune responses by eliminating inappropriate and damaged cells, which plays a vital role in maintaining the tissue homeostasis and health [114]. There are two main apoptotic pathways: the extrinsic pathway and the intrinsic pathway. They are triggered by different stimuli including DNA damage, viral infection, cellular stress, or activation of specific signaling pathways. The activation of Caspases, a family of protease enzymes, is a key event in the process of apoptosis, which ultimately leads to cellular fragmentation and the formation of apoptotic bodies. Apoptotic cells are finally cleared by phagocytes, preventing inflammation and tissue damage.

The extrinsic apoptosis pathway is also known as the death receptor pathway. Pro-apoptotic death receptors are the tumor necrosis factor (TNF) family of proteins, which are activated by their ligands to form the oligomeric platforms at the cell surface, such as Fas activated by the Fas ligand (FasL), TNF-related apoptosis-inducing ligand (TRAIL) receptors DR4 and DR5 activated by TRAIL, and TNF receptor 1 (TNFR1) activated by TNF [115]. This leads to the recruitment of adaptor proteins Fas-associated death domain protein (FADD) and TNFR1-associated death domain protein (TRADD) through the homotypic death domain. FADD recruits and activates the apoptotic initiator caspase Caspase-8 (formerly called FADD-like IL-1β-converting enzyme, FLICE) to promote the formation of the death-inducing signaling complex (DISC) [116, 117]. The effector caspases Caspase-3 and Caspase-7 are cleaved by initiator caspases to promote apoptosis and then degrade critical cellular components. This process is regulated by the cellular FLICE inhibitor protein (c-FLIP) preventing autocatalytic activation [118]. The TNFR1 receptor recruits the adaptor TRADD, which subsequently recruits FADD, TNF-associated factor-2 (TRAF-2), the receptor-interacting protein kinase 1 (RIPK1). FADD then binds and activates Caspase-8, which subsequently activates the effector caspases (Figure 7) [119].

The intrinsic apoptosis pathway is also known as the mitochondrial pathway. A variety of non-receptor stimuli inside the cells such as DNA damage, ER stress, and growth factor deprivation, can induce mitochondrial outer membrane permeabilization (MOMP) [120]. MOMP allows mitochondrial proteins such as Cytochrome c (cyt$C$), Smac/DIABLO, and HtrA2/Omi to be released into the cytosol from the mitochondrial intermembrane space between the outer (OMM) and inner (IMM) mitochondrial membranes. The apoptosome, a multimeric complex involving APAF1, cyt$C$, and the cofactor dATP/ATP, promotes the activation of Caspase-9 and the downstream effector caspases that are the same in both apoptotic pathways [121, 122]. These mitochondrial events are regulated by members of the B-cell lymphoma 2 (BCL-2) family of proteins, which include pro-apoptotic proteins such as BCL-2-associated X protein (BAX), BCL-2 antagonist or killer (BAK) and BH3-only proteins such as BID; and anti-apoptotic proteins such as BCL-2, BCL-XL and BCL-W. Cross talk between the extrinsic and intrinsic pathways exists through sequestering BH3-only protein BID, which can be cleaved by the activated Caspase-8. The truncated BID (t-BID) promotes the activation of BAX and BAK [123].

Introduction

Slow growing viruses such as CMVs are expected to evolve mechanisms to evade apoptosis. CMVs indeed encode viral proteins to inhibit the host's apoptotic pathways at different levels, ensuring viral replication within infected cells (Figure 7). CMVs encode viral inhibitor of Caspase-8 activation (vICA) to inhibit the activation of Caspase-8, a key initiator caspase in the extrinsic apoptosis pathway. UL36 in HCMV and M36 in MCMV directly interact with the death effector domains of pro-Caspase-8 inhibiting FADD association and pro-Caspase-8 cleavage [124, 125]. The UL37exon 1(UL37x1) of HCMV was identified as viral mitochondria-localized inhibitor of apoptosis (vMIA), which interferes with the function of pro-apoptotic BCL-2 family members such as BAX and possibly BAK [126, 127]. By contrast, MCMV encodes protein m38.5 that binds BAX and prevents its activation and protein m41.1 that associates with BAK and blocks its oligomerization [128, 129]. The UL38 protein of HCMV was reported to inhibit ER stress-induced apoptosis by accumulation of the activating transcription factor 4 (ATF4) that helps to resolve ER stress and by suppression of c-Jun N-terminal kinase (JNK) activity that phosphorylates Bcl-2 [130, 131].
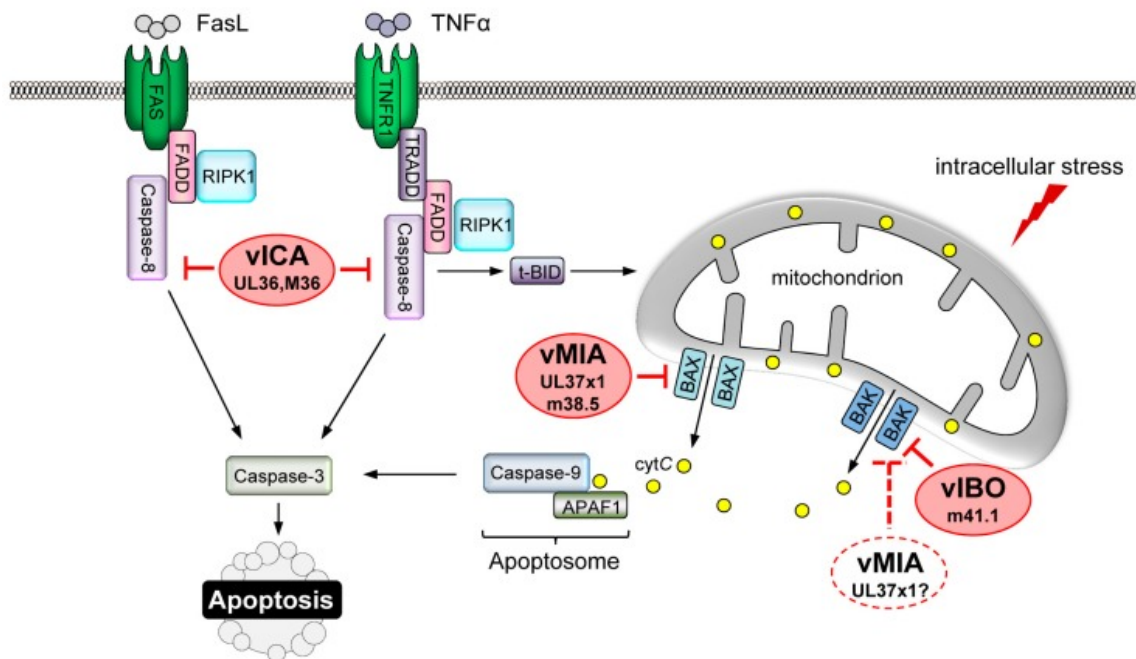
Figure 7. Inhibition of apoptosis by cytomegalovirus (CMV).

UL36 in HCMV and M36 in MCMV function as viral inhibitors of Caspase-8 activation (vICA) to inhibit the extrinsic apoptosis pathway. The UL37 exon 1(UL37x1) protein in HCMV, which is viral mitochondria-localized inhibitor of apoptosis (vMIA), interferes with BAX and possibly BAK. MCMV encodes vMIA m38.5 to prevent BAX and the viral inhibitor of BAK oligomerization (vIBO) m41.1. Figure is taken from [132]**.**

3.4.2 Manipulation of necroptosis by cytomegalovirus

Necroptosis is a form of regulated necrosis, which shares some death inducers molecules with apoptosis such as TNF-α, FasL, and TRAIL, but has distinct morphological changes and molecular features [133]. Necroptosis is triggered by Toll-like receptors (TLRs), death receptors TNFR1 and Fas, and the intracellular sensors Z-DNA binding protein 1/DNA-dependent activator of IFN regulatory factors (ZBP1/DAI) [134-136]. Upon activation of these receptors, necroptosis is mediated by specific signaling molecules such as RIPK1 and RIPK3, which ultimately activate the necroptosis executioner mixed-lineage kinase domain-like protein (MLKL) [137]. Activation of these proteins triggers a cascade leading to a series of events such as cell membrane rupture and the release of intracellular contents, which can induce pro-inflammatory response.

The indirect activation of necroptosis is also known as canonical pathway. The best characterized canonical necroptotic pathway is stimulated through death receptors TNFR. The formation of TNF-receptor-associated complex (complex I) independently recruits RIPK1 and the adaptor TRADD through the death domains (DDs) [138]. At the complex I, RIPK1 is ubiquitylated in its intermediary domain (ID) and recruits the IκB kinase complex (NEMO, IKKα and IKKβ) [139]. The IKK complexes activate the NF-κB pathway, which promotes cell survival by activating the expression of cFLIP. Phosphorylation of RIPK1 is IKKα- and IKKβ-dependent, which directly inhibits RIPK1 kinase activity, preventing its dissociation from the receptor and the formation of complex II [140]. Complex II has two different forms (IIa and IIb) defined by the protein composition and activity [141]. While complex IIa and IIb induce apoptosis, when Caspase-8 is absent or inactivated they can also induce necroptosis. The RIPK1 in complex II recruits and activates RIPK3, which interact through unique RIP homotypic-interacting motifs (RHIMs) forming a complex [142]. The RIPK1/RIPK3 complex recruits and phosphorylates MLKL resulting in the formation of the necrosome [137]. MLKL functions as an executor of necroptosis by its oligomerization and translocation to the plasma membrane where it forms membrane-disrupting pores [143].

RIPK1-independent but RIPK3-dependent mechanisms have been described as non-canonical necroptosis. It has been shown that the intracellular nucleotide sensor ZBP1/DAI triggers RIPK3 dependent necroptosis. ZBP1/DAI can bind and activate RIPK3 through its RHIM domain to form a RHIM-dependent complex that contributes to

activate the necroptotic pathway [144]. In addition, stimulation of TLR3 and TLR4 results in RIPK3-MLKL-dependent necroptosis by the adaptor TRIF, which associates with RIPK3 by RHIM domain [135].

Caspase-8 suppresses necroptosis by inhibiting the activity of RIPK1 and RIPK3 (reviewed in [145]). Thus, the inhibition of Caspase-8 activity greatly sensitizes cells to the initiation of necroptosis [146]. The vICA of CMVs inhibit Caspase-8 activation during infection (described in 3.4.1), which could sensitize cells to necroptosis. The M45 protein of MCMV, which is the first identified RHIM-dependent inhibitor and is also called viral inhibitor of RIP activation (vIRA), is the large subunit of the viral ribonucleotide reductase (RNR). M45 bind RHIM containing proteins RIPK1, RIPK3 and ZBP1/DAI, effectively sequestering RHIM-dependent necroptotic machinery, inhibiting MLKL activation and necroptosis (Figure 8) [144, 147]. However, the UL45 protein of HCMV, the homologous protein of M45, does not contain a RHIM domain. In contrast, the homologous proteins ICP6 of HSV-1 and -2 carry a RHIM domain. The HSV-1 protein ICP6 inhibits necroptosis in infected human cells whereas it activates necroptosis in mouse cells [148, 149]. The UL36 protein of HCMV functions as a dual cell death pathway inhibitor: UL36 as a vICA inhibits extrinsic apoptosis pathway (described in 3.4.1) and UL36 blocks necroptosis by targeting MLKL and inducing its degradation (Figure 8) [150].
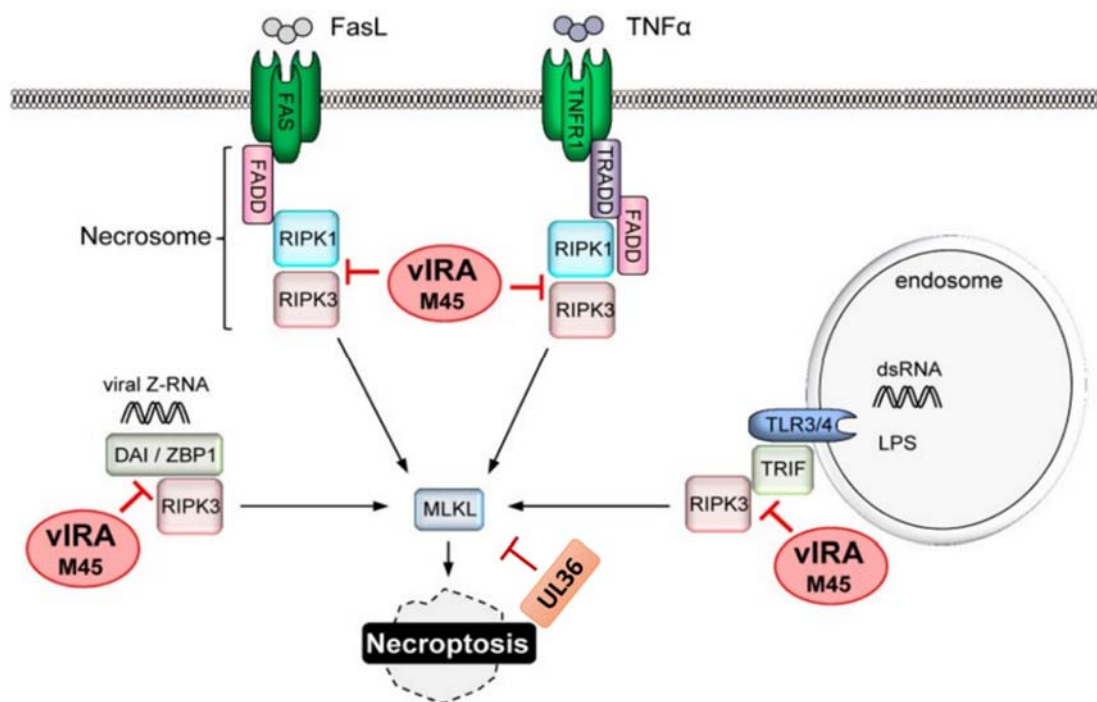
Figure 8. Inhibition of necroptosis by MCMV.

MCMV M45 protein, the viral inhibitor of RIP activation (vIRA), contains a RIP homotypic interaction motif (RHIM) and inhibits RHIM-dependent activation of RIPK3. The UL36 of HCMV inhibits necroptosis by targeting MLKL and inducing its degradation. Figure is modified from [132].

3.4.3 Manipulation of pyroptosis by viruses

Pyroptosis is a form of lytic and highly inflammatory programmed cell death that serves as a host defense mechanism against microorganisms in vertebrates. Cytoplasmic contents such as inflammatory cytokines and alarmins can be released from pyroptotic cells due to the rupture of the plasma membrane (Figure 9).

Assembly of the oligomeric inflammasome complex is initiated upon detection of PAMPs or damage-associated molecular patterns (DAMPs) by the PRRs, such as NLRs, ALRs and RLRs (described in 3.3). The inflammasomes that act as molecular platforms for the activation of inflammatory caspases are mediated through ASC-dependent or -independent signaling. Caspase-1-mediated monocyte death has been the term used to describe pyroptosis for many years [151]. A variety of canonical inflammasomes have been identified, which has revealed that Caspase-1-mediated pyroptosis is involved in crucial immune defense mechanisms. Of note, recognition and binding of the bacterial LPS by the human Caspases-4 and 5 and the mouse orthologue Caspase-11 are able to induce the assembly of the noncanonical inflammasome complex. The noncanonical inflammasomes contribute to antibacterial immune responses, but likely not to antiviral defenses [152]. Thus, the induction of pyroptosis is initiated by proteolytic activation of Caspase-1 or Caspase-11/4/5. The pore-forming protein GSDMD, a substrate of these inflammatory caspases, is an executioner of pyroptosis. The oligomerized gasdermin-N domain of GSDMD forms membrane pores to disrupt the osmotic potential, causing cell swelling and eventual lysis [153]. Nearly all gasdermin family members possess the pore-forming and pyroptotic activity of GSDMD (reviewed in [154]), pyroptosis thus has been defined as gasdermin-mediated cell death. Additionally, Caspase-8, a mediator of extrinsic apoptosis, has also been recognized to contribute to GSDMD cleavage and pyroptosis [155, 156]. In a recent study, it was shown that the protein ninjurin-1 (NINJ1), which acts downstream of GSDMD, induces plasma membrane rupture by inserting its extracellular α-helices into the plasma membrane, causing the polymerization of NINJ1

monomers into amphipathic filaments that ultimately lead to the rupture of the plasma membrane [157].

In addition, the activation of Caspase-1 processes the pro-inflammatory cytokines pro-IL-1β and pro-IL-18 into their mature forms. The GSDMD pores facilitate the release of IL-1β and IL-18 and other cellular components. Therefore, pyroptosis occurs accompanying IL-1β and IL-18 release. A variety of immunomodulatory effects are induced by these cytokines, which can lead to both host protection and damaging pathological response. IL-1β is capable of recruiting neutrophils [158], polarizing T cells to adopt a Th17 phenotype [159], and promoting DCs activation for priming [160, 161]. IL-18 promotes IFN-γ production [162] and cytotoxic activity in a variety of cell types [163].

In response of viral infection, various inflammasomes are involved in mediating pyroptosis including the NLRP3, NLRP6, and NLRP9 inflammasomes, AIM2 inflammasome, and the IFI16 inflammasome (described in 3.3). Many viruses were identified to encode proteins preventing inflammasomes at different levels which contribute to optimal viral replication. Some poxviruses express viral pyrin-only proteins (vPOPs) that directly interact with the adaptor protein ASC by homotypic interactions via pyrin domains [164]. The vaccinia viral protein F1L has the capacity to block NLRP1-mediated Caspase-1 activation [165]. Kaposi's sarcoma-associated herpesvirus (KSHV) encodes the viral protein ORF63 that is homologue of NLRP1, therefore blocks NLRP1 inflammasome activation [166]. The HSV-1 protein VP22 directly interacts with AIM2 to block the assembly of inflammasome complex and the release of inflammatory cytokines [167]. The ubiquitin ligase activity of HSV-1 protein ICP0 targets IFI16 for proteasomal degradation [168]. HCMV UL83 supresses IFI16-dependent inflammasome by targeting PYD [34]. HCMV encodes UL97, a viral kinase that can phosphorylate IFI16 and export IFI16 from the nucleus, thereby preventing detection of viral DNA [169]. Furthermore, viruses have evolved to inhibit pyroptosis by directly processing GSDMD in addition to targeting inflammasome components. The viral protease 3C of enterovirus 71 is able to cleave in the GSDMD-N for inactivation [170]. In human monocytes, the coronavirus SARS-CoV-2 nucleocapsid protein is able to block pyroptosis and IL-1β secretion by preventing Caspase-1-mediated cleavage of GSDMD [171]. Together, an array of viral evasion mechanisms

shows that inflammasome-pyroptosis pathways play important roles in host immunity against viral infection.
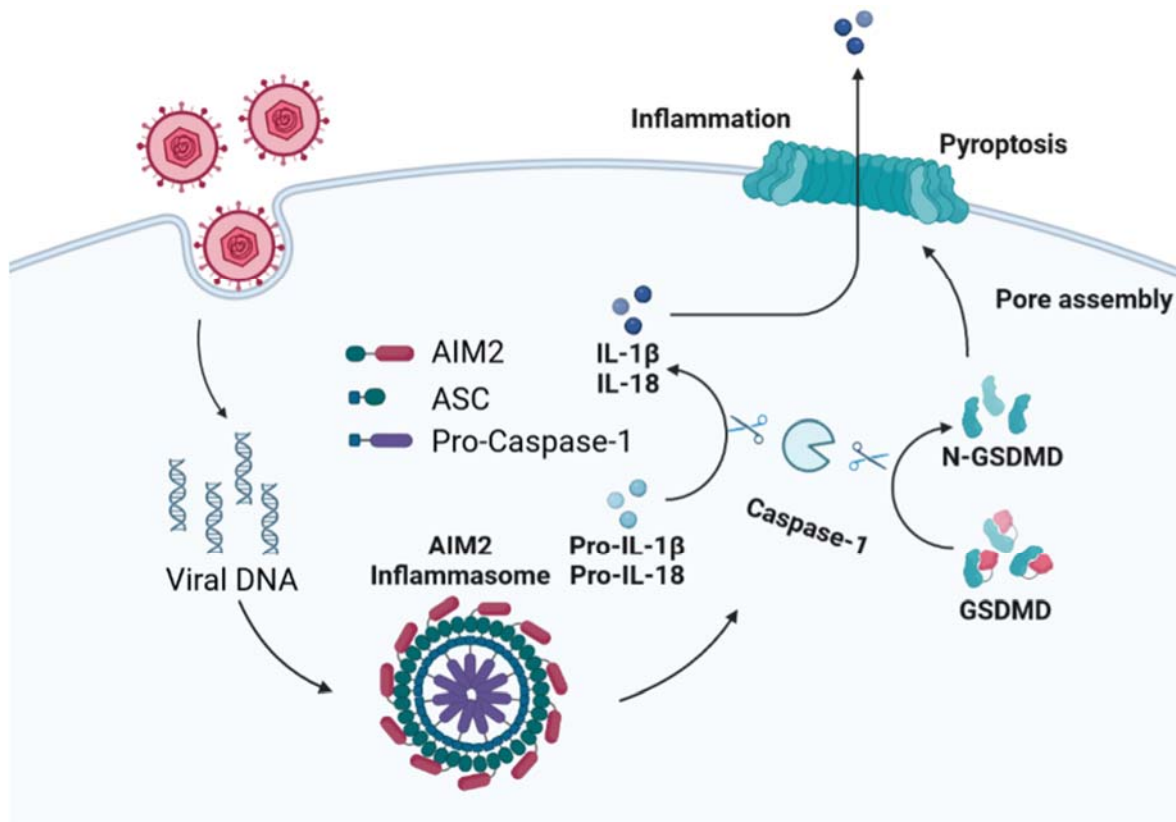
Figure 9. AIM2 inflammasome dependent pyroptosis.

AIM2 senses viral DNA in the cytoplasm and recruits ASC to assemble the AIM2 inflammasome complex leading to Caspase-1 activation. The activated Caspase-1 induces IL-1β and IL-18 maturation and GSDMD cleavage which forms pore on the cell membrane inducing pyroptosis.

4 Aims of the study

Programmed cell death (PCD), comprising the three major forms apoptosis, necroptosis and pyroptosis, is one of the host immune responses against viral infection. PCD serves the host by eliminating infected cells and preventing viral dissemination in the host organism. The CMVs encode several proteins suppressing apoptosis and necroptosis. However, how CMVs modulate pyroptosis has not been described, yet. The AIM2 inflammasome, a multiprotein complex, is expressed in cells of the myeloid lineage (such as macrophages) and is responsible for processing and release of the inflammatory cytokines IL-1β and IL-18 [172] and the induction of pyroptosis. Initial studies have shown that vaccinia virus, MCMV [99, 173], and other DNA viruses (reviewed in [174]) activate the AIM2 inflammasome. By contrast, little is known about viral suppression of AIM2 inflammasome activation and subsequent pyroptosis. Therefore, the first aim of this study was to identify an MCMV protein inhibiting AIM2 inflammasome signaling and to evaluate its inhibitory effect in infected macrophages, *in vitro*.

To investigate the importance of a viral immune evasion protein for pathogenesis *in vivo*, it is crucial to note that the investigation can only be explored if the virus infects laboratory animals (preferably mice) and causes a similar pathology. MCMV is a natural mouse pathogen and perfectly suited for studies in the mouse model [4]. Therefore, the secondary aim of this project was to investigate the biological impact of MCMV mediated inhibition of the AIM2 inflammasome in its natural host, the mouse, *in vivo*.

It is expected that the results of this study will provide the first evidence of MCMV inhibiting AIM2 inflammasome dependent pyroptosis and a better understanding of how MCMV modulates programmed cell death.

5 Results

5.1 Identification of MCMV M84 as an inhibitor of the Aim2 inflammasome activation

To identify MCMV proteins that inhibit the AIM2 inflammasome signaling, I tested the inhibitory effect of viral proteins on AIM2 inflammasome activation in transfected HEK293A cells by detecting IL-1β secretion. HEK-293A cells were co-transfected with plasmids encoding AIM2, ASC, Pro-Caspase-1, Pro-IL-1β, proteins of the AIM2 inflammasome pathway, together with plasmids from a MCMV ORF library [175].

During CMV infection in macrophages, it has been reported that the viral capsid is degraded, thereby releasing the viral DNA into the cytoplasm, which can activate the cytosolic DNA sensor AIM2 inflammasome [173]. Consequently, the viral manipulation of DNA sensing is expected to take place early in infection, and for this reason, I focused on known or predicted tegument and related proteins [176, 177] for the screening assay. The protein product of the non-canonical ORF L147C, which was identified as a putative interactor of Caspase-1 in a proteomic screen [178], was cloned to pcDNA3 and also tested for the inhibitory effect on IL-1β secretion. The HSV-1 protein VP22, a previously described inhibitor of the AIM2 inflammasome, was included as a positive control [167]. The empty vector pcDNA3 was used as a negative control for the general IL-1β secretion level. At 24 hours post transfection, the cells were collected in 2x SDS-PAGE sample buffer for detecting the activation of Caspase-1 by immunoblot analysis (Figure 10A) and the cell-free supernatant was harvested for measuring the IL-1β secretion by ELISA (Figure 10B). Unfortunately, this transfection-based assay and ELISA measurement of IL-1β yielded quite variable results with many MCMV ORF expression plasmids producing a moderate degree of inhibition.
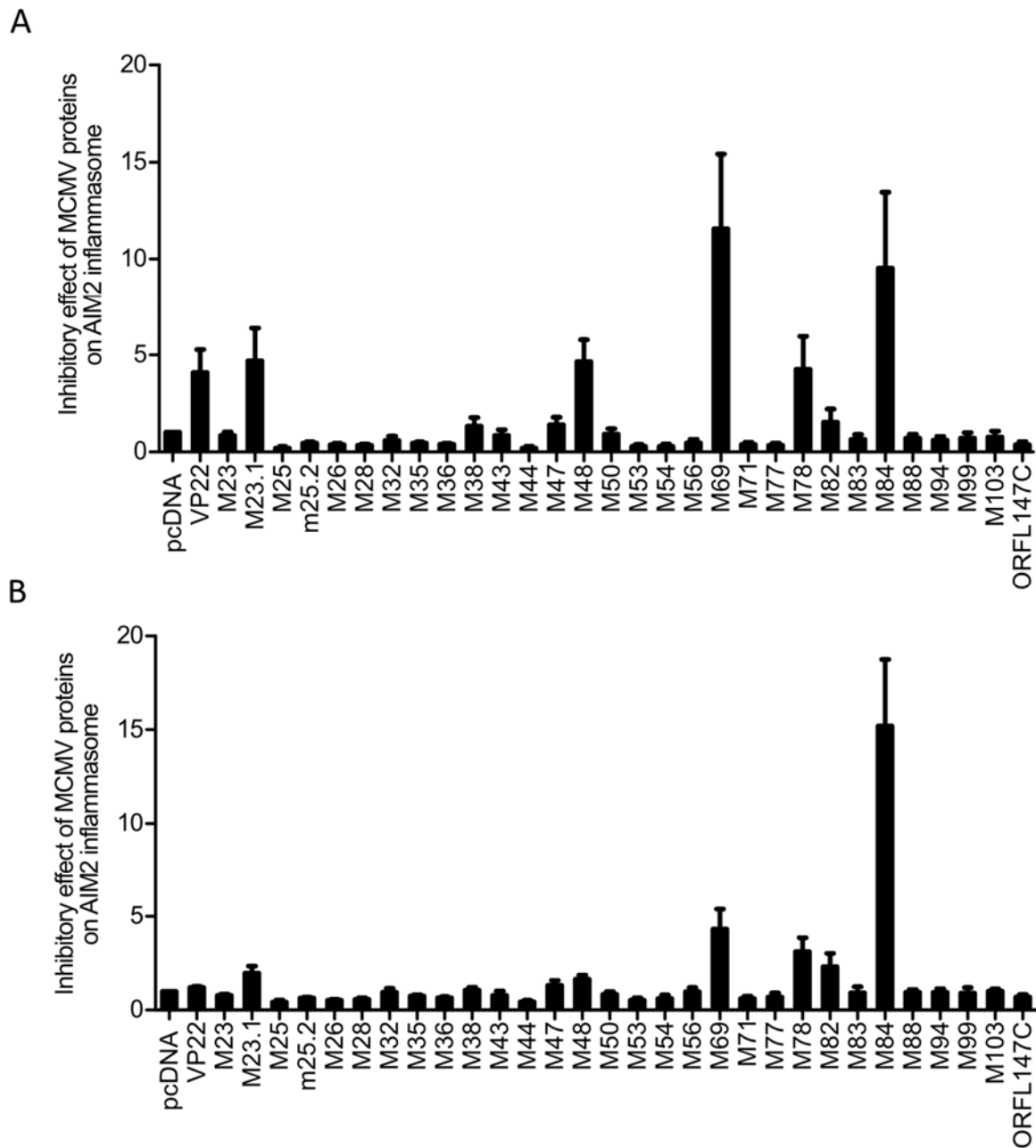
Results
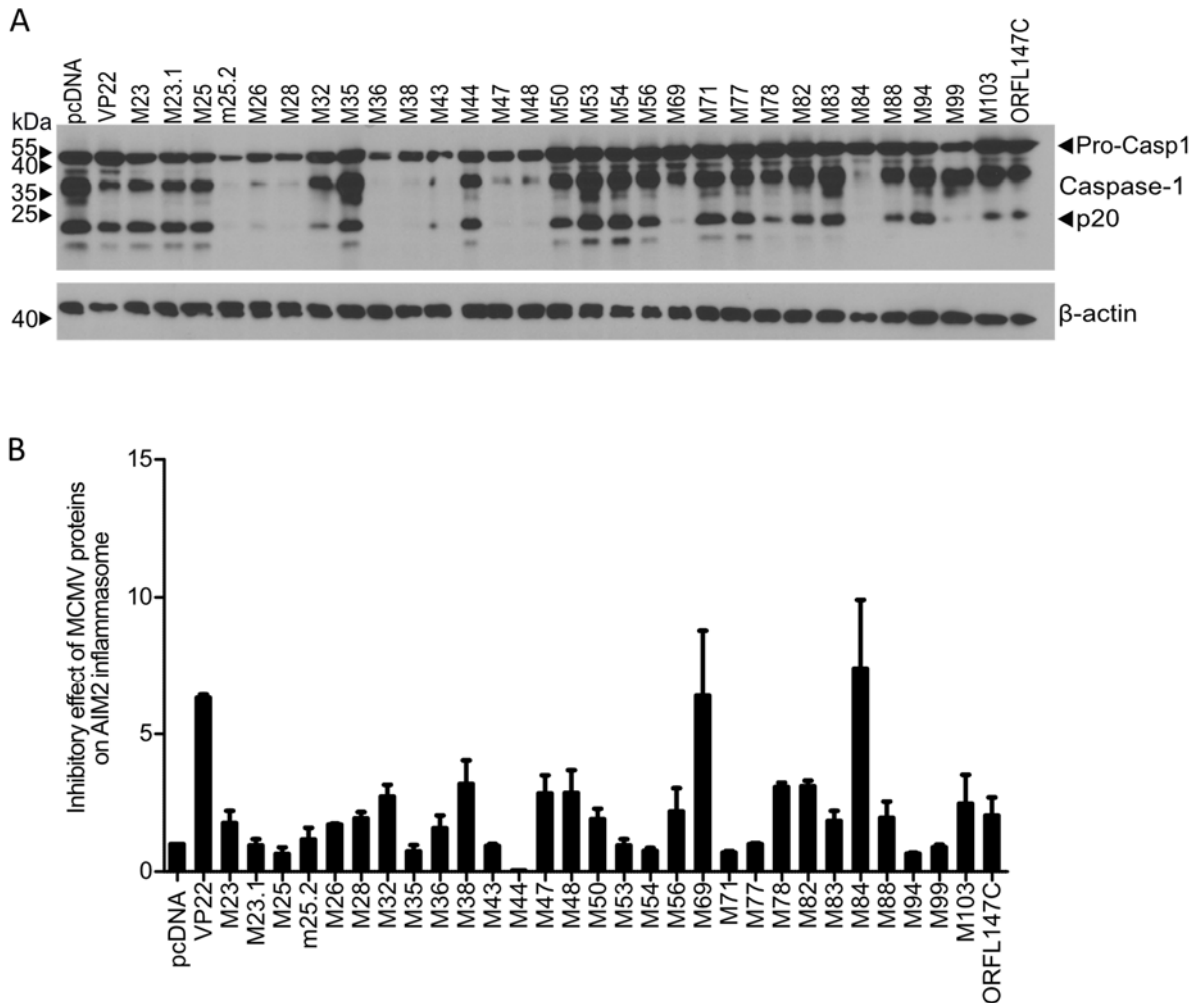
Figure 10. Identification of MCMV AIM2 inflammasome inhibitors.
(A and B) HEK 293A cells were co-transfected with plasmids encoding murine AIM2, ASC, pro-Caspase-1, pro-IL-1β, and individual MCMV proteins. 24 h post transfection, cell lysates were harvested to detect Caspase-1 activation by immunoblot analysis (A). Supernatants were collected to determine IL-1β release by ELISA. The inhibitory effect was calculated by dividing the IL-1β level of vector-transfected cells by those from cells expressing MCMV ORFs. Mean ± SEM of three independent experiments are shown (B).

Due to the variable results of the commercial ELISA assays, a pro-interleukin-1β-*Gaussia* luciferase (iGLuc) fusion protein [179] was used as a better quantifiable reporter for the transfection-based screening assay. The iGLuc ORF was PCR-amplified and cloned into the expression vector pcDNA3. IL-1β secretion was detected by the measurement of the *Gaussia* luciferase activity (Figure 11A). Compared to the results of the ELISA, the luciferase reporter system efficiently reduced the number of unspecific hits. Intriguingly, when the inflammasome activation was increased by transfecting 5 times more ASC expression plasmid, the viral protein M84 showed the most efficient inhibitory effect on IL-1β cleavage and secretion (Figure 11B). These

results suggest that MCMV M84 may function as an inhibitior of the AIM2 inflammasome signaling.

Figure 11. Identification of MCMV M84 as an AIM2 inflammasome inhibitor.
(A) HEK 293A cells were co-transfected with plasmids encoding murine AIM2, ASC, pro-Caspase-1, a pro-IL-1β-*Gaussia* luciferase (iGLuc) reporter, and individual MCMV proteins. 24 h post transfection, supernatants were collected to determine IL-1β release by luciferase assay. The inhibitory effect was calculated by dividing the luciferase reads of pcDNA transfected cells by those from cells expressing MCMV ORFs. (B) Cells were transfected as described above, but 5 times more ASC plasmid was used. Mean ± SEM of three independent experiments are shown (A and B).

5.2 M84 inhibits proinflammatory cytokine release and pyroptosis

To confirm that M84 is an inhibitor of AIM2 inflammasome signaling, the inhibitory effect of M84 was further investigated during viral infection. J774A.1 macrophages were infected with WT MCMV or the M84*stop* mutant virus lacking the expression of M84. This mutant was generated by introducing a point mutation in codon 61 of the M84 ORF resulting in a stop codon. Caspase-1 is an essential mediator of inflammasome signaling, thus its activation serves as a marker of inflammasome activation. The release of mature Caspase-1 was detected by precipitating proteins in the supernatant and analyzed by immunoblot. Upon high multiplicity of infection (MOI) with WT MCMV, the fully processed Caspase-1 p20 fragment was detected at the indicated time points (Figure 12A). Infection with different clones of M84*stop* MCMV resulted in increased p20 levels compared to WT MCMV-infected macrophages (Figure 12A). These results suggest that M84 inhibits Caspase-1 activation during MCMV infection in J774A.1 macrophages.

M84 is able to inhibit Caspase-1 activation already at early time points post infection (Figure 12A), suggesting that M84 is expressed as an early protein. To verify this, a cycloheximide (CHX) release assay was performed. In this assay, 10.1 fibroblasts were infected with MCMV M84HA in the presence of CHX, an inhibitor of translation elongation to allow immediate-early gene transcription but not translation. At 4 hours post infection, cells were washed and incubated with either fresh medium or medium containing actinomycin D (Act D), a transcription inhibitor to selectively allow the translation of viral immediate-early transcripts. As shown in Figure 12B, the cells treated only with CHX expressed immediate-early protein 1 (IE1), early protein 1 (E1) and M84, whereas the cells treated with CHX and Act D expressed only IE1 but not E1 or M84. Furthermore, the expression kinetic of M84HA MCMV in 10.1 fibroblasts showed that M84 was able to be detected at 3 hpi. (Figure 12C). Taken together, these results suggest that M84 is an early protein.
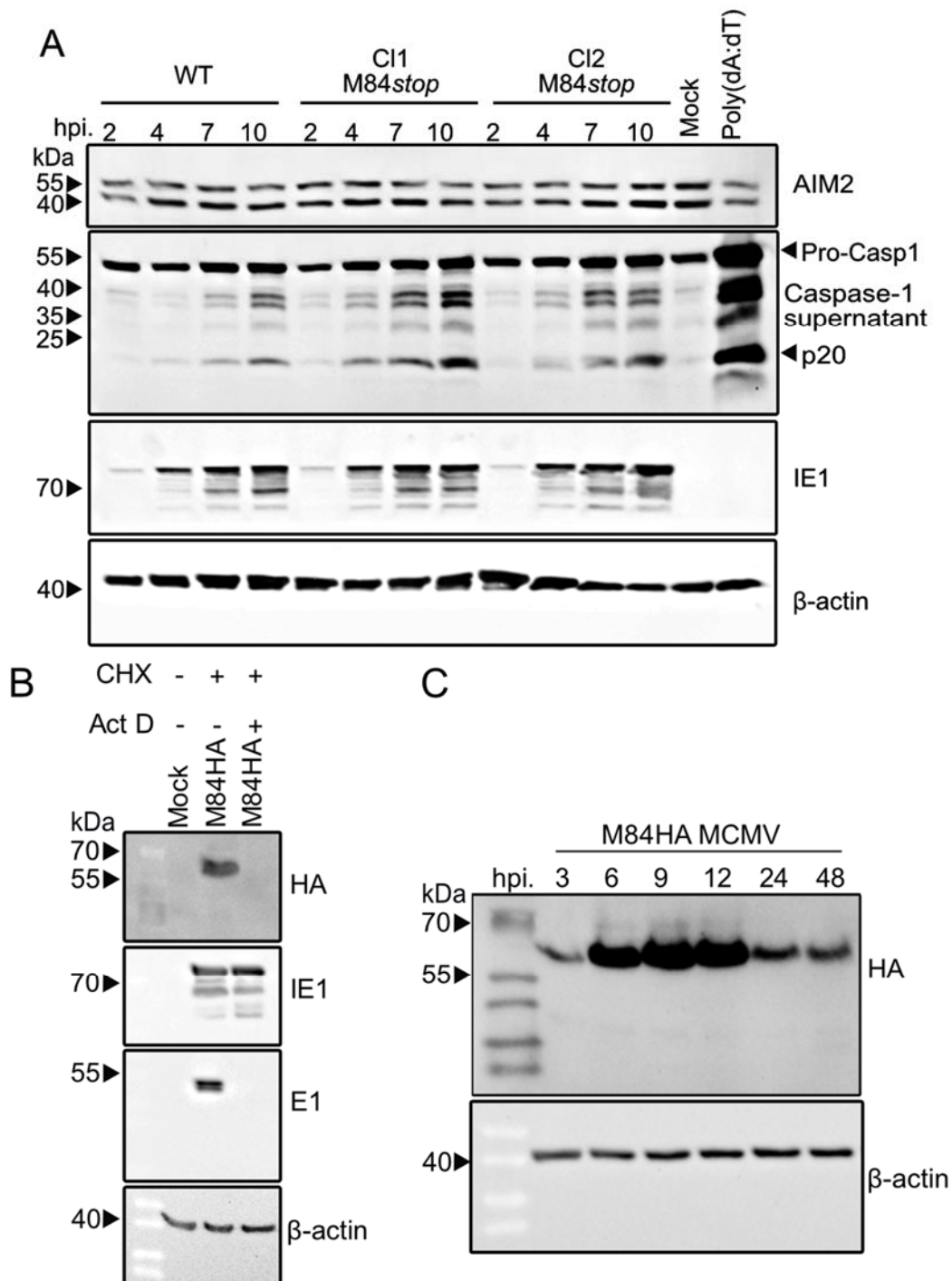
Figure 12. M84 inhibits Caspase-1 activation upon infection.
(A) J774A.1 macrophages were infected with WT MCMV or M84*stop*. At the indicated time points, proteins in the supernatant were precipitated and Caspase-1 was analyzed by immunoblot. Mock-infected cells served as negative control and cells treated with LPS plus poly (dA:dT) as positive control. (B) 10.1 fibroblasts were infected with MCMV M84HA at MOI of 3 and treated for 4 hours with 50 µg/ml cycloheximide (CHX). Afterwards, cells were washed and treated with 5 µg/ml Actinomycin D (Act D) or left untreated (–) for 6 hours and analyzed by immunoblot. (C) 10.1 fibroblasts were infected with MCMV M84HA at MOI of 5. Cell lysates were collected at indicated time points and M84HA expression was analyzed by immunoblot.

33

Upon activation, Caspase-1 proteolytically cleaves the cytokines IL-1β and IL-18 from their inactive precursors. To detect the secretion of cytokines from MCMV-infected macrophages, cell-free supernatant was collected at 4 and 7 hours post infection. The levels of IL-18 released into the supernatant were measured by ELISA. As shown in Figure 13A, infection with the M84*stop* MCMV resulted in significantly higher IL-18 secretion levels compared to infection with WT MCMV. Due to the poor sensitivity of the commercial ELISA assays, it is difficult to detect IL-1β released into the supernatant from infected macrophages. Therefore, the iGLuc ORF was PCR-amplified and cloned into pMSCV-puro, a retroviral vector. Immortalized bone marrow derived macrophages (iBMDMs) stably expressing iGLuc were generated by retroviral transduction and single-cell clones were obtained by limiting dilution. The luciferase activity in the supernatant of infected macrophages was measured at 7 hours post infection. Again, infection with M84*stop* MCMV significantly increased IL-1β-*Gaussia* luciferase activity compared to WT MCMV infection in different single-cell clones (Figure 13B). These results indicate that M84 inhibits the release of pro-inflammatory cytokines IL-18 and IL-1β in MCMV infected macrophages.
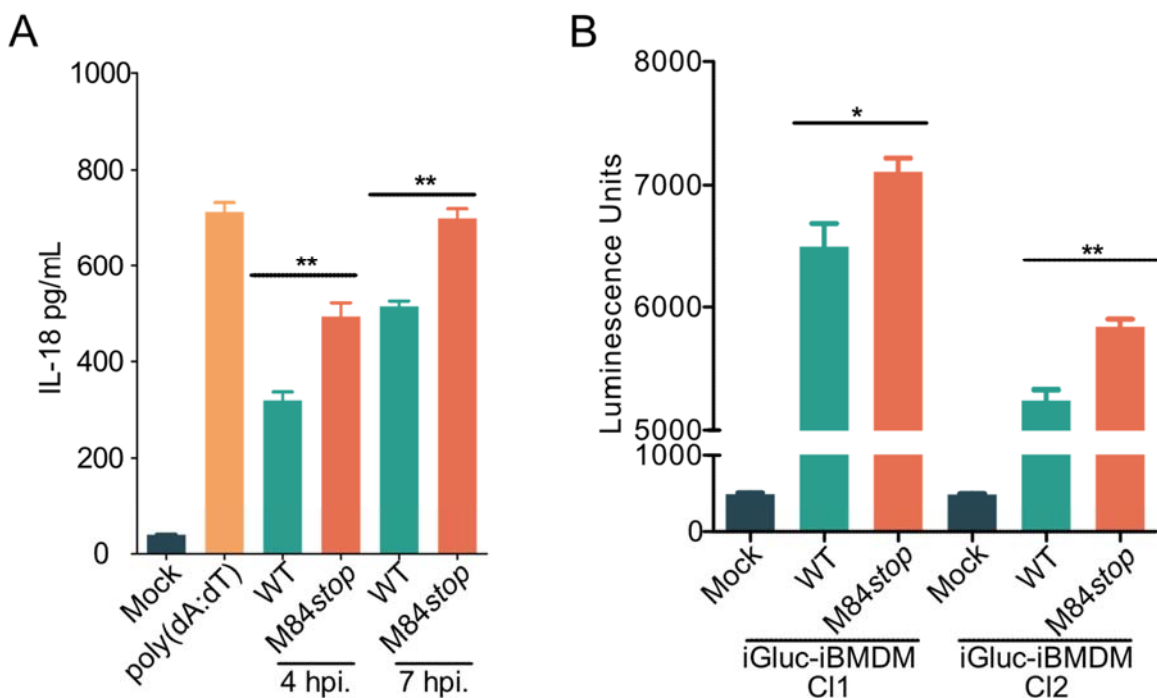
Figure 13. M84 inhibits IL-18 and IL-1β release.
(A) J774A.1 macrophages were infected with WT MCMV or M84*stop*. The release of IL-18 into the supernatant was analyzed by ELISA at 4 and 7 hpi. Mean ± SEM of three biological replicates are shown. (B) iBMDMs expressing an IL-1β-*Gaussia* luciferase reporter were infected with WT MCMV or M84*stop*. Luciferase activity was

measured at 7 hpi and is shown as mean ± SEM of three biological replicates. Two transduced iBMDM single-cell clones (cl1 and cl2) were used. Statistical analysis was performed by the two-tailed Student's *t*-test. n.s., not statistically significant; *p < 0.05, ** p < 0.01.

Caspase-1 specifically cleaves the linker between the N-terminal and C-terminal domains in Gasdermin D (GSDMD) and the N-terminal fragment of cleaved GSDMD (GSDMD-N) forms GSDMD pores within the plasma membrane to trigger pyroptotic cell death. Thus, the cleavage of GSDMD is a hallmark of pyroptosis [153]. To test whether M84 is responsible for the inhibition of pyroptosis during MCMV infection, J774A.1 macrophages were infected with either WT or M84*stop* MCMV. The levels of the GSDMD-N were analyzed at 10 and 24 h post infection by immunoblot. As shown in Figure 14A, the M84*stop* mutant induced higher levels of cleaved GSDMD than WT MCMV.

To test whether the increased GSDMD cleavage also results in a higher level of pyroptosis, the loss of membrane integrity associated cell death was quantified. J774A.1 macrophages were infected with either WT or M84*stop* MCMV and stained with the cell-impermeable dye propidium iodide (PI) and cell-permeable dye Hoechst 33342. PI staining showed the identification of cells that have lost membrane integrity. Consistent with the results of the GSDMD assay, infection with the M84*stop* MCMV resulted in more PI-positive cells than the WT MCMV, in J774A.1 macrophages (Figure 14B).

Taken together, these results demonstrate that MCMV activates the AIM2 inflammasome in macrophages, resulting in Caspase-1 activation, the release of mature IL-1β and IL-18, GSDMD cleavage, and pyroptosis. In the absence of M84, activation of this signaling cascade is substantially increased, suggesting that M84 inhibits the activation of AIM2 inflammasome and dampens cytokine release as well as pyroptosis.
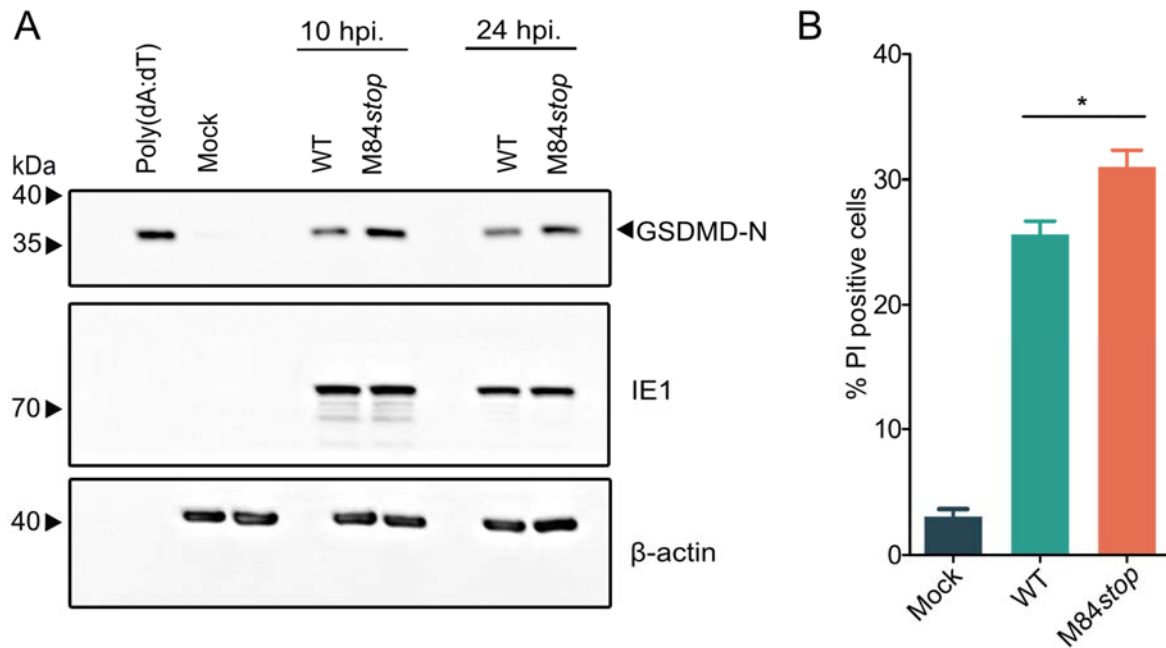
Figure 14. M84 inhibits GSDMD cleavage and pyroptosis.
(A) J774A.1 macrophages were infected with WT MCMV or M84*stop* MCMV. GSDMD cleavage was detected by immunoblot at 10 and 24 hpi. (B) J774A.1 macrophages were infected with WT MCMV or M84*stop* MCMV and stained at 7 hpi with propidium iodide (PI) and Hoechst 33342. The percentage of PI positive cells is shown with mean ± SEM of three biological replicates. Statistical analysis was performed by the two-tailed Student's *t*-test. n.s., not statistically significant; *p < 0.05, ** p < 0.01.

5.3 M84 is required for efficient MCMV replication in macrophages

Considering the clear inhibitory effects of M84 on AIM2 inflammasome signaling, it is important to investigate the impact of M84 on MCMV replication. For this purpose, a MCMV M84*stop* mutant based on MCMV M84HA was constructed by introducing a point mutation in codon 61 of the M84 ORF resulting in a stop codon (Figure 15A). The integrity of the viral genomes of MCMV M84HA and M84*stop* was verified by Illumina sequencing to rule out unintended mutations elsewhere in the viral genome. As shown in Figure 15B, M84*stop* mutant is not able to express M84.

Then the replication properties of the two viruses were investigated by multistep replication kinetics in 10.1 fibroblasts, J774A.1 macrophages, and iBMDMs. In 10.1 fibroblasts, which lack the expression of the AIM2 inflammasome components, the M84*stop* MCMV replicated with the same kinetics as the parental virus, M84HA MCMV (Figure 15C). By contrast, in J774A.1 macrophages and iBMDMs, the M84*stop* MCMV

36

displayed a clear growth defect (Figures 15D and E). These results suggest that M84 is required for efficient MCMV replication in AIM2-inflammasome expressing macrophages but not in fibroblasts. Furthermore, M84HA MCMV replicated to similar titers as WT MCMV in J774A.1 macrophages, suggesting that the C-terminal HA tag of M84 does not negatively affect MCMV replication (Figure 15F).
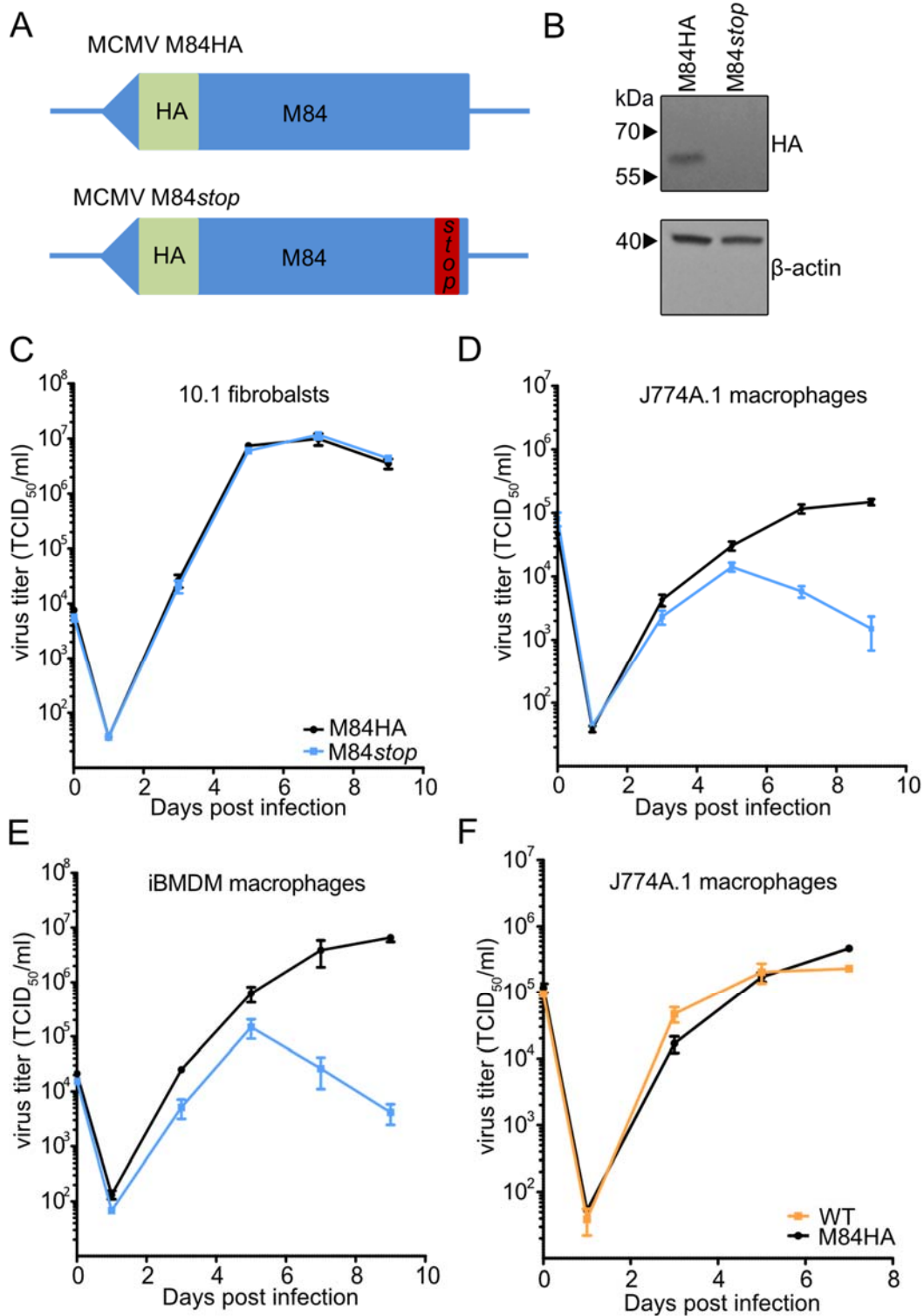

Figure 15. M84 is required for efficient MCMV replication in macrophages.
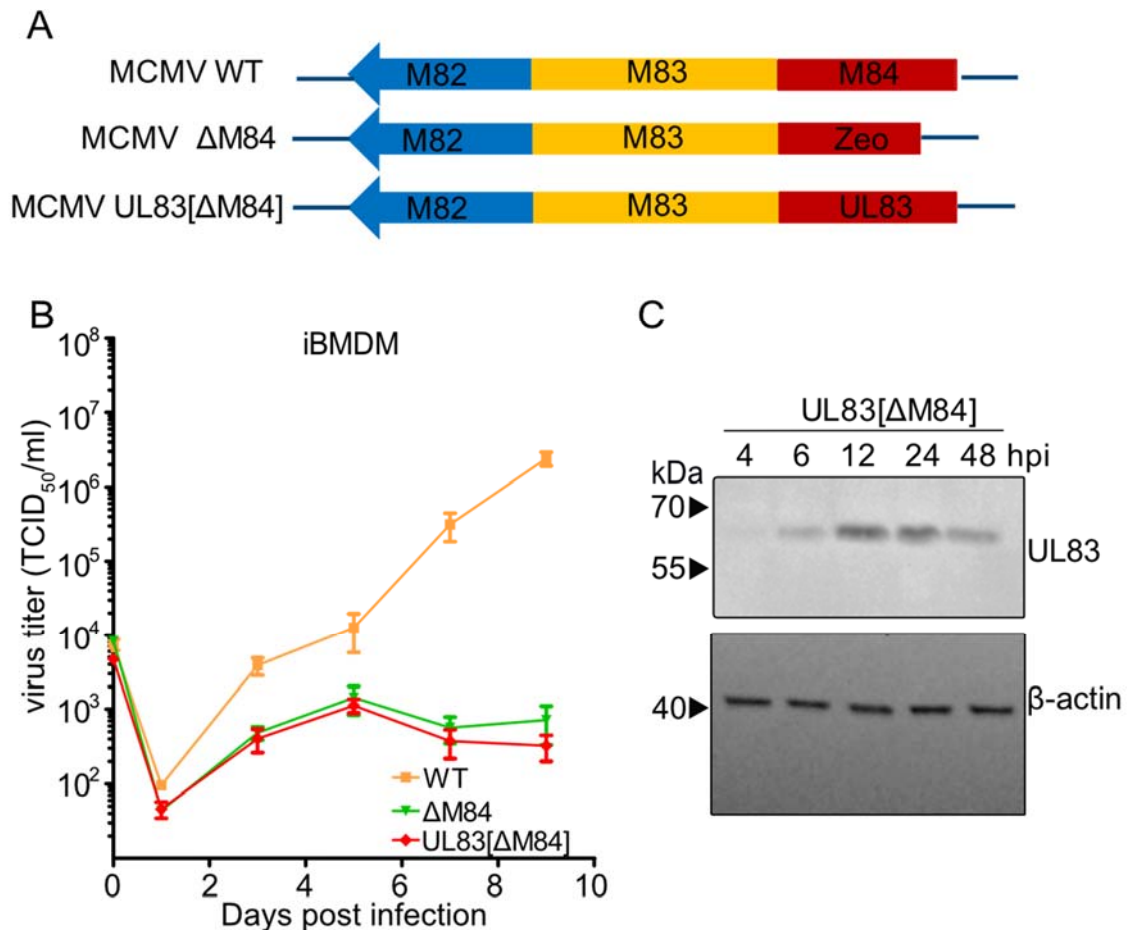
(A) Schematic representation of MCMV M84HA and M84*stop* mutant. (B) 10.1 fibroblasts were infected with MCMV M84HA or M84*stop* at MOI of 3. Cell lysates were collected at 6 hpi and M84HA expression was analyzed by immunoblot. (C) Multistep replication kinetics of MCMV M84HA and M84*stop* in murine 10.1 fibroblasts, (D) J774A.1 macrophages, (E) immortalized bone marrow-derived macrophages (iBMDMs), (F) Multistep replication kinetic of WT or M84HA MCMV in J774A.1 macrophages. Fibroblasts were infected at MOI of 0.01, J774A.1 were infected at MOI of 0.5 and iBMDMs were infected at MOI of 0.025. Viral titers are shown as mean ± SEM of three biological replicates.

MCMV M84 is a member of the M82-84 gene family, which is homologous to the UL82-84 gene family of HCMV [180]. This raises my curiosity of whether M84 has a functional ortholog in HCMV. UL83 and UL84 are speculated to be the strongest candidates as they share a similar level of amino acid identity to M84 [180]. UL83 was shown to interact with IFI16 and to inhibit activation of STING [34]. Another study has detected the interaction of UL83 with AIM2 [181], whereas the consequences of this proposed interaction have not been investigated in virus-infected cells. To elucidate this aspect, an M84 deletion MCMV mutant (ΔM84), in which the M84 ORF is replaced by a zeocin cassette, was generated. This mutant served as the basis for generating a chimeric virus, in which the M84 locus was replaced by the HCMV ORF encoding UL83 (MCMV UL83 [ΔM84]) (Figure 16A).

Next, multistep replication kinetics of these two recombinant mutant viruses were assessed in iBMDMs (Figure 16B). Similar to what was observed with the M84*stop* mutant (Figure 15C), the ΔM84 mutant showed a clear growth defect. The introduction of UL83 did not rescue the phenotype of the absence of M84, indicating that UL83 in MCMV might not functionally substitute for M84 in mouse macrophages. Figure 16C shows that UL83 is already expressed at early time points in MCMV UL83 [ΔM84] infected 10.1 fibroblasts. However, being a tegument protein, it has a late expression kinetic in HCMV infection. This differential expression might explain the functional differences between both proteins. The role of UL83 on AIM2 imflammasome signaling should be clarified in future studies in HCMV infected human cells.

Figure 16. Replication kinetics of UL83 recombinant virus in macrophages.

(A) Schematic representation of WT, ΔM84 and UL83 [ΔM84] MCMV mutants. (B) Multistep replication kinetics of WT, ΔM84 and UL83 [ΔM84] MCMV in iBMDMs infected at MOI of 0.025. Viral titers are shown as mean ± SEM of three biological replicates. (C) 10.1 fibroblasts were infected with MCMV UL83 [ΔM84] at MOI of 3. Cell lysates were collected at indicated time points and UL83 expression was analyzed by immunoblot.

Another candidate that I wanted to test is the non-canonical ORF L147C, which was identified as an interactor of Caspase-1 in a proteomic screen [178]. Although its inhibitory effect in the transfection based screening assay (Figure 2) is less pronounced, the biological impact of its interaction with Caspase-1 should be tested during infection. Thus, an ORF L147C*stop* mutant was generated by introducing a point mutation in codon 45 of the ORF L147C resulting in a stop codon (GAA to TAA). ORF L147C overlaps with M56, which is an essential gene for MCMV replication. To avoid modifying the amino acid sequence of M56, the point mutation in ORF L147C was designed to result in a synonymous mutation (CTG to CTT) in M56 (Figure 17A). This point mutation was also introduced into M84*stop* backbone to generate a M84 and ORF L147C double stop mutant virus (M84+ORF L147C*dstop*).

39

Results

Infection with ORF L147C*stop* MCMV induced similar p20 and GSDMD-N levels compared to WT MCMV-infected macrophages (Figure 17B). These results suggest that ORF L147C is not able to inhibit Caspase-1 activation during MCMV infection in J774A.1 macrophages. Next, the multistep replication kinetics of WT, ORF L147C*stop*, M84*stop* and M84+ORF L147C*dstop* viruses were assessed in J774A.1 macrophages (Figure 17C). The ORF L147C*stop* mutant replicated to similar titers as WT MCMV. Moreover, M84+ORF L147C*dstop* replicated to similar levels as M84*stop* MCMV. These results indicate that the absence of ORF L147C has no impact on viral replication in J774A.1 macrophages. The expression kinetics of ORF L147C were tested in HA-tagged ORF L147C MCMV infected 10.1 fibroblasts (Figure 17D). Unlike the early protein M84, ORF L147C was found to be expressed only at late time points post infection.

Taken together, these results suggest that MCMV ORF L147C is not able to inhibit AIM2 inflammasome activation in infected macrophages and is not required for efficient viral replication in macrophages.
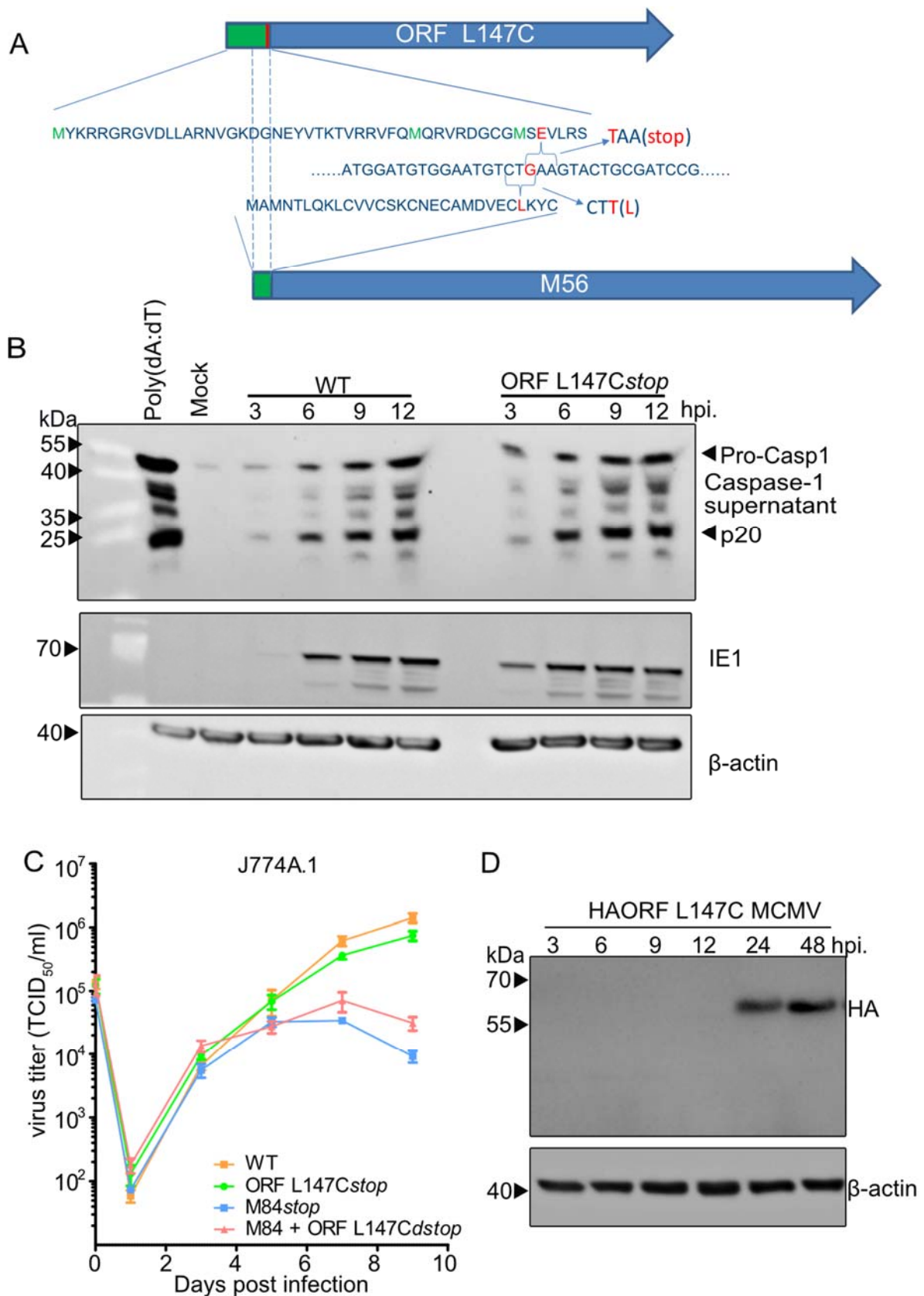
Figure 17. Impact of ORF L147C recombinant viruses on AIM2 inflammasome activation and viral replication in macrophages.
(A) Schematic diagram of ORF L147Cstop MCMV mutant construct. (B) J774A.1 macrophages were infected with WT MCMV or ORF L147Cstop MCMV. At the

indicated time points, proteins in the supernatant were precipitated for analyzing Caspase-1 activation by immunoblot. Mock-infected cells served as negative control and cells treated with LPS plus poly (dA:dT) as positive control. (C) Multistep replication kinetics of WT, ORF L147C*stop*, M84*stop* and M84+ORF L147C*dstop* MCMV in J774A.1 macrophages at MOI of 0.5. Viral titers are shown as mean ± SEM of three biological replicates. (D) 10.1 fibroblasts were infected with MCMV HAORF L147C at MOI of 5. Cell lysates were collected at indicated time points and HAORF L147C expression was analyzed by immunoblot.

5.4 M84 inhibits AIM2 inflammasome-mediated restriction of MCMV replication in macrophages

To find out whether the inhibitory effect of M84 in macrophages was AIM2-inflammasome dependent, gene knockouts of *Aim2* or *Asc* in iBMDMs were generated by CRISPR/Cas9 gene editing. Two independent single-cell clones generated with different guide RNAs were tested for each gene knockout (Figure 18). iBMDMs transduced with an empty vector (EV, without gRNA) were used as control cells. Macrophages were either mock treated or stimulated with LPS for 3 hours prior to transfection with poly (dA:dT) for activation of the AIM2 inflammasome. As shown in Figure 18, Caspase-1 activation and GSDMD cleavage were detectable in AIM2-inflammasome stimulated WT and EV iBMDMs but not in *Aim2* or *Asc* knockout iBMDMs.
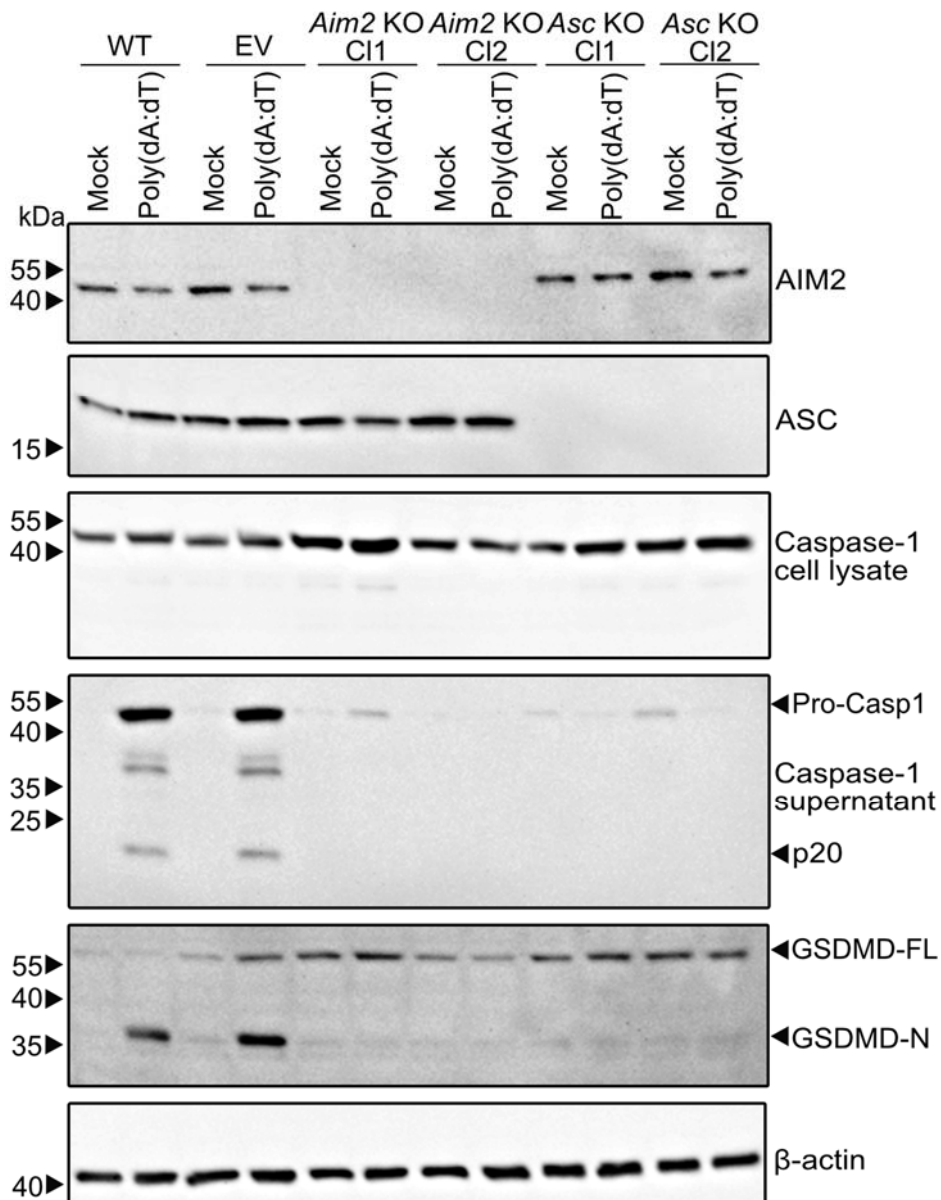
Figure 18. Generation of AIM2 inflammasome deficient cell lines.
Aim2 and *Asc* KO iBMDMs were generated by CRISPR/Cas9 gene editing. WT iBMDMs and iBMDMs transduced with an empty vector (EV, without gRNA) were used as control cells. AIM2 and ASC expression were verified by immunoblot analysis. Caspase-1 activation and GSDMD cleavage in LPS plus poly (dA:dT) stimulated WT, EV, *Aim2* KO and *Asc* KO iBMDMs were also detected by immunoblot analysis.

In addition to knocking out *Aim2* or *Asc*, iBMDMs treated with VX-765, a specific inhibitor of Caspase-1, is another way of shutting down AIM2-inflammasome dependent cell death. Pyroptotic cells of these AIM2-inflammasome deficient macrophages were quantified with the same method as described in Figure 14B. As shown in Figure 19, infection of WT iBMDMs with the MCMV M84*stop* mutant resulted in more PI-positive cells compared to the WT MCMV. However, in the VX-765 treated

WT iBMDMs and *Aim2* or *Asc* knockout iBMDMs, MCMV infection resulted in very low levels of PI-positive cells, both with WT MCMV and the M84*stop* mutant. Furthermore, there was no difference regarding pyroptosis between WT and M84*stop* MCMV infected AIM2-inflammasome deficient iBMDMs (Figure 19). These results suggest that M84 inhibits AIM2-inflammasome dependent pyroptosis.
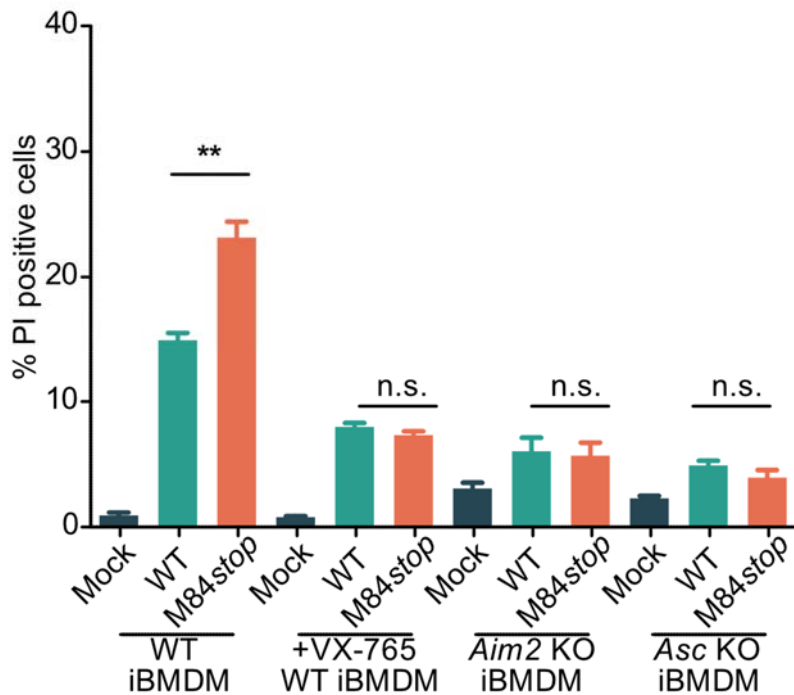
Figure 19. M84 inhibits AIM2 inflammasome dependent pyroptosis.
WT, *Aim2* KO and *Asc* KO iBMDMs, and iBMDMs treated with VX-765 were infected with WT or M84*stop* MCMV and stained at 7 hpi with propidium iodide (PI) and Hoechst 33342. The percentage of PI positive cells is shown with mean ± SEM of three biological replicates. Statistical analysis was performed by the two-tailed Student's *t*-test. n.s., not statistically significant; *p < 0.05, ** p < 0.01.

In addition, multistep replication kinetics were performed in AIM2-inflammasome deficient iBMDMs. Remarkably, the replication defect of M84*stop* MCMV in WT iBMDMs and EV iBMDMs (Figures 15C and 20A) was rescued to WT levels in *Aim2* KO (Figures 20C and D) as well as in *Asc* KO iBMDMs (Figures 20E and F). When macrophages were treated with the Caspase-1-specific inhibitor VX-765, the growth defect of M84*stop* MCMV was also rescued (Figure 20B). These findings indicate that the AIM2 inflammasome restricts MCMV replication in macrophages and that M84 counteracts this restriction.
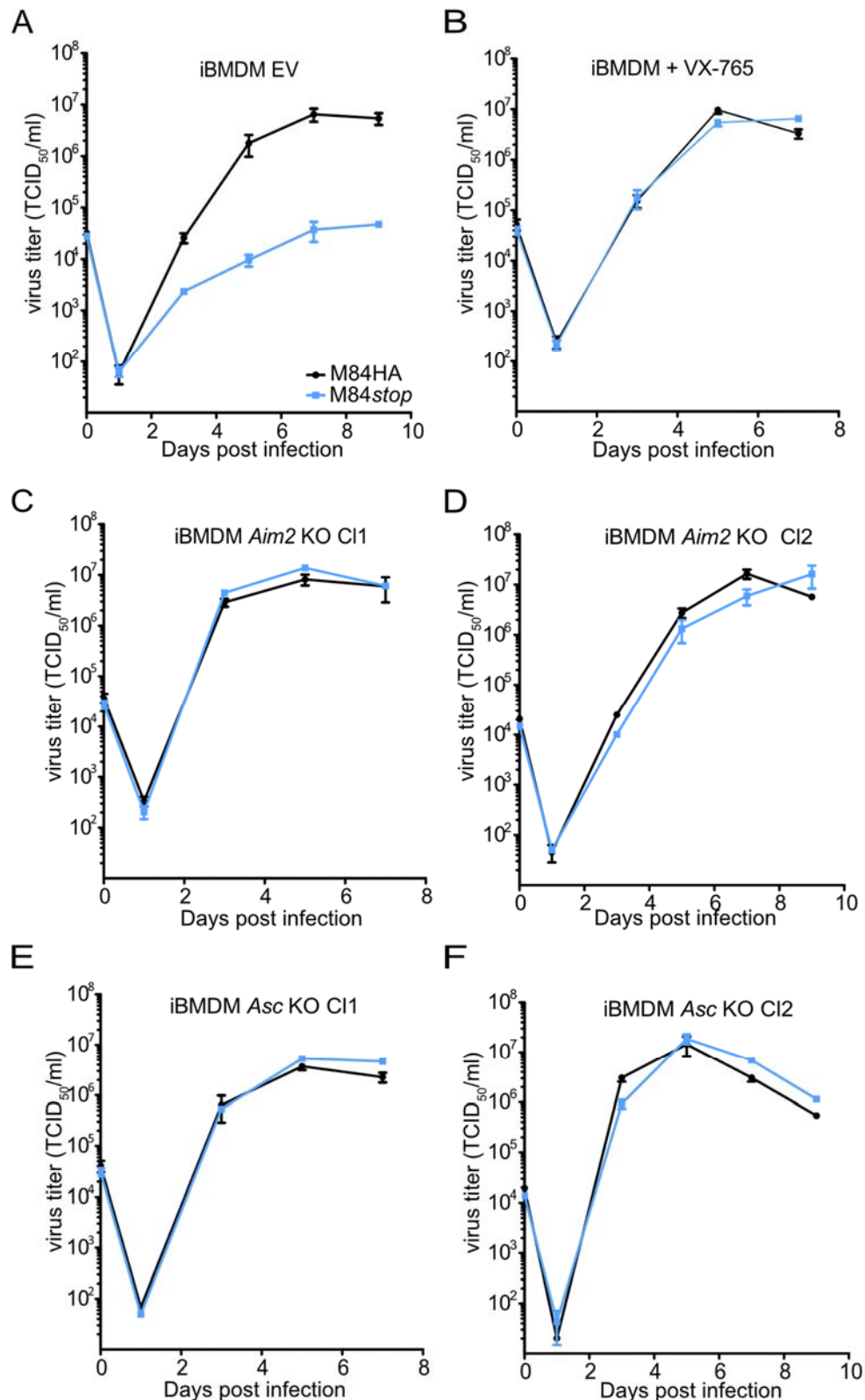
Figure 20. M84 counteracts AIM2 inflammasome restriction of MCMV replication in macrophages.
Multistep replication kinetics of MCMV M84HA and M84*stop* in (A) Empty vector transduced iBMDMs, (B) iBMDMs treated with Caspase-1 inhibitor VX-765, (C, D) *Aim2* KO iBMDMs, and (E, F) *Asc* KO iBMDMs were infected at MOI of 0.025. Viral titers are shown as mean ± SEM of three biological replicates.

5.5 MCMV M84 interacts with AIM2 and ASC

Based on the results showing that M84 inhibits Caspase-1 activation and its downstream signaling, it is important to know more precisely at which level of the Aim2 inflammasome M84 could play a role. The DNA sensor AIM2 recruits the adaptor protein ASC by homotypic interaction of the pyrin domains to form the inflammasome complex [182]. It could be speculated that M84 might interact with the components upstream of Caspase-1, AIM2 and/or ASC. In order to investigate such an interaction, HEK-293A cells were co-transfected with plasmids encoding Flag-tagged AIM2 or ASC and HA-tagged MCMV proteins M84, M83, or M82. M82 and M83 were used as control proteins as they are phylogenetically related to M84 and belong to the same gene family [180]. Flag-tagged AIM2 or ASC were immunoprecipitated from lysates of the transfected cells, and the HA-tagged M82, M83, and M84 proteins were analyzed by immunoblot. As shown in Figures 21A and B, M84, but not M83 or M82, co-precipitated with AIM2 and ASC. These results indicate that M84 specifically interacts with AIM2 and ASC.
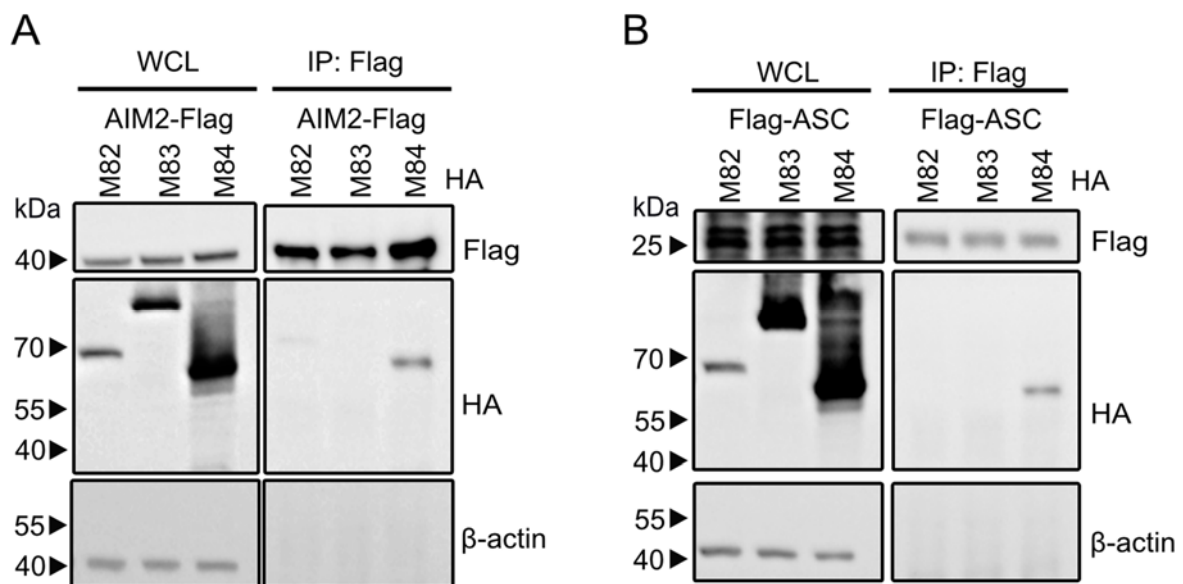
Figure 21. Interaction of M84 with AIM2 and ASC in transfected HEK293A cells. HEK-293A cells were transfected with plasmids encoding AIM2-Flag (A) or Flag-ASC (B) and HA-tagged MCMV proteins M82, M83 or M84. Cell lysates were collected 24 h post transfection for IP. Co-precipitating proteins were detected by immunoblot analysis.

It is important to confirm whether the interaction of M84 with AIM2 and ASC also occurred during MCMV infection in macrophages. As an M84-specific antibody was not available, a recombinant MCMV expressing a C-terminally HA-tagged M84 was used. The iBMDMs were mock treated or infected with MCMV M84HA or MCMV M28HA, a MCMV virus with HA tagged M28, which was used as a negative control. At 10 hpi, iBMDMs were lysed in NP-40 lysis buffer. HA tagged viral proteins were immunoprecipitated by using an anti-HA affinity matrix. The endogenous AIM2 and ASC proteins were detected by immunoblot analysis with the specific antibodies. As shown in Figure 22, AIM2 and ASC co-precipitated with M84 but not with M28.
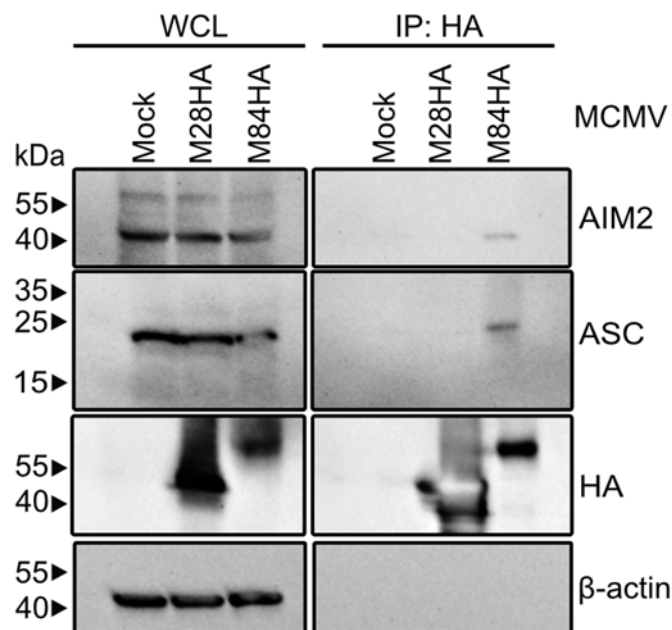
Figure 22. Interaction of M84 with AIM2 and ASC in macrophages.
iBMDMs were infected with MCMV M84HA or M28HA at MOI of 5. At 10 hpi, cell lysates were collected for IP using an anti-HA affinity matrix. Co-precipitating proteins were detected by immunoblot analysis with AIM2 and ASC-specific antibodies.

To support this finding, immunofluorescence assays were performed in MCMV-infected macrophages. Primary BMDMs isolated from transgenic mice expressing mCherry-tagged ASC [183] were infected with MCMV M84HA. M84 was detected in the both the cytoplasm and the nucleus. In the cytoplasm, M84 co-localized with ASC specks (Figure 23A). In 10.1 fibroblasts that lack the expression of the AIM2 inflammasome components, M84 was detected only in the nucleus and co-localizing with E1 that is a marker of viral replication compartments (Figure 23B). Taken together, these results suggest that M84 interacts with the inflammasome components AIM2 and ASC.
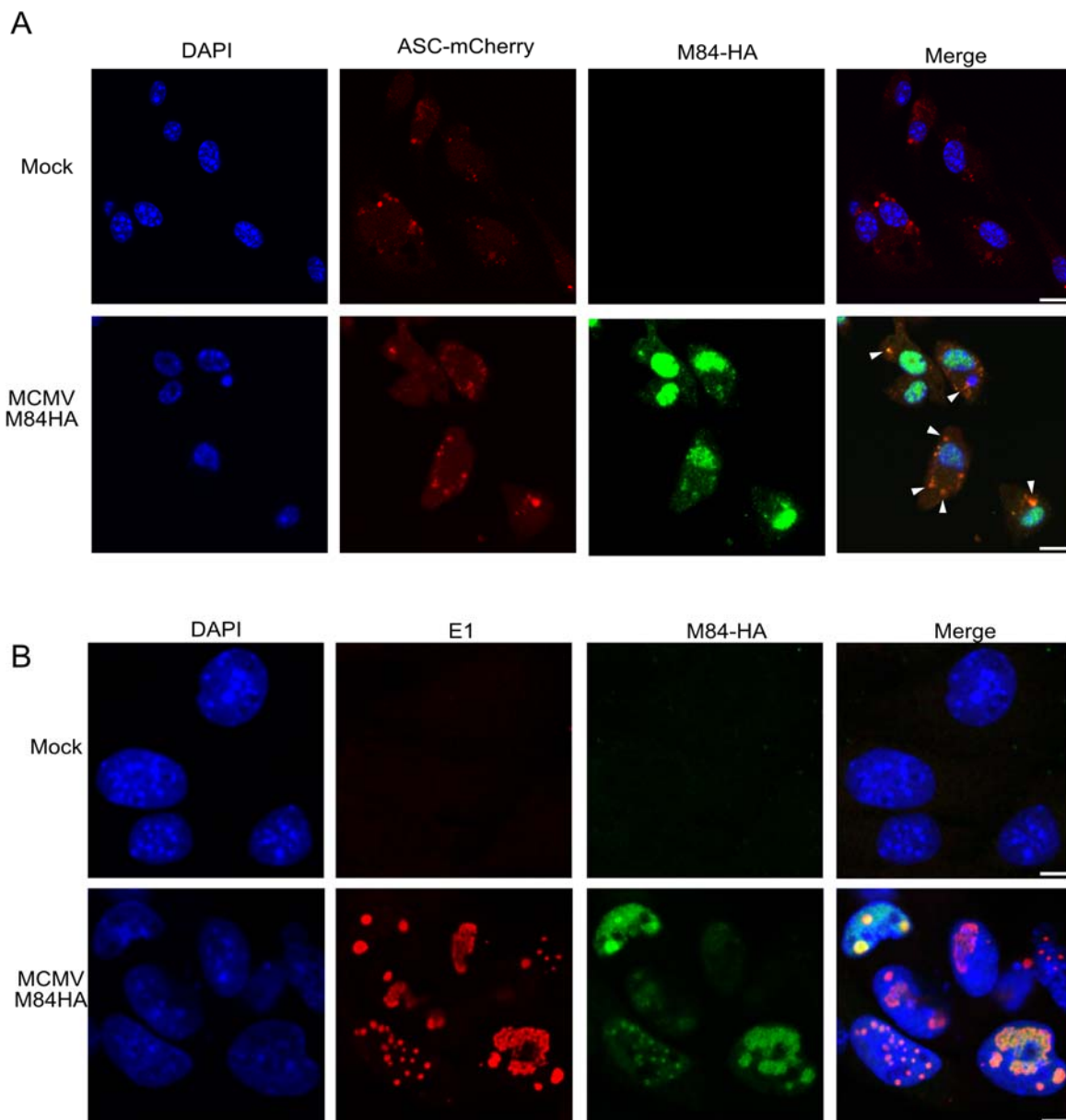
Figure 23. M84 co-localizes with ASC in primary BMDMs.
(A) Primary BMDMs from ASC-mCherry mice were infected with MCMV-M84HA at MOI of 3. Mock-infected BMDMs were used as a control. (B) 10.1 fibroblasts were mock or infected with M84HA at MOI of 3. M84HA was detected with an anti-HA antibody and a secondary antibody coupled to AlexaFluor488. E1 was detected with an anti-E1 antibody and a secondary antibody coupled to AlexaFluor555. Nuclei were stained with Hoechst33342. Representative images taken by confocal microscopy are shown (scale bar, 10 µm). The results are representative of three independent experiments.

As both AIM2 and ASC were involved in impairing the replication of the M84*stop* mutant, the next step was to investigate whether the interaction of M84 with these two proteins is interdependent. Therefore, co-immunoprecipitation experiments were performed in AIM2 and ASC-deficient iBMDMs. While ASC co-precipitated with M84 in AIM2-

deficient iBMDMs (Figure 24A), AIM2 co-precipitation with M84 was not detectable in ASC-deficient iBMDMs (Figure 24B), suggesting that the interaction of M84 with AIM2 in macrophages is ASC-dependent.
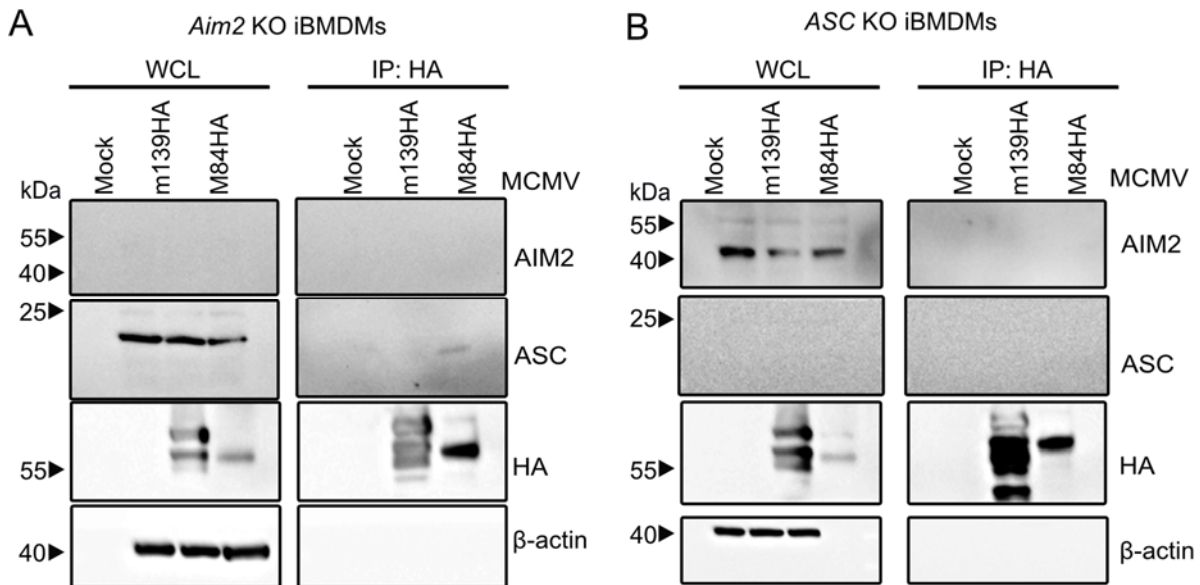
Figure 24. The interaction of M84 with AIM2 and ASC is interdependent.
(A) *Aim2* KO and (B) *Asc* KO iBMDMs were infected with MCMV M84HA or m139HA (MOI 5). At 10 h post-infection, cell lysates were collected for co-IP using an anti-HA affinity matrix. Co-precipitating proteins were analyzed by immunoblot with AIM2 and ASC-specific antibodies.

5.6 M84 is required for efficient MCMV dissemination *in vivo*

Next step was to investigate the biological impact of M84-mediated AIM2 inflammasome inhibition on MCMV dissemination *in vivo*. With the help of Dr. Eléonore Ostermann and Michaela Bockelmann, WT and *Asc$^{-/-}$* mice [83] were infected with WT MCMV and M84*stop* MCMV. The viral titers in the spleens and livers were determined at 3 days post infection with plaque assay. The viral titers in the spleens of WT mice infected with M84*stop* MCMV were significantly (12-fold) lower than those of mice infected with WT MCMV (Figures 25A and B). However, in the spleens of *Asc$^{-/-}$* mice, the viral titers of MCMV M84*stop* were partially rescued to only 4-fold lower than those of WT MCMV. Similarly, the viral titers in the livers of M84*stop* were 17-fold lower than those of WT MCMV in WT mice but only 6-fold lower in *Asc$^{-/-}$* mice (Figures 25C and D). These results indicate that MCMV dissemination to the spleen and liver is impaired in the absence of M84. This defect is partially, but not completely, rescued in *Asc$^{-/-}$*

mice, suggesting that M84 may have additional functions besides inhibition of the AIM2 inflammasome signaling.
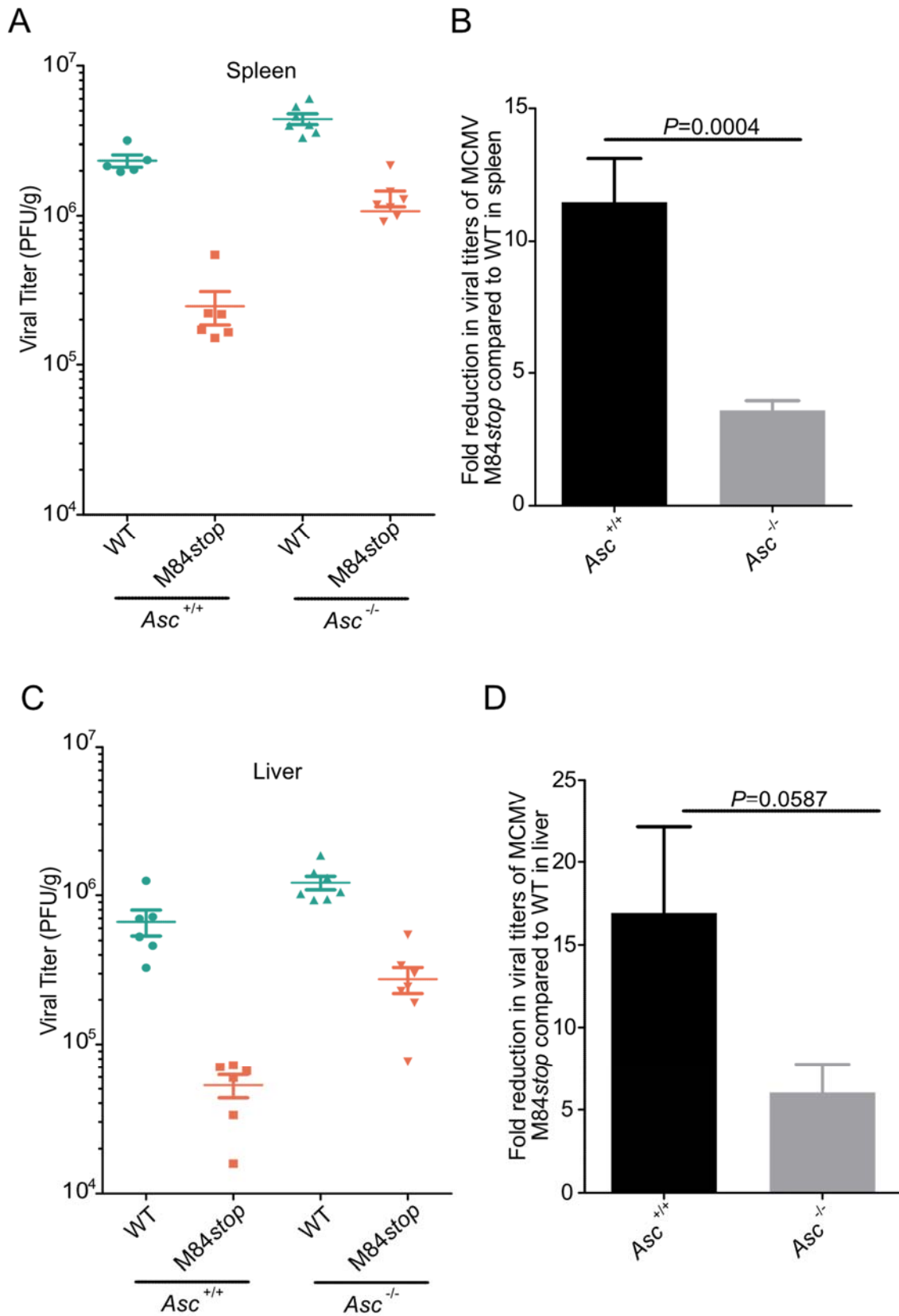
Figure 25. M84 is required for efficient viral replication *in vivo*.

6-week-old female WT and *Asc*^{-/-} mice were infected intraperitoneally with WT MCMV or M84*stop* MCMV. The viral titers in spleen (A) and liver (C) determined at 3 days post-infection by plaque assay are shown as mean titers ± SEM. The fold reduction in viral titers of MCMV M84*stop* compared to WT MCMV in spleen (B) and liver (D) of WT or *Asc*^{-/-} mice are shown as mean ± SEM. Statistical analysis was done by using the two-tailed Student's *t*-test.

IL-18 is an important cytokine in the early stage of host defense against MCMV infection [184]. To further investigate the role of M84 in regulating IL-18 levels *in vivo*, I measured the concentration of IL-18 in the serum of MCMV infected mice at 1.5 and 3 days post-infection. M84*stop* MCMV induced higher IL-18 levels than WT MCMV at 1.5 days post infection (Figure 26) in the serum of WT mice. However, at 3 days post infection, IL-18 levels were higher in the serum of WT MCMV-infected mice (Figure 26), which may be explained by the significantly higher viral loads on day 3 (Figures 25A and C). In *Asc*^{-/-} mice, IL-18 levels in the serum were not detectable, consistent with previously published data [173]. Similar to macrophages *in vitro*, IL-1β levels in the serum of infected mice *in vivo* were not detectable with commercial ELISA kit.

Taken together, these results suggest that M84 is required for efficient MCMV dissemination *in vivo* and inhibits the release of the pro-inflammatory cytokine IL-18 in the early stage of MCMV infection *in vivo*.
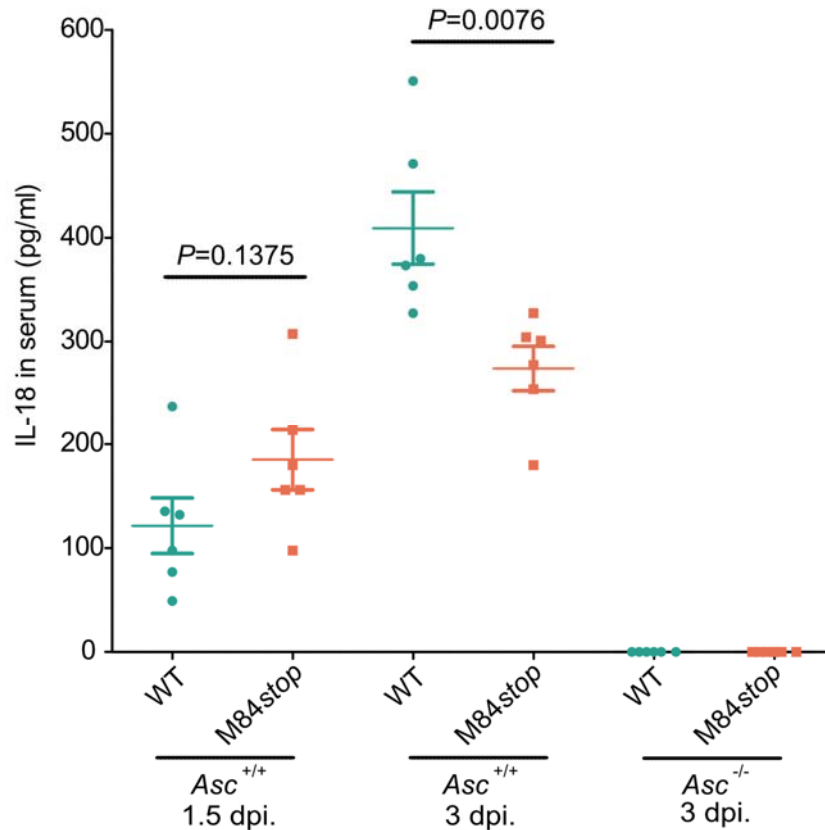
Figure 26. M84 inhibits the release of IL-18 at the early stage of infection *in vivo*.
6-week-old female WT and *Asc*^{-/-} mice were infected intraperitoneally with WT MCMV or M84*stop* MCMV. IL-18 levels in the serum were measured at 1.5 and 3 days post-infection by ELISA. Mean ± SEM are shown. Statistical analysis was done by using the two-tailed Student's *t*-test.

5.7 M84 interacts with other PYHIN family proteins

The viral dissemination defect of M84*stop* was partially, but not completely, rescued in *Asc*-deficient mice (Figures 25A and C), suggesting that M84 might have additional functions besides interacting with the components of the AIM2 inflammasome. ASC contains a PYD and a CARD domain, and AIM2 contains a PYD and a HIN domain and is a member of the PYHIN (IFI200/HIN-200) family of proteins. PYHIN proteins are known to be involved in the host defense against viral infection [185]. Therefore, the interaction of M84 with other members of the PYHIN family was investigated with a special focus on the interferon-inducible proteins IFI202, IFI203 and IFI204. (Figure 27).
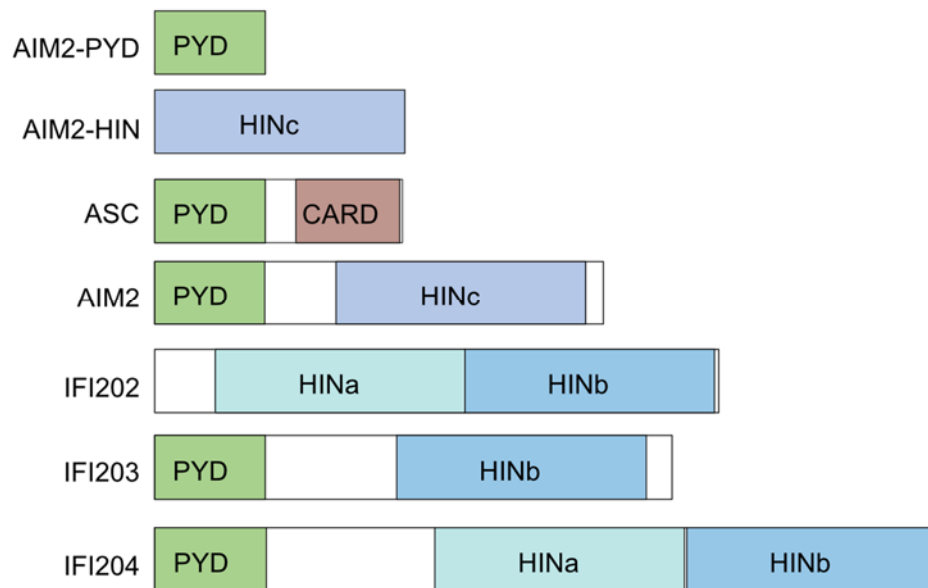
Figure 27. Schematic representation of ASC and PYHIN family proteins.
Schematic representation of the domain structures of ASC and PYHIN family proteins. ASC contains a pyrin domain (PYD) and a CARD domain. PYHIN family proteins contain an N-terminal PYD and one or two C-terminal HIN domains, classified as three subtypes. IFI202 contains two HIN domains but lacks PYD.

For this purpose, I transfected HEK-239A cells with plasmids encoding Flag-tagged IFI202, IFI203, or IFI204 and HA-tagged M83 or M84. Flag-tagged proteins were immunoprecipitated, and co-precipitating proteins were analyzed by immunoblot. In all three cases, M84 co-precipitated with the PYHIN family proteins, whereas M83 did not (Figures 28A and B).
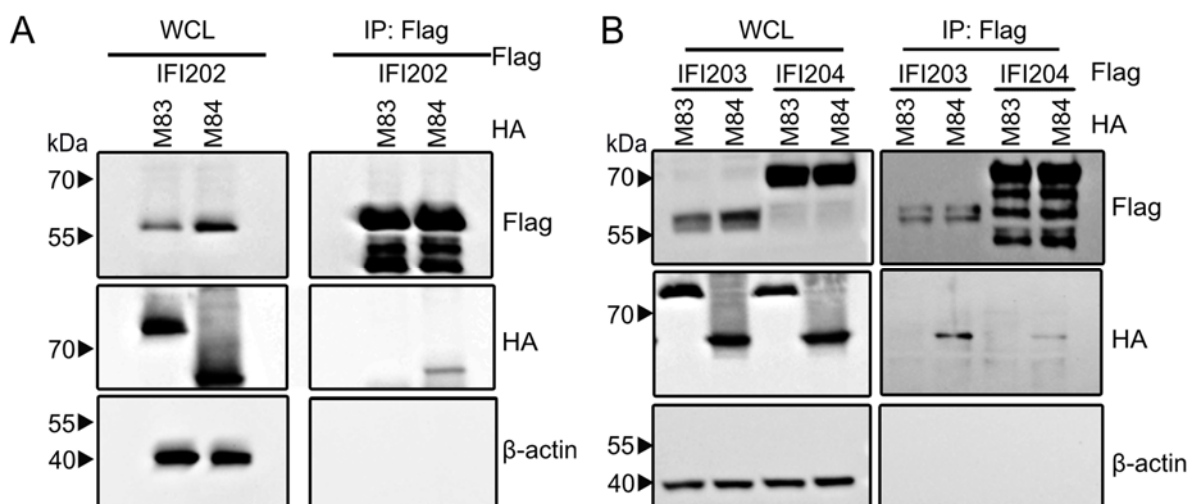
Figure 28. M84 interacts with other PYHIN proteins.
HEK-293A cells were transfected with plasmids encoding HA-tagged MCMV proteins M83 or M84 and IFI202-Flag (A), IFI203-Flag, or IFI204-Flag (B). Cell lysates were collected 24 h post transfection for immunoprecipitation. Co-precipitating proteins were detected by immunoblot.

As ASC contains a pyrin but no HIN domain, and IFI202 contains two HIN domains but no pyrin domain (Figure 27), it was intriguing to investigate the interaction of M84 with PYHIN proteins in more detail. The Flag-tagged pyrin and HIN domains of AIM2 were cloned respectively in the expression vector pcDNA and tested for their interaction with M84. Interestingly, M84 interacted with both, the pyrin and the HIN domain, whereas M83 interacted with none of the two domains (Figure 29). These results suggest that M84 can interact with PYHIN family proteins by association with either the PYD or the HIN domain. These additional interactions of M84 may explain why the attenuation of the MCMV M84*stop* mutant was partially but not completely rescued in *Asc*-deficient mice (Figures 25A and C).
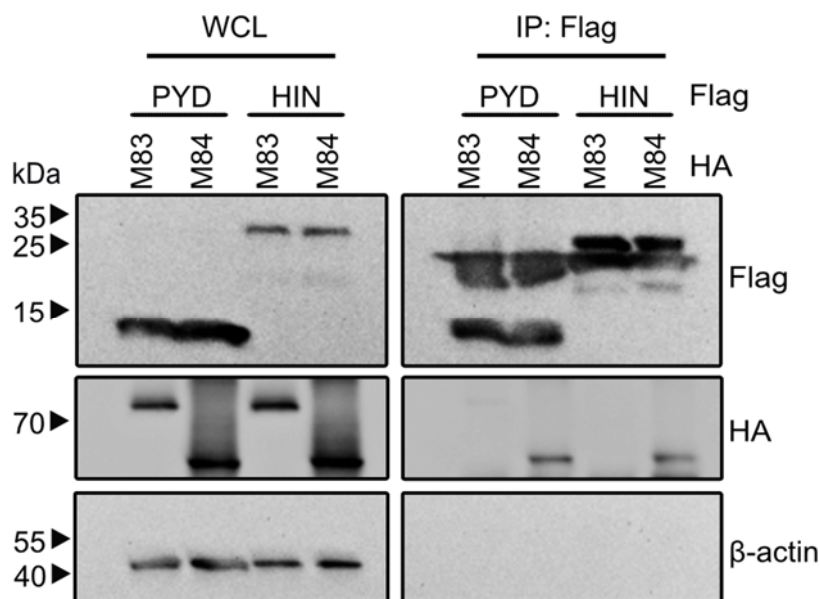
Figure 29. M84 interacts with PYD and HIN domains of AIM2.

HEK 293A cells were co-transfected with plasmids encoding the Flag-tagged AIM2 pyrin domain (PYD) or HIN domain and HA-tagged MCMV proteins M83 or M84. Cell lysate was collected 24 h post transfection for immunoprecipitation and immunoblot analysis.

6 Discussion

6.1 Identification of M84 as a viral inhibitor of the AIM2 inflammasome signaling

CMVs were demonstrated encoding several cell death inhibitors, which suppress apoptosis and necroptosis, but a CMV inhibitor of pyroptosis, the third major PCD modality, has not been identified yet (reviewed in [186]). Pyroptosis is triggered by inflammasome activation and MCMV is known to activate AIM2 [173, 187], but not NLRP3 or NLRC4 inflammasome (Sester et al., 2015). In my study, I identified the MCMV protein M84, which interacts with AIM2 and ASC and inhibits Caspase-1 activation, release of IL-1β and IL-18, GSDMD cleavage and pyroptosis.

The aim of my project was to identify an MCMV inhibitor of the AIM2 inflammasome-pyroptosis pathway. Some viruses interfere directly with the cleavage of GSDMD, which is a hallmark of pyroptosis [153]. Indeed, coronaviruses and picornaviruses express proteins interfering with GSDMD cleavage, thereby preventing pore formation by the GSDMD N-terminal fragment [171, 188, 189]. However, a viral inflammasome inhibitor would be a more powerful immune modulator as it would inhibit both pro-inflammatory cytokine release and pyroptosis. Indeed, some DNA viruses encode proteins with structural similarity to inflammasome components, which block inflammasome assembly or signaling. For instance, Kaposi's sarcoma-associated herpesvirus encodes an NLRP1 homolog [166], and some poxviruses encode viral pyrin-only proteins (vPOPs) [164, 190]. The genomes of other viruses do not harbor such homologs, but still encode potent antagonists. Examples are the HSV-1 VP22 protein that interacts with AIM2 [167] and the MCMV M84 protein, which interacts with ASC and PYHIN proteins, as shown in my study. These two viral inflammasome inhibitors were not identified on the basis of sequence similarity to inflammasome components but rather with functional screening assays. The evaluation of an Alphafold prediction of the M84 protein structure did not show a structural similarity to inflammasome components. Thus, structure predictions cannot substitute for systematic functional screens but may accelerate the discovery of viral protein functions in some cases.

In my study, IL-1β cleavage was used as the readout for the functional screening that identified MCMV M84 protein as an inhibitor of the AIM2-inflammasome signaling. ELISA kits for detecting the release of IL-1β are available and were used for the screening of the MCMV ORF library, however these commercial ELISA assays yielded quite variable results with many MCMV ORF expression plasmids producing a moderate degree of inhibition (Figure 10B). I also tried to check the activation of Caspase-1 by western blot (Figure 10A), which is not optimal for a high throughput method to screen a large number of viral proteins. In contrast, the luciferase reporter system, also based on the transfection assay, efficiently reduced the number of unspecific hits. A possible explanation for this difference is the single-step addition of the luciferase substrate, which may reduce the error rate, compared to a multi-step assay, such as ELISA. In addition, the sensitivity and accuracy of the commercial ELISA kit were a potential limitation in my experiments.

Several different proportions of plasmids transfection for the AIM2-inflammasome inhibitor screening was tested according to the literatures [167, 179, 191]. I could observe the best results of AIM2 inflammasome activation by transfecting HEK 293A cells with AIM2 (200 ng), ASC (20 ng), pro-Caspase-1 (100 ng), pro-IL-1β (200 ng) in 12-well plates. It was shown that the overexpression of ASC lead to an autoactivation of the inflammasome signaling [179]. By adding 5 times more ASC in the screening assay, I could reduce the number of candidates, with M84 showing the strongest inhibitory effect on IL-1β secretion (Figure 11B). Thus, this functional screening assay based on the luciferase reporter system provides an efficient method for identifying inflammasome inhibitors.

6.2 The role of M84 in regulation of pro-inflammatory cytokines

Pro-inflammatory cytokines are important components of the host immune responses against viral infection. MCMV infection activates the AIM2 inflammasome and triggers the release of pro-inflammatory cytokines IL-1β and IL-18, as shown in this study (Figure 13) and in a previous study [173]. In my study, M84*stop* MCMV showed higher levels of IL-1β and IL-18 secretion compared to WT MCMV during infection in macrophages indicating that M84 inhibits IL-1β and IL-18 secretion (Figure 13).

IL-1β is regulated by transcription factors such as nuclear factor-κB (NF-κB) and

activator protein-1 (AP-1). This transcriptional induction activates the production of pro-IL-1β, which is processed into mature IL-1β by Caspase-1 in the inflammasome complex upon inflammasome activation. It has been shown that the inflammatory responses were reduced and the viral loads increased in HSV-1 infected IL-1β-deficient mice compared to WT mice, indicating that IL-1β plays an important role in a host protective response to viral infection [192]. In contrast, the absence of the viral VP22 protein of HSV-1 induced higher levels of IL-1β secretion compared to the WT HSV-1 infected macrophages [167]. Similar to VP22, the absence of the viral M84 in MCMV resulted in increased IL-1β release (Figure 13B) leading to crippled viral replication in macrophages (Figure 15). Unfortunately, the IL-1β levels in infected mice were not detectable due to the difficulties encountered with the commercial ELISA kit. IL-1β release is controlled at multiple levels, including transcription, mRNA stability, cleavage by Caspase-1 and secretion [193]. MCMV has been shown to inhibit the activation of NF-κB [194]. This may inhibit the transcription of pro-IL-1β resulting in a lower level of IL-1β, which could be under the detection limit. A further study using IL-1β$^{-/-}$ mice infected with WT and M84*stop* MCMV would be a potential way to investigate the importance of IL-1β in MCMV infection and how M84 regulates AIM2 inflammasome-dependent IL-1β release *in vivo*.

In contrast to IL-1β, *de novo* transcriptional induction of pro-IL-18 is not needed, as it is constitutively expressed in multiple cell types [195]. Mature bioactive IL-18 can stimulate IFN-γ production from natural killer (NK) cells, which is crucial in the early defense against viral infection. The importance of IL-18 in antiviral responses may vary between different viruses due to different roles and sites of action (reviewed in [196]). For instance, influenza virus infection of IL-18$^{-/-}$ mice has been shown to result in increased mortality and viral loads [198]. In contrast, IL-18$^{-/-}$ mice do not show reduced survival upon MCMV infection. Furthermore, IL-18 contributes to systemic and splenic but not hepatic IFN-γ responses in MCMV infected mice [197].

In this study, I could show that M84 inhibits AIM2-inflammasome dependent IL-18 release during the early stage of infection (Figure 13A and Figure 26), which is critical for MCMV replication *in vitro* and dissemination *in vivo*. M84*stop* MCMV induced higher IL-18 levels in the serum at 1.5 dpi. (Figure 26), which may have an effect on IFN-γ to restrict viral replication. However, this was not the case at 3 dpi. (Figure 26), which might be due to significantly lower viral loads of M84*stop* MCMV (Figure 25) restricted

by AIM2 inflammasome and pyroptosis. In *Asc*-deficient mice, IL-18 serum levels were not detectable (Figure 26), consistent with previously published data [173] and highlighting the importance of AIM2 inflammasome in regulating the release of IL-18. All in all, this study provides a piece of evidence for the important role for M84 in regulating pro-inflammatory cytokines during MCMV replication and dissemination at the early stage of infection.

The viral M84 protein dampens AIM2 inflammasome activation, pro-inflammatory cytokines release, and pyroptotic cell death, but does not completely suppress these effects. The reasons for this remain unclear. M84 has not been classified as a tegument protein [176] and is therefore not imported into cells at the time of virus entry. Since MCMV first activates and later inhibits NF-kB, a transcription factor driving pro-inflammatory gene expression [199, 200], it is conceivable that a certain level of inflammasome activation is advantageous for the viral infection. Therefore, the mechanism by which MCMV manipulates inflammasome activation, cytokine release and pyroptosis needs to be further investigated.

6.3 Effect of AIM2 inflammasome inhibition by M84 on MCMV dissemination *in vivo*

Studies with knockout mice have demonstrated that inflammasome activation by MCMV is dependent on AIM2 and ASC, but not on NLRP3 or NLRC4, suggesting that the AIM2 inflammasome is activated by viral DNA in murine cells [100, 173]. However, a recent study demonstrated that AIM2 is dispensable for DNA-mediated inflammasome activation in human myeloid cells and that cytosolic DNA is sensed by the cGAS-STING signaling axis, which triggers the activation of the NLRP3 inflammasome [201]. These studies indicate that the functional importance of AIM2 as a DNA sensor may have diverged between mice and humans during mammalian evolution. To investigate the importance of a viral immune evasion protein for pathogenesis *in vivo*, it is crucial to note that the investigation can only be explored if the virus infects laboratory animals (preferably mice) and causes a similar pathology. However, most human herpesviruses, such as HCMV, EBV, and KSHV, are highly species-specific and do not replicate in mice [202]. Therefore, related animal viruses are widely used for pathogenesis studies *in vivo*. For instance, MCMV, a natural mouse pathogen, is perfectly suited for studies in the mouse model [4].

The AIM2 inflammasome is mainly expressed in cells of the myeloid lineage such as macrophages. In mice, the expression level of AIM2 varies between different organs and is the highest in the spleen [203]. In this study, I chose the commonly used experimental MCMV infection route, intraperitoneal (i.p.) inoculation [204], which results in MCMV colonizing circulating monocytes and the virions reaching the bloodstream directly [205]. In the tissues, the macrophages from the spleen and liver have the capability of capturing cell-free virions, leading to an early viral replication mainly carried out in these two organs upon acute MCMV infection *in vivo*. Indeed, the highly organized and dense network macrophages serve as the major target cells in the spleen [206] and the overall virulence of MCMV appears to be influenced by its replication ability in this organ [207]. In contrast, numerous tissue macrophages diffusely disperse throughout the sinusoids in the liver and the hepatocytes are the preferred target cells for MCMV infection [208]. In macrophages *in vitro*, the M84*stop* MCMV displayed a clear growth defect (Figures 15 D and E) which was rescued to WT levels in the absence of AIM2 inflammasome signaling (Figures 15F and 20). Furthermore, in the spleen and liver of WT mice, the viral titers of M84stop MCMV were significantly lower compared to WT MCMV. (Figure 25). Thus, the inhibitory effect of M84 on AIM2 inflammasome plays an important role in MCMV dissemination *in vivo*.

6.4 M84 interacts with PYHIN proteins

The M84*stop* MCMV has a clear growth defect in macrophages (Figure 15), which is completely rescued by treatment of a Caspase-1 inhibitor or by knocking out *Aim2* or *Asc* (Figure 20). However, the replication defect is not completely recued in *Asc* knockout mice (Figure 25), suggesting that M84 might have additional functions besides inflammasome inhibition *in vivo*. These might be mediated by the ALRs IFI202, IFI203, and IFI204, which also interacted with M84 in co-immunoprecipitation experiments (Figure 28). The functions of these proteins are not fully understood, but all of them can interact with other PYHIN proteins through homotypic interactions [209]. IFI202 is thought to function as a negative regulator of AIM2 inflammasome, due to direct interactions between HINb-IFI202 and HIN-AIM2 and the competition of HINa-IFI202 with HIN-AIM2 for DNA binding [210]. In addition, IFI202 can negatively regulate NF-κB, which may result in a lower level of cytokine secretion [211]. It has been reported that IFI202 regulates cell cycle by inhibiting p53 transcriptional activity through p53-binding protein 1 [212]. IFI204 is a functional ortholog of IFI16 in human cells,

Discussion

which recognizes viral DNA in the cytoplasm and nucleus to activate the inflammasome signaling and to induce the production of IFNβ and pro-inflammatory cytokines [213, 214]. IFI204 was also shown to initiate innate antiviral responses in adipose cells [215]. In this study, I showed that IFI202, IFI203 and IFI204 co-precipitate with M84 upon overexpression in HEK293A cells (Figure 28). These PYHIN proteins are expressed in a wide variety of cell types, whereas the AIM2 inflammasome is not. Thus, the M84-mediated modulation of these functions in different cell types would not be rescued in the *Asc* knockout mice.

It has been demonstrated that translocation of ASC from the nucleus to the cytoplasm is essential for inflammasome activation [216]. In this study, M84 was identified as an early protein and was detected in both the nucleus and the cytoplasm of MCMV infected macrophages (Figure 23A). Although M84 is mainly detected in the nucleus, it co-localized with ASC only in the cytoplasm (Figure 23A). Notably, M84 was only found in the nucleus in MCMV infected 10.1 fibroblasts that lack the expression of the AIM2 inflammasome components (Figure 23B). These different localizations of M84 in different cell types thus suggest multiple different functions of this protein.

In this study, I could show that M84 interacted with both AIM2 and ASC of the AIM2 inflammasome components (Figures 21 and 22). ASC co-precipitated with M84 in *Aim2* knockout iBMDMs (Figure 24A), whereas AIM2 co-precipitation with M84 was not detected in *Asc* knockout iBMDMs (Figure 24B), suggesting that the interaction of M84 with AIM2 in macrophages was ASC-dependent. Interestingly, M84 had the capacity of binding to both PYD and HIN domain of AIM2 in a co-IP experiment upon overexpression (Figure 29). In the absence of dsDNA, the PYD binds to the HIN domain keeping AIM2 in an auto-inhibited state [68], indicating the interaction happens between PYD and HIN domain. Furthermore, the HEK 293A cells, used for co-IP experiments in this study, express a large amount of proteins that are associated with PYHIN interactions and are conserved across significantly different cell types [217]. Therefore, many direct and indirect interactions with PYHIN proteins are expected in these cells. This may explain why M84 interacted with all the proteins tested in this study (Figure 27) that contain either PYD or HIN domain or both. A cell line without PYHIN interactive proteins should be used instead to further investigate the direct and indirect interactions.

6.5 Homologous proteins of M84 in HCMV

MCMV M84 is a member of the M82-84 gene family, which is homologous to the UL82-84 gene family of HCMV [180]. This raises the question of whether M84 has a functional ortholog in HCMV.

In HCMV, UL82 encodes the protein pp71, which is a major tegument protein and has multiple functions in viral infection. The pp71 protein is localized to both the cytoplasm and the nucleus [218]. It is characterized as a transactivator, which can activate a number of viral promoters including the major immediate early promoter and initiates viral gene expression [219]. In addition, pp71 enhances the infectivity of viral DNA in a manner independent from its function as a transactivator of the IE1 and IE2 genes [220]. It has also been described that pp71 interferes with the transport and cell surface expression of MHC class I complexes [221]. Additionally, pp71 acts as an inhibitor of the STING-mediated signaling to evade immune response by interacting with STING to prevent its cellular trafficking and formation of the TBK1/IRF3 complex thereby interfering the experssion of the type I IFN. [222]. It is unlikely that UL82 is the functional homolog of M84 because there is no evidence of pp71 interference with inflammasome activation.

In contrast, UL83 and UL84 are the strongest candidates for being homologs of M84 as they share a similar level of amino acid identity with M84 [180]. UL83 encodes the protein pp65, which is the most abundant HCMV tegument protein and the major component of cell-free viral particles [223]. pp65 protein is responsible for inhibiting multiple levels of immune responses in HCMV infection. For instance, pp65 is involved in the downregulation of MHC class II expression [224] and it can inhibit NK cell cytotoxicity by targeting the NKp30 activating receptor during HCMV infection [225]. Moreover, pp65 has been shown to interact directly with the PYD of IFI16 in order to block its nuclear aggregation and inhibit IFI16-mediated DNA sensing for immune evasion [34]. pp65 prevents the type I interferon response, which has been investigated at different levels, by inhibiting its nuclear accumulation associated with a reduced IRF3 phosphorylation state [226] and by inactivating the DNA sensor cGAS without affecting STING [227]. pp65 is also able to impair the transcriptional upregulation of IL-1β by HCMV infection through inhibition of NF-kB activity [228]. Another study has shown an interaction of UL83 with AIM2 [181], but the consequences of this proposed interaction have not been investigated in HCMV

infected cells. It is also unknown whether UL83 interacts with ASC as M84 does. These evidences highlight the important role of pp65 as a critical molecular hub in viral evasion strategies against the host immune responses. In this study, I generated a chimeric virus in which the M84 locus is replaced by the HCMV ORF encoding UL83 (MCMV UL83 [ΔM84]). However, the introduction of UL83 did not rescue the growth defect caused by the absence of M84, indicating that UL83 in MCMV might not functionally substitute for M84 in mouse macrophages. The role of pp65 protein on AIM2 imflammasome signaling should be clarified in future studies in HCMV infected human cells.

UL84 is characterized as a "very early" gene as its mRNA can be detected as early as 2.5 hpi. [231]. UL84 protein is a multifunctional protein that interacts with several cellular and other virus-encoded factors. UL84 plays a key role in the virus life cycle, which is proposed as initiator for lytic viral DNA synthesis or acts as the origin-binding protein in lytic viral replication [232]. UL84 specifically interacts with IE2, which is the major viral transactivator in lytic viral replication and known to govern UL84 expression [233]. Furthermore, proteomics analysis shows the interaction between UL84 with both UL44 and pp65 in infected cells [234]. Due to the importance of pp65 in HCMV immune evasion, the functional consequence of the interaction between pp65 and UL84 remains to be investigated. Similar to MCMV M84, UL84 localizes in the nucleus in HCMV infected HFF fibroblasts. However, the effect of UL84 on AIM2 inflammasome signaling in HCMV infected macrophages remains unclear.

6.6 Summary

In the present study, the inhibition of pro-inflammatory cytokine release and pyroptosis during MCMV infection was investigated.

The MCMV M84 protein was identified as an inhibitor of the AIM2 inflammasome signaling using a luciferase report system based screening assay. M84 is expressed with early kinetics and was detected in both the nucleus and the cytoplasm of MCMV infected macrophages. M84 interacted with the inflammasome components AIM2 and ASC to block Caspase-1 activation, release of pro-inflammatory cytokines IL-1β and IL-18, cleavage of GSDMD, and pyroptosis of MCMV infected macrophages.

Growth attenuation of an M84*stop* MCMV in infection of macrophages was rescued by knocking out of either *Aim2* or *Asc* or by a Caspase-1 inhibitor treatment, and its

attenuation in infected mice was partially rescued in *Asc⁻/⁻* mice. M84 was found to be required for efficient MCMV dissemination *in vivo* and to inhibit the release of the inflammasome-activated cytokine IL-18 in the early stage of MCMV infection *in vivo*.

Taken together, these results demonstrate that viral inhibition of the inflammasome-pyroptosis pathway is important to promote viral replication and dissemination *in vivo*. This study provides the first evidence of MCMV inhibiting AIM2-inflammasome dependent pyroptosis and a better understanding of how MCMV modulates programmed cell death.

6.7 Graphical Summary
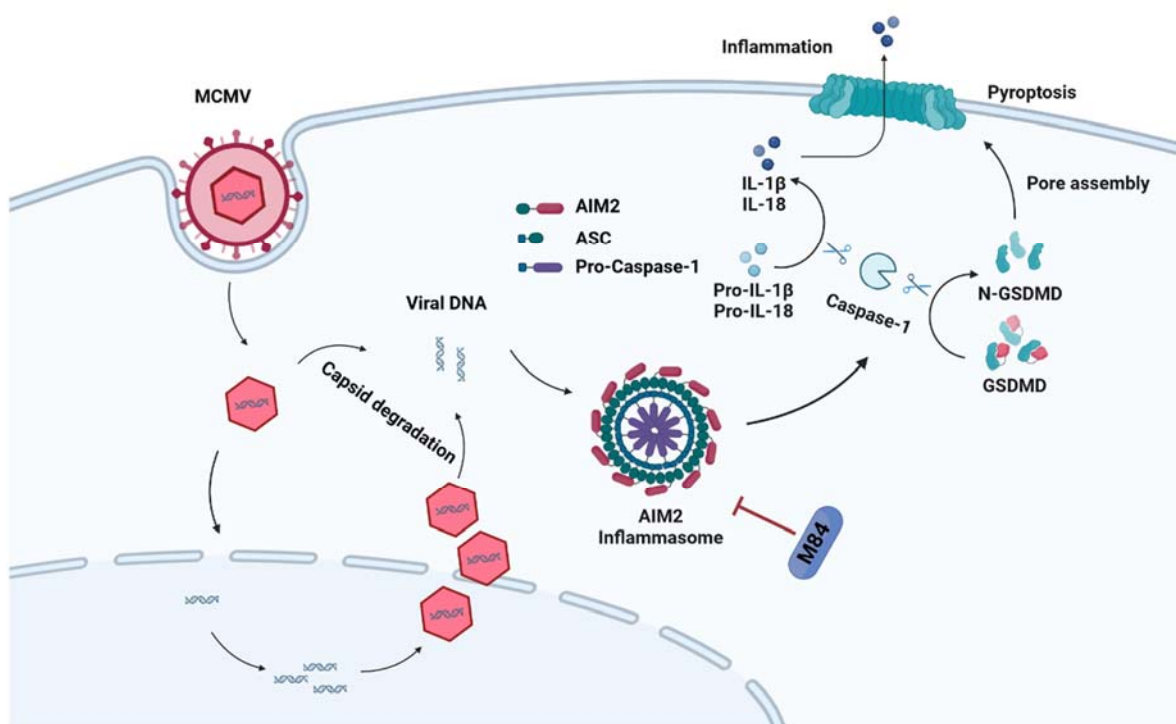
Figure 30. Graphical Summary

M84 interacts with the inflammasome components AIM2 and ASC to block Caspase-1 activation, release of IL-1β and IL-18, cleavage of Gasdermin D, and pyroptosis.

7 Materials

7.1 Cells

Name	Description	Reference
M2-10B4	Murine bone marrow stromal cells	ATCC (CRL-1972)
HEK-293T	Human embryonic kidney epithelial cells transformed with large T antigen	ATCC (CL-11268)
HEK-293A	Human embryonic kidney epithelial cells, subclone of the 293 Cell	Invitrogen (R705-07)
Phoenix	HEK-293T cells stably expressing retroviral packaging proteins: gag, pol and env	[235]
10.1	Spontaneously immortalized murine embryonal fibroblasts isolated from BALB/c mice	[236]
J774A.1	Murine macrophages derived from a tumor in a female BALB/c mouse	ECACC (91051511)
iBMDM WT	Wild-type immortalized murine bone marrow-derived macrophage	NIAID NIH (NR9456)
iBMDM-iGluc	iBMDMs stably transduced with iGluc- pMSCV-puro	This study
Asc ^{-/-} iBMDM	ASC knock-out generated using CRISPR/Cas9	This study
Aim2 ^{-/-} iBMDM	AIM2 knock-out generated using CRISPR/Cas9	This study
ASC-mCherry BMDM	Primary bone marrow derived macrophages were isolated from mice expressing ASC-mCherry	Kindly provided by Mathias Gelderblom (UKE, Hamburg, Germany)

7.2 Viruses

Name	Description	Reference
MCMV WT	MCMV Smith strain pSM3fr-MCK-2fl	[237]
MCMV M28HA	MCMV Smith strain pSM3fr-MCK-2fl with insertion of the HA epitope tag sequence at the 3' end of the M28 ORF	[238]
MCMV m139HA	MCMV Smith strain pSM3fr-MCK-2fl with insertion of the HA epitope tag sequence at the 3' end of the m139 ORF	[239]
MCMV M84HA	MCMV Smith strain pSM3fr-MCK-2fl with insertion of the HA epitope tag sequence at the 3' end of the M84 ORF	This study
MCMV M84*stop*	MCMV Smith strain pSM3fr-MCK-2fl with introduction of a C-to-G point mutation at the 183rd nucleotide of the M84 ORF leading to a stop codon	This study
MCMV Δm157	MCMV Smith strain pSM3fr-MCK-2fl with deletion of m157 as described [240]	This study
MCMV Δm157-M84*stop*	MCMV Δm157 strain with introduction of a C-to-G point mutation at the 183rd nucleotide of the M84 ORF leading to a stop codon	This study
MCMV ΔM84	MCMV Smith strain pSM3fr-MCK-2fl with deletion of M84 ORF	This study
MCMV UL83 [ΔM84]	MCMV ΔM84 strain with introduction of HCMV gene UL83 cloned from TB40E BAC into M84 ORF	This study
MCMV HAORFL147C	MCMV Smith strain pSM3fr-MCK-2fl with insertion of the HA epitope tag sequence at the 5' of the non-canonical ORFL147C protein	This study
MCMV ORFL147C*stop*	MCMV Smith strain pSM3fr-MCK-2fl with introduction of a G-to-T point mutation at the 133rd nucleotide of the ORF L147C leading to a stop codon	This study
MCMV M84-ORFL147Cdouble*stop*	MCMV Smith strain pSM3fr-MCK-2fl with M84 and ORF L147C stop mutant	This study

7.3 Plasmids

Name	Description	Reference
pcDNA3	Expression vector, ampR, neoR	Life Technologies
pEPkan-S	Template plasmid for en passant mutagenesis, contains I-Sce-aphA1 cassette, kanR	[241]
pMSCV-puro	Retroviral expression vector to generate retrovirus for transduction of eukaryotic cells, ampR, puroR	Clontech Laboratories
pSicoR-CRISPR-PuroR	Lentiviral expression vector, contains Cas9 gene, PuroR and site for cloning of gRNA	[242]
pMDG.2	Lentiviral second-generation packaging plasmid, ampR	[242]
pCMVR8.91	Lentiviral second-generation packaging plasmid, ampR	
MCMV ORF expression library	Expression plasmids of MCMV ORFs [175]	kindly provided by Niels Lemmermann (University of Mainz, Mainz, Germany)
pcDNA3-mAIM2-Flag	Express mouse AIM2 with a C-terminal Flag tag	Addgene, #51537
pcDNA3-N-Flag-ASC	Express mouse ASC with a N-terminal Flag tag	Addgene, #75134
pCMV-Caspase-1-Flag	Express mouse Caspase-1 with a C-terminal Flag tag	Addgene, #21142
pCMV-pro-IL-1β-c-Flag	Express mouse IL-1β with a C-terminal Flag tag	Addgene, #75131
pCMV-p202-Myc-DDK	Express Mouse interferon activated gene 202 (Ifi202)	Origene (NM_008327)
pCMV-p203-Myc-DDK	Express Mouse interferon activated gene 203 (Ifi203)	Origene (NM_008328)
pCMV-p204-Myc-DDK	Express Mouse interferon activated gene 204 (Ifi204)	Origene (BC010546)
pcDNA-M82HA	Express murine cytomegalovirus M82 with a C-terminal HA tag	This study

Materials

pcDNA-M83HA	Express murine cytomegalovirus M83 with a C-terminal HA tag	This study
pcDNA-M84HA	Express murine cytomegalovirus M84 with a C-terminal HA tag	This study
pcDNA-VP22HA	Express HSV-1 VP22 with a C-terminal HA tag	This study
pcDNA-HA-ORFL147C	Express murine cytomegalovirus ORF L147C with a N-terminal HA tag	This study
pEFBOS-iGluc	Express pro-interleukin -1β-Gaussia luciferase [179]	A gift from Veit Hornung (Gene Center of the LMU Munich, Germany)
pcDNA-iGluc	Express pro-interleukin -1β-Gaussia luciferase in pcDNA	This study
pMSCV-puro-iGluc	Pro-interleukin -1β-Gaussia luciferase in retroviral expression vector	This study

7.4 Bacteria

Name	Description	Reference
E.coli DH10B	*F- mcrA Δ(mrr-hsdRMS-mcrBC) Φ80dlacZΔM15 ΔlacX74 endA1 recA1 deoR Δ(ara,leu)7697 araD139 galU GalK nupG rpsL λ-* Growth at 37°C	Life Technologies
E. coli GS1783	DH10B I *cI857Δ(cro-bioA)<>araC-*PBAD*I-sceI* Growth at 30°C	[241]

7.5 Primers

Name	Sequence	Description
ASC-105 sm105-cASC	CTAAGCACAGTCATTGTGAGCTCC	Genotyping of ASC^{-/-} mice
ASC-99 sm99-gASC	CTAGTTTGCTGGGGAAAGAAC	

ASC-Neo sm141-NEOseq6	AAGACAATAGCAGGCATGCTGG	
BgLII-iGluc FW	GGAAGATCTATGGCAACTGTTCCTGAACTC	Cloning of iGluc
EcoRI-iGluc REV	CCGGAATTCCTACTTGTCGTCATCGTCTTTGT	
Aim2-HIN-BamHI FW	CTCGGATCCATGAATAGAAGTCAAGCTGAAAACT	Cloning of AIM2-HIN-Flag from pcDNA3-mAIM2-Flag
Aim2-HIN-Flag-ApaI REV	GCT CTA GCA TTT AGG TGA CAC	
Aim2-PYD-BamH FW	CTCGGATCCATGGAGAGTGA	Cloning of AIM2-PYD-Flag from pcDNA3-mAIM2-Flag
Aim2-PYD-Flag-ApaI REV	ATAGGGCCCTCTAGCTACTTGTCGTCATCGTCTTTGTAGTCCTCGAGCTGTTTCTTCTGAGGCTTAGC	
VP22-HA HindIII FW	CCCAAGCTTATGACCTCTCGCCGCTCCG	Cloning of Vp22-HA from HSV-1
VP22-HA HindIII FW	CGCGGATCCTCAAGCGTAGTCTGGGACGTCGTATGGGTACTCGACGGGCCGTCTGGG	
M82-HA HindIII FW	TATAAGCTTATGGCCGAGGAATTTAACTTCCTGAC	Cloning of MCMV M82-HA from MCMV
M82-HA EcoRII REV	ATATTGAATTCTCAAGCGTAGTCTGGGACGTCGTATGGGTAGGGTTGTAGATGTGGGG	
M83-HA HindIII FW	TATAAGCTTATGAACGCCATGAACAACAGGAC	Cloning of MCMV M83-HA from MCMV
M83-HA EcoRII REV	ATATTGAATTCTCAAGCGTAGTCTGGGACGTCGTATGGGTATGAACGCAGCAGTCTCC	
M84-HA HindIII FW	TATAAGCTTATGTCGGTCAACGTTTACTTGCC	Cloning of MCMV M84-HA from MCMV
M84-HA EcoRII REV	ATATTGAATTCTCAAGCGTAGTCTGGGACGTCGTATGGGTAGATGTTCTGCTGCAGC	
MCMV delta m157_zeo_FW	CGTGGTCAAGCCGGTCGTGTTGTACCAGAACTCGACTTCGGTCGCGTTCATGTTGACAATTAATCATCGGCAT	Deletion of m157 from MCMV

Materials

MCMV delta m157_zeo_Rev	CCTAGTAAAATTACTCTTGATTGTGTT TATCTCGGAACGTGCTGTAACAATCA GTCCTGCTCCTCGGCCA	
M84-HA MCMV FW	CTTCCACCCGCTCGGCGCGCTCCAG AGGCTGCAGCAGAACATCTACCCATA CGACGTCCCAGACTACGCTTAGGGAT AACAGGGTAATCGATTT	Insertion of HA tag at 3' end of the M84 in MCMV
M84-HA MCMV REV	TCCGATCGGGCTCTGTCTGTTTGTCT ATGTCCTCAAGCGTAGTCTGGGACGT CGTATGGGTAGATGTTCTGCTGCGCC AGTGTTACAACCAATTAACC	
M84*stop* MCMV FW	GTCCGCAGGCGCCCTGCGTCCTGTG TGTGGGGAAGATGTAGCGGCACCCG GACAACCACCCTAGGGATAACAGGG TAATCGATTT	Introduction of a stop codon into M84 in the M84-HA MCMV
M84*stop* MCMV REV	TGGCGAAGTTCACCAGGTGTGGGTG GTTGTCCGGGTGCCGCTACATCTTCC CCACACACAGGCCAGTGTTACAACCA ATTAACC	
ΔM84-zeo MCMV FW	TTCACGGCGCCGTCCGTCCTTCCTTC TTCCTTCGTTCGACTGTTGACAATTAA TCATCGGCAT	Deletion of M84 from MCMV
ΔM84-zeo MCMV REV	ATCTTGATTCCGATCGGGCTCTGTCT GTTTGTCTATGTCCTCAGTCCTGCTC CTCGGCCA	
M84-UL83-Gibson-FW1	AGACCCAAGCTTGGTACCGAGCTCG GGCGCCGTCCGTCCTTCCTTCTTCCT TCGTTCGACTTGGTCGCCTGCCTATA GGGATAACAGGGTAATCGATTT	Cloning of UL83 from HCMV for Gibson assembly and insertion of UL83 into ΔM84 MCMV
M84-UL83-Gibson-REV1	TCTGCGGCCGCCGCCTTACATAGGC AGGCGACCAAGTCGAACGAAGGAAG AAGGAGCCAGTGTTACAACCAATTAA CC	
M84-UL83-Gibson-FW2	TTGGTCGCCTGCCTATGTAA	
M84-UL83-Gibson-REV2	CCGCCAGTGTGATGGATATCTGCAGA TCTTGATTCCGATCGGGCTCTGTCTG TTTGTCTATGTCCTGGCTCAACCTCG ATGCTT	

HA-ORF L147C-MCMV FW	GCGGTGTCTGTATCGCCGTTCGGGG TTGTCTGTGCGCGGTATGTACCCATA CGACGTCCCAGACTACGCTTAGGGAT AACAGGGTAATCGATTT	Insertion of HA tag at 5' end of the ORF L147C in MCMV
HA-ORF L147C-MCMV REV	CAGGTCGACTCCCCTACCCCTCCGCT TATAAGCGTAGTCTGGGACGTCGTAT GGGTACATACCGCGCACAGCCAGTG TTACAACCAATTAACC	
HA-ORF L147Cstop-MCMV FW	GTTCCAAATGCAACGAGTGCGCGATG GATGTGGAATGTCTTAAGTACTGCGA TCCGAATATTGTAGGGATAACAGGGT AATCGATTT	Introduction of a stop codon into ORF L147C in the HA-ORF L147C MCMV
HA-ORF L147Cstop-MCMV REV	GGCCGTCGAATCCATCGACACAATAT TCGGATCGCAGTACTTAAGACATTCC ACATCCATCGCGCCAGTGTTACAACC AATTAACC	
M84-seq-FW	AGGAGAGAGGGATAGAGGGTG	Sequencing of the modifications in MCMV M84
M84-seq-REV	TCCTGTTGTTCATGGCGTTC	
ORFL147C-seq-FW	AAGCTCGTTGAAATCACGG	Sequencing of the modifications in MCMV ORF L147C
ORFL147C-seq-REV	GAGCCTCTTGTGCACGAG	
ORFL147Cm-seq-FW	GTACATCAACGACGCGGA	
ORFL147Cm-seq-REV	TCC GCG TCG TTG ATG TAC	
gRNA-Ms-AIM2-1 FW	ACC GACCACCTGATTCAAAGTGC	Generation of the gRNAs for AIM2 CRISPR/Cas9 knock-out
gRNA-Ms-AIM2-1 REV	AAAC GCACTTTGAATCAGGTGGT	
gRNA-Ms-AIM2-2 FW	ACC GCAGCCTTAGTTCTCAACTC	
gRNA-Ms-AIM2-2 REV	AAAC GAGTTGAGAACTAAGGCTG	
gRNA-Ms-AIM2-3 FW	ACC GACCGGCCTGGACCACATCA	
gRNA-Ms-AIM2-3 REV	AAAC TGATGTGGTCCAGGCCGGT	

gRNA-Ms-ASC-1 FW	ACC GTGCAACTGCGAGAAGGCTA	
gRNA-Ms-ASC-1 REV	AAAC TAGCCTTCTCGCAGTTGCA	
gRNA-Ms-ASC-2 FW	ACC GGACGCTCTTGAAAACTTGT	Generation of the gRNAs for ASC CRISPR/Cas9 knock-out
gRNA-Ms-ASC-2 REV	AAAC ACAAGTTTTCAAGAGCGTC	
gRNA-Ms-ASC-3 FW	ACC GCTCAGAGTACAGCCAGAAC	
gRNA-Ms-ASC-3 REV	AAAC GTTCTGGCTGTACTCTGAG	

7.6 Antibodies

7.6.1 Primary antibodies

Antigen	Clone	Specie	Application (dilution)	Reference
AIM2	63660	Rabbit	western blot (1:1000)	Cell Signaling
ASC	D2W8U	Rabbit	western blot (1:1000)	Cell Signaling
Caspase-1	AG-20B-0042-C100	Mouse	western blot (1:1000)	AdipoGen
GSDMD	ab209845	Rabbit	western blot (1:1000)	Abcam
Flag	M2	Mouse	western blot (1:1000)	Sigma-Aldrich
HA	3F10	Rat	western blot (1:500) immunofluorescence (1:300)	Roche
MCMV IE1	Croma 101	Mouse	western blot (1:1000)	Stipan Jonjic (University of Rijeka, Rijeka, Croatia)
β-actin	AC-74	Mouse	western blot (1:3000)	Sigma

7.6.2 Secondary antibodies

Antigen	Conjugate	Species	Application (dilution)	Source
Rat Ig	HRP	goat	western blot (1:5000)	Jackson ImmunoResearch
Mouse Ig	HRP	goat	western blot (1:5000)	Jackson ImmunoResearch
Rabbit Ig	HRP	goat	western blot (1:5000)	Jackson ImmunoResearch
Mouse Ig	HRP	goat	western blot (1:10000)	Dako Cytomation
Rabbit Ig	HRP	goat	western blot (1:10000)	Dako Cytomation
Rat Ig	Alexa 488	goat	immunofluorescence (1:1000)	Invitrogen
Mouse Ig	Alexa 488	goat	immunofluorescence (1:1000)	Invitrogen
Rabbit Ig	Alexa 488	goat	immunofluorescence (1:1000)	Invitrogen
Mouse Ig	Alexa 555	goat	immunofluorescence (1:1000)	Invitrogen
Rabbit Ig	Alexa 555	goat	immunofluorescence (1:1000)	Invitrogen
Rabbit Ig heavy chain	HRP	mouse	western blot (1:4000)	Abcam (ab99702)
Mouse Ig light chain	HRP	goat	western blot (1:5000)	Jackson ImmunoResearch
Rabbit light chain Ig	HRP	goat	western blot (1:5000)	Jackson ImmunoResearch

7.7 Chemical and reagents

7.7.1 Antibiotics

Name	Application	Concentration	Reference
Ampicillin	Selection of bacteria	100 µg/ml	Roth
Kanamycin	Selection of bacteria	50 µg/ml	Roth
Zeocin	Selection of bacteria	50 µg/mL	Thermo Fisher
Chloramphenicol	Selection of bacteria	15 µg/ml	Roth

Penicillin	cell culture supplement	100 µg/ml	PAA
Streptomycin	cell culture supplement	100 µg/ml	PAA
Puromycin	Selection of transduced cells	5 µg/ml	Sigma-Aldrich

7.7.2 Enzymes

Name	Reference
Dream Taq Green DNA polymerase and buffer	Thermo Fischer Scientific
Fast Digest restriction enzymes and buffer	Thermo Fischer Scientific
PRECISOR DNA polymerase and buffer	BioCat
Q5 High-Fidelity DNA polymerase and buffer	NEB
DNAse	Thermo Fischer Scientific
T4-DNA-ligase and buffer	Thermo Fischer Scientific
Gibson Assembly Ultra Master Mixes	BioCat GmbH

7.7.3 Molecular mass standards

Name	Reference
O'GeneRuler™ DNA Ladder Mix	Thermo Fisher Scientific
PageRuler™ Prestained Protein Ladder	Thermo Fisher Scientific

7.7.4 Other reagents and chemicals

Name	Reference
Polyethylenimine (PEI), branched	Sigma-Aldrich
PolyFect Transfection reagent	Qiagen
Lipofectamine 2000	Life Technologies GmbH
Polybrene	Millipore
Protease inhibitor cocktail cOmplete™ mini, EDTA free	Roche
ECL Prime Western Blotting Detection Reagent	GE-Healthcare
Lumigen ECL Ultra (TMA-6)	Beckman Coulter

Albumin Fraction V pH 7.0 (BSA)	Applichen Panreac
Anti-HA Affinity Matrix (anti-HA rat, clone 3F10)	Roche
Protein A-Sepharose	GE-Healthcare
Protein G-Sepharose	GE-Healthcare
DMSO (dimethyl sulfoxide)	Roth
VX-765	Invivogen
Methylcellulose (viscosity 4000 cPs)	Sigma-Aldrich
Poly (dA: dT)	Invivogen
Nitrocellulose membrane (0.2 µm and 0.45µm)	GE Healthcare Life Science
LPS-EB (LPS from E. coli O111:B4)	Invivogen
Whatman® gel blotting paper, Grade GB003	Sigma-Aldrich
Hoechst 33342	Thermo Fisher Scientific
Propidium Iodide	Sigma-Aldrich
Coelenterazine-h	Promega
L-(+)-Arabinose	Sigma-Aldrich

7.8 Medium

7.8.1 Cell culture medium

Name	**Reference**
Dulbecco's Modified Eagle's Medium (DMEM) with glucose	Sigma-Aldrich
Dulbecco's Phosphate Buffered Saline	Sigma-Aldrich
Trypsin-EDTA (1×)	Sigma-Aldrich
Fetal calf serum (FCS)	Pan Biotech GmbH
Opti-MEM	Thermo Fisher Scientific
Penicillin/streptomycin (100×)	Sigma-Aldrich
10×MEM	Thermo Fisher Scientific
L-Glutamine	Thermo Fisher Scientific

Methylcellulose overlay:

10×MEM	40mL
Methylcellulose 2.5% (m/v)	360mL
Penicillin/streptomycin (100×)	4mL
L-Glutamine	5mL
NaHCO$_3$ (1M)	15mL
Fetal calf serum (FCS)	16mL

7.8.2 Bacteria medium

Name	Reference
Luria Bertani (LB) liquid medium	Roth
Luria Bertani (LB) agar	Roth

7.9 Buffers

7.9.1 Agarose gel electrophoresis

Name	Components	pH
50 × TAE buffer (used 1× for pouring agarose gel and running buffer)	2M Tris-HCl	8.0
	50 mM EDTA	
	5.7 % (v/v) acetic acid	
TBE electrophoresis buffer (10×) (used 0.5 × for pouringagarose gel and running buffer)	1M Tris-HCl	8.0
	0.02M EDTA	
	1M boric acid	

7.9.2 SDS polyacrylamide gel electrophoresis (Tricine-SDS-Page)

Name	Components	PH
4×SDS sample loading buffer	150 mM Tris	6.8
	2 mM EDTA	

	20 % (v/v) glycerol	
	4 % (v/v) SDS	
	10 % β-mercaptoethanol	
	bromophenol blue	
10 × TBS-T (used 1 ×)	100 mM Tris	7.5
	1,5 M NaCl	
	1 % (v/v) Tween	
Transfer buffer (semi-dry)	50 mM Tris	--
	150 mM NaCl	
	0.04 % (v/v) SDS	
	20 % (v/v) methanol	
10× cathode buffer (used 1 ×)	1 M Tris Base	--
	1 M Tricine	
	1 % SDS	
10× Anode Buffer (used 1 ×)	2 M Tris	8.9
SDS-Resolving Gel	3M Tris-HCl	8.45
	12.5 % Acrylamide	
	50 % Glycerol	
	0.3 % SDS	
SDS-Stacking Gel	3M Tris-HCl	8.45
	4% Acrylamide	
	0.3 % SDS	

7.9.3 Buffers for immunoprecipitation

Buffer	Components	PH
RIPA lysis buffer	50 mM Tris	7.2
	150 mM NaCl	
	1 % (v/v) Triton X-100	
	0.1 % (v/v) SDS	

	1 % deoxylcholate	
NP-40 lysis buffer	50 mM Tris-HCl	7.5
	150 mM NaCl	
	1 % Nonidet P-40	
IP Washing Buffer 1	10 mM Tris-HCl	7.6
	150 mM NaCl	
	0.2 % Nonidet P-40	
	2 mM EDTA	
IP Washing Buffer 2	10 mM Tris-HCl	7.6
	500 mM NaCl	
	0.2 % Nonidet P-40	
	2 mM EDTA	
IP Washing Buffer 3	10 mM Tris-HCl	7.6

7.9.4 Buffers for Immunofluorescence

Buffer	Components
Fixation Buffer	4% Paraformaldehyd in PBS
Quenching Buffer	50 mM NH4Cl in PBS
Permeabilization Buffer	0.3 % or 0.5 % Triton X-100 in PBS
Blocking Buffer (0.2 % Gelatine)	0.2 % Gelatine in PBS
Blocking Buffer (TBS-BG)	Tris buffered saline with 5% glycine, 5% BSA 0.05% Tween20 and 0.05% NaN3

7.9.5 DNA preparation from bacteria ("Mini Prep")

Buffer	Components	PH
S1 Buffer	50 mM Tris-HCl	8.0
	100 µg/mL RNAse A	
	10 mM EDTA	
S2 Buffer	200 mM NaOH	--

	1 % (v/v) SDS	
S3 Buffer	2.8 M calcium acetate	5.2
Tris-HCl	10 mM Tris	8.0

7.10 Kit

Name	Reference
innuPREP DNA mini kit	Analytik Jena
mi-Plasmid Miniprep Kit	Metabion
NucleoBond Xtra Midi	Macherey-Nagel
NucleoBond Gel and PCR Clean-up	Macherey-Nagel
Mouse IL-1β ELISA kit	Invivogen
Mouse IL-18 ELISA kit	Invivogen

8 Methods

8.1 Molecular biology methods

8.1.1 E.coli DH10B Electrocompetent bacteria preparation

A single colony of *E.coli* DH10B was inoculated to 10ml LB-broth medium and cultured overnight with continuous shaking at 37°C. 5ml of the overnight culture was added to 200ml pre-warmed LB-broth medium and cultured with continuous shaking at 37°C. Once the concentration of bacteria reached an OD600 value between 0.5 and 0.6, the culture was immediately transferred on ice for 20 minutes. The bacteria were centrifuged at 4°C and 5000 × *g* for 10 minutes. The pellet was then washed twice with 100ml ice-cold sterile water and once with ice-cold sterile 10% glycerol. The pellet of bacteria was dissolved in 1ml ice-cold sterile 10% glycerol and immediately aliquoted with 50µl/tube on ice and then stored at -80°C.

8.1.2 E.coli GS1783 Electrocompetent bacteria preparation

A single colony of *E.coli* GS1783 was inoculated to 10ml LB-broth medium with 15 µg/ml chloramphenicol and cultured overnight with continuous shaking at 30°C. 5ml of the overnight culture was added to 200ml pre-warmed LB-broth medium with 15 µg/ml chloramphenicol and cultured with continuous shaking at 30°C. Once the OD600 value was measured between 0.5 and 0.6, the culture was immediately transferred into a water bath shaker at 42°C for 15 minutes and then was placed on ice for 20 minutes. The bacteria were centrifuged at 4°C and 5000 × *g* for 10 minutes. The pellet was then washed twice with 100ml ice-cold sterile water and once with ice-cold sterile 10% glycerol. The pellet of bacteria was resuspended in 1ml ice-cold sterile 10% glycerol and immediately aliquoted with 50µl/tube on ice and then stored at -80°C.

8.1.3 Polymerase Chain Reaction (PCR)

PCR was performed by using DreamTaq, PRECISOR or Q5 High-Fidelity DNA polymerase according to the manufacture's protocol. The DreamTaq was used for colony PCR and genotyping of *Asc* knockout mice, Precisor and Q5 polymerase were used for cloning or sequencing that require high-fidelity amplifications.

Reaction Setup:

PRECISOR /Q5		Dream Taq	
5X Q5 / HiFi Reaction Buffer	10µl	10X DreamTaq Green Buffer	5µl
10 mM dNTPs	1µl	10 mM dNTPs	1µl
10 µM Forward Primer	2µl	10 µM Forward Primer	2µl
10 µM Reverse Primer	2µl	10 µM Reverse Primer	2µl
Template DNA (10 -100 ng)	Xµl	Template DNA (10 -100 ng)	Xµl
PRECISOR /Q5 High-Fidelity DNA Polymerase	1µl	DreamTaq DNA Polymerase	0.25µl
Autoclaved distilled water	Up to 50µl	Autoclaved distilled water	Up to 50µl

Cycling Conditions:

	PRECISOR /Q5			Dream Taq		
Cycle Step	Temperature	Time	Cycle(s)	Temperature	Time	Cycle(s)
Initial denaturation	98°C	2min/30sec	1	95°C	2min	1
Denaturation	98°C	30/10sec		95°C	30sec	
Annealing	Tm	30s	25-30	Tm	30sec	25-30
Extension	72°C	15-30s/kb		72°C	1min/kb	
Final Extension	72°C	5/2min	1	72°C	5min	1

8.1.4 Restriction digestion of DNA

DNA digestion was performed by using FastDigest restriction enzymes according to the manufacturer's instructions.

Reaction set up and digestion conditions:

Plasmid digestion	PCR product digestion

10X FastDigest Green Buffer	2µl	10X FastDigest Green Buffer	6µl
Plasmid	1µg	DNA	50µl PCR reaction
FastDigest restriction enzyme	1µl/enzyme	FastDigest restriction enzyme	1µl/enzyme
Fast Akaline Phosphatase	1µl	DpnI	1µl
Autoclaved distilled water	Up to 20µl	Autoclaved distilled water	Up to 60µl

37°C for 10-20 min

8.1.5 Agarose gel electrophoresis

PCR products or other DNA fragments were loaded on a 0.8%-1% (w/v) TAE agarose gel and run at 120 V for 1 hour. The BAC DNA fragments were loaded on a 0.6% (w/v) TBE agarose gel and run at 60 V overnight. Both TAE and TBE gels contain 0.5 µg/ml ethidium bromide. The O'GeneRuler was loaded on the gel as a size ladder. The sizes of DNA fragments were visualized with GelDoc XR + (BioRad). The pictures of the gels were taken using a GelDoc XR+ (BIO-RAD) and analyzed with the Image Lab software.

8.1.6 Purification of DNA fragments

The DNA fragments were cut out from TAE gels and purified by using a NucleoSpin Gel and PCR clean up kit according to the manufacturer's instructions. The concentration and quality of the purified DNA was measured by a NanoDrop-1000 (Peqlab). DNA was stored at -20°C for further using.

8.1.7 DNA ligation

The vector (linearized plasmid) and the insert (digested DNA fragment) were mixed according to the molecular ratio of 1:5 and ligated by using T4-DNA-Ligase.
Reaction set up and ligation conditions:

10X Ligase Reaction Buffer	2 µl
Vector	Xµl (150ng)

Insert	Yµl
T4 DNA Ligase	1µl
Autoclaved distilled water	Up to 20µl

22°C for 1hour / 16°C overnight

8.1.8 Bacteria transformation

The electrocompetent bacteria were transformed by electroporation. 50µl of *E.coli* DH10B was thawed on ice and then mixed with either 1-10 ng of plasmids or 2-4µl of ligation products. 50µl of *E.coli* GS1783 was thawed on ice and then mixed with 150ng of linear PCR amplified DNA. The mixture was then transferred to a 2 mm electroporation cuvettes and pulsed using the Gene Pulser XCell (BioRad) with the following settings: 2500 V, 25 µF and 200 Ω. 900 µL of warm LB-broth medium was added to the bacteria immediately after the pulse. *E.coli* DH10B were incubated at 37°C and *E.coli* GS1783 were incubated at 30 °C for 1 hour. Next, the bacteria were centrifuged for 2 minutes at 2000 × *g*. The pellet was resuspended and plated on LB agar plate with the corresponding antibiotics and incubated overnight at the appropriate temperature in a bacteria incubator.

8.1.9 Extraction of Plasmid DNA and BAC DNA (Mini prep)

A single colony was picked up from LB agar plate and incubated in 5ml of LB-broth medium with required antibiotics for continuous shaking overnight. Plasmid DNA was extracted from *E.coli* DH10B bacteria by using the Mi-Plasmid MiniPrep Kit according to the manufacturing protocol. The overnight culture of *E.coli* GS1783 was centrifuged at 6000 × *g* for 5 minutes and the pellet was resuspended with 300µl of ice-cold S1 buffer. 300µl of ice-cold S2 buffer was then added to the mixture and gently inverted for 3-5 times. After 5 minutes of incubation at RT, 300µl of ice-cold S3 buffer was added and the tubes were gently inverted for 3-5 times. The samples were incubated on ice for another 7 minutes and then centrifuged at 11000 × *g* for 20 minutes at 4 °C. The clear supernatant was transferred into a new tube and mixed with 0.8× volume of isopropanol. After 3 inversions, the tube was centrifuged at 11000 × *g* for 30 minutes at 4°C. The pellet was then washed with 1ml of 70% ethanol and centrifuged again at

11000 × *g* for 5 minutes at 4°C. The DNA pellet was dried and then dissolved in 30µl of 10mM Tris-HCl (pH 8).

8.1.10 Extraction of Plasmid DNA and BAC DNA (Midi prep)

Bacteria were incubated in 200ml LB-broth medium with the required antibiotics for continuous shaking overnight at the appropriate temperature. Plasmid DNA or BAC DNA was extracted from bacteria by using the NucleoBond Midi Xtra Kit according to the manufacturing protocol. The high-copy protocol was used for plasmid DNA extraction while the low-copy protocol was used for extraction of BAC DNA. The DNA pellet was dissolved in Tris-HCl buffer (pH 8.0) and stored at -20°C.

8.1.11 Storage of bacteria

600µl of an overnight culture was mixed with 300µl of autoclaved 86% glycerol and stored at -80°C.

8.1.12 DNA Sequencing

PCR products and plasmid DNA were sequenced by SEQLAB Sequence Laboratories (Maschmühlenweg 36, 37081, Göttingen, Germany). MCMV virus DNA and BACs were sequenced by the NGS facility of LIV.

8.1.13 En passant (BAC) mutagenesis

The mutations of BACs were performed by using *en passant* mutagenesis as described by Tischer and colleagues [241]. The primers containing homologies with the viral genome were used for PCR to amplify the I-SceI-aphAI-cassette from the pEP-Kan-S plasmid. The I-SceI-aphAI-cassette encodes for the Kanamycin resistance gene and contains the unique restriction site I-Sce-I. The PCR product was then digested by DpnI to remove the plasmid templates and loaded on a TAE agarose gel. The correct size of ~1kb fragment was cut from the gel and purified by NucleoSpin Gel and PCR clean up kit. 150ng of the purified PCR product was transformed to *E.coli* GS1783 electrocompetent bacteria carrying MCMV BAC. Transformed bacteria were then plated on LB agar plates containing chloramphenicol and kanamycin. After overnight incubation at 30°C, 10 colonies were picked up and incubated in LB-Broth medium containing chloramphenicol and kanamycin for overnight incubation with continuous shaking at 30°C. BAC DNA from the overnight culture was extracted and digested with

restriction enzymes (HindIII, BamHI or EcoRI). The DNA fragments were analyzed by running a TBE agarose gel. According to the DNA restriction fragment length polymorphism, 3 positive colonies were used for the secondary recombination procedure. Single colony was inoculated in 2ml of LB-broth medium containing chloramphenicol for 2-3 h incubation with continuous shaking at 30°C until medium was turning cloudy. 2ml warm LB-broth medium containing 2% (w/v) L-arabinose was added and cultured for another hour. The culture was then immediately transferred into a 42 °C water bath for 15 minutes with continuous shaking to induce the expression of the red recombinase. The bacteria were incubated back to 30°C for 1 hour with continuous shaking. The culture was then diluted at 1:1000 (OD600<0.5) or 1:10000 (OD600>0.5) according to the OD600 measurement. 100µl of diluted bacteria was plated on the agarose plates containing chloramphenicol and 1% (w/v) L-arabinose at 30°C overnight. Single colonies were picked up for verifying loss of kanamycin resistance and digestion of the BAC DNA. The positive colonies were further checked by colony PCR and sequencing of the modified region. At least 2 of selected positive colonies were prepared with Midi-preps for reconstituting the virus in murine fibroblasts.

8.1.14 Mouse genotyping

The samples of ear punch from mice were mixed with 100µl of 50mM NaOH and incubated at 95°C for 45min. After 5 minutes cooling down to room temperature, 10µl of 1M Tris/HCl (PH 8.0) was added to each sample. The mixture in the tube was then vortexed and centrifuged with full speed for 5 minutes. The supernatants were transferred into new tubes and used as templates for PCR. The rest of extracted DNA was stored at -20°C for further experiments. The PCR products were loaded on a 0.8%(w/v) TAE agarose gel and run at 120 V for 1 hour.

PCR Reaction Setup		Cycling Conditions		
10X DreamTaq Green Buffer	2.5µl	Temperature	Time	Cycle(s)
10 mM dNTPs	0.5µl	95°C	2min	1
10 µM Primer 1	1µl	95°C	30sec	
10 µM Primer 2	1µl	Tm	30sec	25-30
10 µM Primer 3	1µl	72°C	1min/kb	

Template DNA	1µl	72°C	5min	1
DreamTaq DNA Polymerase	0.25µl	4°C	--	
Autoclaved distilled water	Up to 25µl			

8.2 Cell biology and virology methods

8.2.1 Cell culture

All cells were grown on culture dishes (10 or 15 cm^2) or plates (6-well, 12-well, 24-well, 48-well or 96-well) at 37°C in the Hera Cell incubator with 80 % relative humidity and 5 % CO_2. All cell culture work was performed within a Laminar flow hood (HeraSafe, Heraeus). Cells were cultured in complete Dulbecco's modified Eagle medium (DMEM) supplemented with 10% fetal calf serum (FCS) and 100U/ml penicillin/100µg/ml streptomycin. When the cells reached approximately 90% confluence, they were washed with PBS and splitted by using 0.25% Trypsin-EDTA solution at 37°C. The trypsin was neutralized by addition of growth medium containing FCS and the cells were splitted 1:3 to 1:10. For seeding the cells, 10µl of the cell suspension was loaded onto a counting slide and counted by a TC20™ Automated Cell Counter (BIO-RAD).

For freezing the cells, the cell suspension was centrifuged for 10 minutes at 250 × g. The cell pellet was resuspended in FCS containing 10% DMSO and aliquoted to cryotubes. The cells were immediately transferred to a freezing box ("CoolCell LX") at -80°C for at least 4 hours and then transferred to liquid nitrogen.

For thawing cells, the aliquot of frozen cells from the liquid nitrogen were transferred into a 37°C water bath and immediately transferred into a 15ml Falcon tube containing 10ml growth medium and centrifuged for 10 minutes at 250 × g. The cell pellet was resuspended in 10ml growth medium and transferred to a 10cm^2 dish.

8.2.2 Transfection of Plasmid DNA

Plasmid DNA was transfected to cells using polyethylenimine (PEI). 3×10^6 cells were seeded on 10cm^2 dish the day before transfection. 8µg of plasmid DNA was diluted in 100µl of DMEM and 32µl (a ratio of 1:4 with the DNA) of PEI was diluted in another 100µl of DMEM. The dilutions of plasmid and PEI were mixed by vortexing and incubated at room temperature for 20 minutes. 700µl of growth medium was added to

the mixture and then transferred to cells. The mixture was then gently spread to the whole dish. The medium was changed 6 hours post transfection. The cells and supernatant were collected at 24 hours post transfection for further using.

8.2.3 Transfection of BAC DNA

MCMV BAC DNA was transfected to 10.1 murine fibroblasts by using Polyfect transfection reagent for reconstitution of MCMV viruses. 1.5×10^5 cells were seeded on a 6-well plate the day before transfection. On the following day, 3µg of MCMV BAC DNA was diluted in 100µl of DMEM and 10µl of Polyfect was diluted to another 100µl of DMEM. The dilution of BAC DNA and Polyfect were mixed and incubated at room temperature for 20 minutes. 700µl of growth medium was added to the mixture and then transferred to cells. The mixture was then gently spread to the whole dish. The medium was changed 6 hours post transfection. As soon as the cells were confluent in 6-well plate, they were transferred to $15cm^2$ dish. The reconstitution of MCMV was monitored by detection of the cytopathic effects (CPE). The supernatant from the infected cells was harvested for virus stock.

8.2.4 Production of retrovirus and lentivirus

For retrovirus production, 8µg of pMSCV-puro plasmid carrying the target gene was transfected into 3×10^6 Phoenix cells on a $10cm^2$ dish as described in 8.2.2. For lentivirus production, 4µg of pSicoR-CRISPR-PuroR, 3µg of packaging plasmid pCMVdR8.91 and 1µg of envelope plasmid pMD2.G were co-transfected to HEK 293T cells on a $10cm^2$ dish as described in 8.2.2. The supernatant containing retrovirus or lentivirus was harvested 48 hours post transfection and another 8ml of fresh medium was added to the cells for a secondary harvesting at 72 hours post transfection. The supernatant was filtered through a 0.45µm filter and used directly or stored at -80°C.

8.2.5 Transduction of cells

3×10^5 of iBMDMs were seeded on a 6-well plate the day before transduction. The medium was replaced by 3.5 ml of the filtered supernatant containing retrovirus or lentivirus mixed with Polybrene (5 µg/ml). The infection was enhanced by centrifugation at 37 °C, 1000 × g for 30 min. The medium was changed 6 hours post infection. The next day, iBMDMs were infected again with the secondary harvesting supernatant at 72 hours post transfection. In the following days, cells were trypsinized

and transferred to a 10cm^2 dish and selected by application of 4µg/ml puromycin. Non-transduced cells were treated by puromycin as well for a control. The selection finished when the all control cells were dead.

8.2.6 Generation of knockouts using CRISPR/Cas9 system

A lentiviral CRISPR/Cas9 gene editing system (van Diemen et al., 2016) was used to knock out *Aim2* and *Asc* genes in iBMDMs. The following guide RNAs were designed using E-CRISP (http://www.e-crisp.org/E-CRISP): *Aim2* (gRNA1, GACCACCTGATTCAAAG TGC; gRNA2, GCAGCCTTAGTTCTCAACTC; gRNA3, GACCGGCCTGGACCACATC A) and *Asc* (gRNA1, GTGCAACTGCGAGAAGGCTA; gRNA2, GGACGCTCTTGAAA ACTTGT; gRNA3, GCTCAGAGTACAGCCAGAAC). The gRNAs were inserted into the lentiviral vector pSicoR-CRISPR-puroR [242]. The lentiviruses were generated as described in 8.2.4 and the cells were transdused as described in 8.2.5. The cells were selected with 4µg/ml puromycin and single-cell clones were obtained by limiting dilution. The protein expression levels of the selected single-cell clones were tested by immunoblot analysis.

8.2.7 Infection of cells with MCMV

Cells were infected with MCMV by a certain multiplicity of infection (MOI) based on the median tissue culture infective dose (TCID$_{50}$) of the virus stock. The calculation of the amount of virus was performed according to the following equation:

$$volum\ of\ virus\ stock\ (ml) = \frac{number\ of\ cells\ \times MOI}{TCID50/ml}$$

The required amount of virus was diluted in the growth medium and the dilution was added to infect the cells. If needed, the centrifuge enhancement was applied 1000 x *g* for 30 minutes at 37 °C.

8.2.8 Preparation of MCMV stocks

10.1 murine fibroblasts were infected with a MOI of 0.025 in 15cm^2 dishes. 3 days post infection, the supernatant containing virus was harvested and new medium was added for a secondary harvesting 5 days post infection. All of the harvested supernatant was centrifuged at 4°C with 6000 × *g* for 15 minutes to remove the cell debris. The supernatant was then transferred to new tubes and centrifuged at 4 °C with 27000 × *g*

for 3.5 hours to collect the viral particles. The viral pellet was dissolved in 1ml of growth medium on ice overnight. On the next day, the viral pellet was re-suspended gently, and the remaining cell debris was removed by centrifugation at 4 °C with 2000× g for 10 minutes. The supernatant was carefully loaded on top of the sucrose (15%-20%) cushion (18 ml) in an ultra-centrifuge tube. The ultracentrifugation was performed at 4 °C using 26100 x rpm for 1.5 hours with a L70 Ultracentrifuge. The viral pellet was dissolved in 500µl of growth medium (for in $vitro$ experiments) or PBS (for in $vivo$ experiments) at 4 °C overnight. The virus stock was aliquoted with 20-50µl/tube and stored at -80°C.

8.2.9 Titration of MCMV

For in $vitro$ experiments, the TCID$_{50}$/ml method was used to determine the virus concentration of MCMV samples. 2×10^3 of 10.1 murine fibroblasts were seeded in 96-well plates the day before infection. On the next day, individual triplicates of serial log$_{10}$ dilutions (from 10^{-3} to 10^{-10}) were prepared in 4 ml growth medium for each viral samples. 100µl of each dilution was added to an entire row (12 wells) for two plates. One plate was directly put back to the incubator, the other plate was centrifuged at 1000 x g for 30 minutes at 37 °C to apply the centrifugal enhancement. 7 days post infection, the number of infected wells in each dilution was counted and the viral titer was calculated with the Spearman-Kärber method [243].

For in $vivo$ experiments, the plaque assay was used to determine the virus concentration of MCMV samples. 4×10^4 M2-10 B4 cells were seeded in 48-well plates the day before infection. On the next day, individual triplicates of serial log$_{10}$ dilutions (from 10^{-3} to 10^{-10}) were prepared in 1 ml 3% FCS growth medium for each viral samples. 100µl of each dilution was added to one well and 3 hours later 300µl of methylcellulose was added on top. 7 days post infection, the plaques in each well were counted and the viral titer was calculated as described by Zurbach et.al [244].

8.2.10 Growth curves

Multistep replication kinetics were performed on 10.1 fibroblasts with MOI of 0.01, J774A.1 macrophages with MOI of 0.5 and iBMDMs with MOI of 0.025 in 6-well plates. 3 hours post infection, the cells were washed twice with PBS, and fresh medium was

added. The supernatant was harvested from the infected cells on days 1, 3, 5 and 7 and titrated on 10.1 cells.

8.3 Protein biochemistry methods

8.3.1 Preparation of samples

Cells were washed with PBS and lysed with 2× SDS-PAGE sample buffer. The cell lysate was boiled at 95°C for 10 minutes and either used directly or stored at -20°C for later use.

Proteins in the cell-free supernatant were precipitated using the methanol/choloroform method [245]. 500µl of the cell-free supernatant was mixed with 125µl of Choloroform. The samples were vortexed for at least 30 seconds and the centrifuged at 4°C, 13000 × g for 5 minutes. The aqueous phase was removed carefully and 500µl of methanol was added to the tube. The mixture was vortexed for at least 30 seconds and then centrifuged at 4°C, 13000 × g for 5 minutes. The pellet was dried and then dissolved in 2× SDS-PAGE sample buffer. The lysate was boiled at 95°C for 10 minutes and either used directly or stored at -20°C for later use.

8.3.2 SDS polyacrylamide gel electrophoresis (SDS-PAGE) and immunoblot

Protein samples were separated by SDS-PAGE, according to the molecular weight. In this study, the Tricine-SDS-PAGE was used for the separation of proteins under 100 kDa. Resolving gels containing 12.5% acrylamide and stacking gels containing 4% acrylamide were prepared according to the tricine gel recipe. Gels were mounted in the vertical electrophoresis apparatus. The anode buffer was added outside of the gels as the lower electrode buffer and cathode buffer was added in between of the gels as the upper electrode buffer. The boiled protein samples were loaded into each well of the gel. The gels were run at 85 V constantly for 120 min on ice. 3 µl of the protein ruler was loaded as well for a size ladder.

After the SDS-Page, the proteins were transferred to a nitrocellulose membrane by semi-dry blotting. The transfer was done by applying 100mA/gel for 90 minutes.

After the transfer, the membrane was washed with TBST and blocked with 5% nonfat

milk diluted in TBST for 30 minutes at room temperature. After that, the membrane was incubated with the primary antibody overnight at 4 °C. On the next day, the membrane was washed with TBST for 3 × 5 minutes and then incubated with HRP-coupled secondary antibodies for 1 hour at room temperature. The membrane was washed with TBST for 3 × 5 minutes and then detected by Luminescence signals with the enhanced chemiluminescence solution. The pictures were taken with a Fusion Capture Advance FX7 16.15 camera system (Peqlab) or X-ray films.

8.3.3 Immunoprecipitation

iBMDMs were infected with MOI of 3 in 6-well plates for 12 hours. HEK 293A cells were co-transfected for 24 hours in 10 cm^2 dishes. Cells were lysed in 1ml of NP-40 lysis buffer for 30 minutes. Samples were centrifuged with full speed to remove the insoluble material, the supernatant was retained for immunoprecipitation. 100µl of the whole cell lysate (WCL) was mixed with 33µl of 4× SDS-PAGE sample buffer and boiled at 95 °C for 10 minutes. The rest supernatant from transfected cells and infected cells were treated differently. For the transfected HEK 293A cells, the rest of the supernatant was pre-cleared with protein G Sepharose (PGS) beads for at least one hour on a rotating platform at 4°C. After the pre-clearing, the beads-free supernatant was incubated overnight with Flag antibody for immunoprecipitation of the Flag tagged AIM2 and ASC. On the next day, 2 hours incubation with PGS beads for each sample was performed. For the infected iBMDMs, the rest of supernatant was directly incubated overnight with anti-HA affinity matrix for immunoprecipitation of M84HA. All the incubations were performed on a rotating platform at 4°C. After the pulldown, all the precipitates were washed 3 times with IP Washing buffer 1, twice with IP Washing buffer 2, and once with IP Washing buffer 3. Samples were then boiled and eluted in 100µl of 2× SDS-PAGE sample buffer. The whole cell lysate and immunoprecipitation were analyzed by Western blot.

8.4 Immunofluorescence

Primary BMDMs expressing ASC-mCherry were isolated from femurs of transgenic mice [183] as described [240]. Cells were seeded on 8-well µ-slides (Ibidi) and infected on the following day with MCMV-M84HA. Cells were fixed at indicated time points with 4% paraformaldehyde (PFA) for 15 minutes at room temperature. The cells were then washed with PBS for 3 times and treated with 50mM ammonium chloride for 10

minutes to quench free aldehyde groups from fixation. The cells were washed with PBS for 3 times and then permeabilized by incubation in PBS with 0.3% Triton X-100 for 15 minutes. Followed by a 3-time washing with PBS and blocking with blocking buffer for 20 minutes. After that, the cells were incubated with diluted primary antibodies for 1 hour at room temperature. The cells were washed with PBS for 3 times and nuclear DNA were stained with Hoechst 33342 (ThermoFisher). The mixture of diluted Hoechst 33342 and secondary antibodies in PBS were incubated on cells for 30 minutes at room temperature. Fluorescence images were acquired by using a Nikon A1+ confocal laser scanning microscope (cLSM).

For the quantification of pyroptotic cells, macrophages were seeded on 96-well plates and infected on the following day with WT and M84*stop* MCMV at MOI of 3. Cells were stained with 1µg/ml PI and 5µg/ml Hoechst 33342 at indicated time points. The number of PI- and Hoechst-positive nuclei was automated counted by using CellInsight CX5 High-Content Screening Platform.

8.5 Library screening

$1.5×10^5$ of HEK 293A cells in 12-well plates were transfected with pcDNA3-mAIM2-Flag (200ng), pcDNA3-N-Flag-ASC (20ng), pCMV-Caspase-1-Flag (100ng), pCMV-pro-IL-1β-c-Flag (200ng) together with 1µg plasmid of MCMV ORF expression library as described in 8.2.2. 24 hours post transfection, the cell lysate was collected in 2X SDS-PAGE sample buffer for the analysis of Capsase-1 cleavage by immunoblot. Cell-free supernatant was collected for the determination of IL-1β concentration by ELISA. The inhibitory effect was calculated by dividing the IL-1β concentration of pcDNA transfected cells by each MCMV protein transfected cells.

$1.5×10^5$ of HEK 293A cells in 12-well plates were transfected with pcDNA3-mAIM2-Flag (200ng), pcDNA3-N-Flag-ASC (20ng or100ng), pCMV-Caspase-1-Flag (100ng), pcDNA-iGluc (200ng) together with 1µg plasmid of MCMV ORF expression library as described in 8.2.2. 24 hours post transfection, the cell-free supernatant was collected for the determination of IL-1β Gaussia luciferase. The inhibitory effect was calculated by dividing the luciferase value of pcDNA transfected cells by the luciferase value of each MCMV protein transfected cells.

8.6 AIM2 Inflammasome stimulation

iBMDMs or J774A.1 macrophages were pre-treated with 200 ng/ml ultrapure LPS. The medium was replaced 3 hours later with Opti-MEM, and cells were transfected with 2µg/ml poly(dA:dT) by using Lipofectamine 2000. The poly(dA:dT) and Lipofectamine 2000 was diluted in 100µl of Opti-MEM in separate tubes and then mixed together. The mixture was incubated at room temperature for 15 minutes and then added to macrophages. 3 hours post transfection, the cell-free supernatant was harvested for the detection of cleaved Caspase-1, p20 fragment. Proteins in the supernatant were precipitated as described in 8.3.1 and analyzed by Western blot. The cleavage of GSDMD in the cell lysate was analyzed by Western blot. IL-18 levels in the cell-free supernatant of infected macrophages were determined by Mouse IL-18 ELISA Kit.

8.7 Cytokine quantification

For measurement of IL-1β, cell-free supernatant was collected 24 hours post transfection. The concentration of IL-1β was measured by using the mouse IL-1β ELISA kit according to the manufacturer's instructions.

The concentration of IL-18 in the serum of infected mice and in the cell-free supernatant of infected macrophages were determined by Mouse IL-18 ELISA Kit according to the manufacturer's instructions.

The IL-1β Gaussia luciferase (iGLuc) reporter in the supernatants of transfected HEK 293A cells and MCMV-infected iBMDM-iGluc was quantified. The luciferase activity was measured on a FLUOstar Omega reader by using Coelenterazine-h (final concentation 2.5µM) according to the manufacturer's instructions.

8.8 Animal experiments

All animal experiments were performed by Dr. E. Ostermann and M. Bockelmann according to the recommendations and guidelines of the FELASA (Federation for Laboratory Animal Science Associations) and Society of Laboratory Animals (GV-SOLAS) and approved by the institutional review board and local authorities (Behörde für Gesundheit und Verbraucherschutz, Amt für Verbraucherschutz, Freie und Hansestadt Hamburg, reference number N017/2019).

Six-week-old female WT or $Asc^{-/-}$ C57BL/6 mice were infected intraperitoneally with 10^5 PFU MCMV per mouse. Spleens and livers from infected mice were harvested at 3 days post infection. Serum was harvested at 1.5 and 3 days post infection. Viral titers in the organs were determined by plaque assay on M2-10B4 cells as described in 8.2.9. Concentrations of IL-18 in the serum were measured by ELISA as described in 8.5.

9 References

1.   Ho, M., *The history of cytomegalovirus and its diseases.* Med Microbiol Immunol, 2008. **197**(2): p. 65-73.
2.   Smith, M.G., *Propagation of salivary gland virus of the mouse in tissue cultures.* Proc Soc Exp Biol Med, 1954. **86**(3): p. 435-40.
3.   Smith, M.G., *Propagation in tissue cultures of a cytopathogenic virus from human salivary gland virus (SGV) disease.* Proc Soc Exp Biol Med, 1956. **92**(2): p. 424-30.
4.   Brizic, I., et al., *Mouse Models for Cytomegalovirus Infections in Newborns and Adults.* Curr Protoc, 2022. **2**(9): p. e537.
5.   Cannon, M.J., T.B. Hyde, and D.S. Schmid, *Review of cytomegalovirus shedding in bodily fluids and relevance to congenital cytomegalovirus infection.* Rev Med Virol, 2011. **21**(4): p. 240-55.
6.   Kenneson, A. and M.J. Cannon, *Review and meta-analysis of the epidemiology of congenital cytomegalovirus (CMV) infection.* Rev Med Virol, 2007. **17**(4): p. 253-76.
7.   Goodrum, F., *Human Cytomegalovirus Latency: Approaching the Gordian Knot.* Annu Rev Virol, 2016. **3**(1): p. 333-357.
8.   Willame, A., et al., *Awareness of Cytomegalovirus Infection among Pregnant Women in Geneva, Switzerland: A Cross-sectional Study.* International Journal of Environmental Research and Public Health, 2015. **12**(12): p. 15285-15297.
9.   Cannon, M.J., D.S. Schmid, and T.B. Hyde, *Review of cytomegalovirus seroprevalence and demographic characteristics associated with infection.* Rev Med Virol, 2010. **20**(4): p. 202-13.
10.   Deayton, J.R., et al., *Importance of cytomegalovirus viraemia in risk of disease progression and death in HIV-infected patients receiving highly active antiretroviral therapy.* Lancet, 2004. **363**(9427): p. 2116-21.
11.   Lumbreras, C., et al., *Cytomegalovirus infection in solid organ transplant recipients.* Clin Microbiol Infect, 2014. **20 Suppl 7**: p. 19-26.
12.   Fishman, J.A., et al., *Cytomegalovirus in transplantation - challenging the status quo.* Clin Transplant, 2007. **21**(2): p. 149-58.
13.   Cope, A.V., et al., *Quantity of cytomegalovirus viruria is a major risk factor for cytomegalovirus disease after renal transplantation.* Journal of Medical Virology, 1997. **52**(2): p. 200-205.
14.   Humar, A., et al., *Cytomegalovirus (CMV) virus load kinetics to predict recurrent disease in solid-organ transplant patients with CMV disease.* J Infect Dis, 2002. **186**(6): p. 829-33.
15.   Pass, R.F., et al., *Congenital cytomegalovirus infection following first trimester maternal infection: Symptoms at birth and outcome.* Journal of Clinical Virology, 2006. **35**(2): p. 216-220.
16.   Reynolds, D.W., et al., *Maternal cytomegalovirus excretion and perinatal infection.* N Engl J Med, 1973. **289**(1): p. 1-5.
17.   Stagno, S., et al., *Maternal cytomegalovirus infection and perinatal transmission.* Clin Obstet Gynecol, 1982. **25**(3): p. 563-76.
18.   Stagno, S., et al., *Congenital Cytomegalovirus-Infection - Consecutive Occurrence Due to Viruses with Similar Antigenic Compositions.* Pediatrics, 1973. **52**(6): p. 788-794.

References

19.   Stagno, S., et al., *Breast-Milk and the Risk of Cytomegalovirus-Infection.* New England Journal of Medicine, 1980. **302**(19): p. 1073-1076.

20.   Carlson A, N.E., Stiller RJ. , *Cytomegalovirus infection in pregnancy: should all women be screened?* Rev Obstet Gynecol. , 2010 p. 3(4):172-9.

21.   Bhide, A. and A.T. Papageorghiou, *Managing primary CMV infection in pregnancy.* BJOG, 2008. **115**(7): p. 805-7.

22.   Cannon, M.J. and K.F. Davis, *Washing our hands of the congenital cytomegalovirus disease epidemic.* Bmc Public Health, 2005. **5**.

23.   Demmler, G.J., *Infectious Diseases Society of America and Centers for Disease Control. Summary of a workshop on surveillance for congenital cytomegalovirus disease.* Rev Infect Dis, 1991. **13**(2): p. 315-29.

24.   Dolan, A., et al., *Genetic content of wild-type human cytomegalovirus.* J Gen Virol, 2004. **85**(Pt 5): p. 1301-1312.

25.   Chen, D.H., et al., *Three-dimensional visualization of tegument/capsid interactions in the intact human cytomegalovirus.* Virology, 1999. **260**(1): p. 10-6.

26.   Mocarski ES, S.T., Pass RF., *Cytomegalovirus*, in *Fields Virology*, H.P. In Knipe DM, Griffin DE, Lamb RA, Martin MA, Roizman B, Straus SE Editor 2007, Lippincott-Williams & Wilkins: Philadelphia, PA. p. 2701-2772.

27.   Mohammed Ali Jassim, M., M. Mohammed Mahmood, and M. Hafedh Hussein, *Human Herpetic Viruses and Immune Profiles.* 2021.

28.   Sinzger, C., M. Digel, and G. Jahn, *Cytomegalovirus cell tropism.* Curr Top Microbiol Immunol, 2008. **325**: p. 63-83.

29.   Sinclair, J. and P. Sissons, *Latency and reactivation of human cytomegalovirus.* J Gen Virol, 2006. **87**(Pt 7): p. 1763-1779.

30.   Sinclair, J., *Human cytomegalovirus: Latency and reactivation in the myeloid lineage.* J Clin Virol, 2008. **41**(3): p. 180-5.

31.   Reeves, M. and J. Sinclair, *Aspects of human cytomegalovirus latency and reactivation.* Curr Top Microbiol Immunol, 2008. **325**: p. 297-313.

32.   Ogawa-Goto, K., et al., *Microtubule network facilitates nuclear targeting of human cytomegalovirus capsid.* J Virol, 2003. **77**(15): p. 8541-7.

33.   Davison, A.J. and N.D. Stow, *New genes from old: redeployment of dUTPase by herpesviruses.* J Virol, 2005. **79**(20): p. 12880-92.

34.   Li, T., J. Chen, and I.M. Cristea, *Human cytomegalovirus tegument protein pUL83 inhibits IFI16-mediated DNA sensing for immune evasion.* Cell Host Microbe, 2013. **14**(5): p. 591-9.

35.   Stinski, M.F., *Sequence of protein synthesis in cells infected by human cytomegalovirus: early and late virus-induced polypeptides.* J Virol, 1978. **26**(3): p. 686-701.

36.   Tandon, R., E.S. Mocarski, and J.F. Conway, *The A, B, Cs of herpesvirus capsids.* Viruses, 2015. **7**(3): p. 899-914.

37.   Jean Beltran, P.M. and I.M. Cristea, *The life cycle and pathogenesis of human cytomegalovirus infection: lessons from proteomics.* Expert Rev Proteomics, 2014. **11**(6): p. 697-711.

38.   Ma, Z., G. Ni, and B. Damania, *Innate Sensing of DNA Virus Genomes.* Annu Rev Virol, 2018. **5**(1): p. 341-362.

39.   Takeshita, F., et al., *Cutting Edge: Role of Toll-Like Receptor 9 in CpG DNA-Induced Activation of Human Cells.* The Journal of Immunology, 2001. **167**(7): p. 3555-3558.

40. Ahmad-Nejad, P., et al., *Bacterial CpG-DNA and lipopolysaccharides activate Toll-like receptors at distinct cellular compartments.* European Journal of Immunology, 2002. **32**(7): p. 1958-1968.

41. Leifer, C.A., et al., *TLR9 is localized in the endoplasmic reticulum prior to stimulation.* J Immunol, 2004. **173**(2): p. 1179-83.

42. Iwasaki, A. and R. Medzhitov, *Toll-like receptor control of the adaptive immune responses.* Nat Immunol, 2004. **5**(10): p. 987-95.

43. Hemmi, H., et al., *A Toll-like receptor recognizes bacterial DNA.* Nature, 2000. **408**(6813): p. 740-5.

44. Blasius, A.L. and B. Beutler, *Intracellular toll-like receptors.* Immunity, 2010. **32**(3): p. 305-15.

45. Latz, E., et al., *TLR9 signals after translocating from the ER to CpG DNA in the lysosome.* Nat Immunol, 2004. **5**(2): p. 190-8.

46. Honda, K., et al., *Spatiotemporal regulation of MyD88-IRF-7 signalling for robust type-I interferon induction.* Nature, 2005. **434**(7036): p. 1035-40.

47. Guiducci, C., et al., *Properties regulating the nature of the plasmacytoid dendritic cell response to Toll-like receptor 9 activation.* J Exp Med, 2006. **203**(8): p. 1999-2008.

48. Lakadamyali, M., M.J. Rust, and X.W. Zhuang, *Ligands for clathrin-mediated endocytosis are differentially sorted into distinct populations of early endosomes.* Cell, 2006. **124**(5): p. 997-1009.

49. O'Neill, L.A. and A.G. Bowie, *The family of five: TIR-domain-containing adaptors in Toll-like receptor signalling.* Nat Rev Immunol, 2007. **7**(5): p. 353-64.

50. Kawagoe, T., et al., *Essential role of IRAK-4 protein and its kinase activity in Toll-like receptor-mediated immune responses but not in TCR signaling.* J Exp Med, 2007. **204**(5): p. 1013-24.

51. Deng, L., et al., *Activation of the IkappaB kinase complex by TRAF6 requires a dimeric ubiquitin-conjugating enzyme complex and a unique polyubiquitin chain.* Cell, 2000. **103**(2): p. 351-61.

52. Sato, S., et al., *Essential function for the kinase TAK1 in innate and adaptive immune responses.* Nat Immunol, 2005. **6**(11): p. 1087-95.

53. Kawai, T., et al., *Interferon-alpha induction through Toll-like receptors involves a direct interaction of IRF7 with MyD88 and TRAF6.* Nat Immunol, 2004. **5**(10): p. 1061-1068.

54. Sun, L.J., et al., *Cyclic GMP-AMP Synthase Is a Cytosolic DNA Sensor That Activates the Type I Interferon Pathway.* Science, 2013. **339**(6121): p. 786-791.

55. Wu, J.X., et al., *Cyclic GMP-AMP Is an Endogenous Second Messenger in Innate Immune Signaling by Cytosolic DNA.* Science, 2013. **339**(6121): p. 826-830.

56. Ma, R., et al., *The cGAS-STING pathway: The role of self-DNA sensing in inflammatory lung disease.* FASEB J, 2020. **34**(10): p. 13156-13170.

57. Zhang, X., et al., *The cytosolic DNA sensor cGAS forms an oligomeric complex with DNA and undergoes switch-like conformational changes in the activation loop.* Cell Rep, 2014. **6**(3): p. 421-30.

58. Hooy, R.M. and J. Sohn, *The allosteric activation of cGAS underpins its dynamic signaling landscape.* Elife, 2018. **7**.

59. Li, X., et al., *Cyclic GMP-AMP Synthase Is Activated by Double-Stranded DNA-Induced Oligomerization.* Immunity, 2013. **39**(6): p. 1019-1031.

60. Barber, G.N., *STING: infection, inflammation and cancer.* Nat Rev Immunol, 2015. **15**(12): p. 760-70.

References

61.	Saitoh, T., et al., *Atg9a controls dsDNA-driven dynamic translocation of STING and the innate immune response.* Proc Natl Acad Sci U S A, 2009. **106**(49): p. 20842-6.

62.	Mukai, K., et al., *Activation of STING requires palmitoylation at the Golgi.* Nat Commun, 2016. **7**: p. 11932.

63.	Taguchi, T., et al., *STING Operation at the ER/Golgi Interface.* Front Immunol, 2021. **12**: p. 646304.

64.	Tanaka, Y. and Z.J. Chen, *STING specifies IRF3 phosphorylation by TBK1 in the cytosolic DNA signaling pathway.* Sci Signal, 2012. **5**(214): p. ra20.

65.	Ishikawa, H. and G.N. Barber, *STING is an endoplasmic reticulum adaptor that facilitates innate immune signalling.* Nature, 2008. **455**(7213): p. 674-8.

66.	Ishikawa, H., Z. Ma, and G.N. Barber, *STING regulates intracellular DNA-mediated, type I interferon-dependent innate immunity.* Nature, 2009. **461**(7265): p. 788-92.

67.	Cridland, J.A., et al., *The mammalian PYHIN gene family: phylogeny, evolution and expression.* BMC Evol Biol, 2012. **12**: p. 140.

68.	Jin, T., et al., *Structure of the absent in melanoma 2 (AIM2) pyrin domain provides insights into the mechanisms of AIM2 autoinhibition and inflammasome assembly.* J Biol Chem, 2013. **288**(19): p. 13225-35.

69.	Jin, T., et al., *Structures of the HIN domain:DNA complexes reveal ligand binding and activation mechanisms of the AIM2 inflammasome and IFI16 receptor.* Immunity, 2012. **36**(4): p. 561-71.

70.	Lu, A., et al., *Plasticity in PYD assembly revealed by cryo-EM structure of the PYD filament of AIM2.* Cell Discov, 2015. **1**: p. 15013-.

71.	Morrone, S.R., et al., *Assembly-driven activation of the AIM2 foreign-dsDNA sensor provides a polymerization template for downstream ASC.* Nat Commun, 2015. **6**: p. 7827.

72.	Liu, X., et al., *Inflammasome-activated gasdermin D causes pyroptosis by forming membrane pores.* Nature, 2016. **535**(7610): p. 153-8.

73.	Kumari, P., et al., *AIM2 in health and disease: Inflammasome and beyond.* Immunological Reviews, 2020. **297**(1): p. 83-95.

74.	Kerur, N., et al., *IFI16 Acts as a Nuclear Pathogen Sensor to Induce the Inflammasome in Response to Kaposi Sarcoma-Associated Herpesvirus Infection.* Cell Host Microbe, 2011. **9**(5): p. 363-375.

75.	Unterholzner, L., et al., *IFI16 is an innate immune sensor for intracellular DNA.* Nat Immunol, 2010. **11**(11): p. 997-U42.

76.	Morrone, S.R., et al., *Cooperative assembly of IFI16 filaments on dsDNA provides insights into host defense strategy.* Proc Natl Acad Sci U S A, 2014. **111**(1): p. E62-71.

77.	Brazda, V., et al., *Preferential binding of IFI16 protein to cruciform structure and superhelical DNA.* Biochem Biophys Res Commun, 2012. **422**(4): p. 716-20.

78.	Ablasser, A., et al., *RIG-I-dependent sensing of poly(dA:dT) through the induction of an RNA polymerase III-transcribed RNA intermediate.* Nat Immunol, 2009. **10**(10): p. 1065-U40.

79.	Chiu, Y.H., J.B. MacMillan, and Z.J.J. Chen, *RNA Polymerase III Detects Cytosolic DNA and Induces Type I Interferons through the RIG-I Pathway.* Cell, 2009. **138**(3): p. 576-591.

80.	Yoneyama, M., et al., *The RNA helicase RIG-I has an essential function in double-stranded RNA-induced innate antiviral responses.* Nat Immunol, 2004. **5**(7): p. 730-737.

81. Kolakofsky, D., E. Kowalinski, and S. Cusack, *A structure-based model of RIG-I activation.* RNA, 2012. **18**(12): p. 2118-27.

82. Pothlichet, J., et al., *Type I IFN triggers RIG-I/TLR3/NLRP3-dependent inflammasome activation in influenza A virus infected cells.* PLoS Pathog, 2013. **9**(4): p. e1003256.

83. Mariathasan, S., et al., *Differential activation of the inflammasome by caspase-1 adaptors ASC and Ipaf.* Nature, 2004. **430**(6996): p. 213-8.

84. Martinon, F., A. Mayor, and J. Tschopp, *The inflammasomes: guardians of the body.* Annu Rev Immunol, 2009. **27**: p. 229-65.

85. Petrilli, V., et al., *The inflammasome: a danger sensing complex triggering innate immunity.* Curr Opin Immunol, 2007. **19**(6): p. 615-22.

86. Ting, J.P., et al., *The NLR gene family: a standard nomenclature.* Immunity, 2008. **28**(3): p. 285-7.

87. Allen, I.C., et al., *The NLRP3 Inflammasome Mediates In Vivo Innate Immunity to Influenza A Virus through Recognition of Viral RNA.* Immunity, 2009. **30**(4): p. 556-565.

88. Ichinohe, T., I.K. Pang, and A. Iwasaki, *Influenza virus activates inflammasomes via its intracellular M2 ion channel.* Nat Immunol, 2010. **11**(5): p. 404-10.

89. Chen, I.Y. and T. Ichinohe, *Response of host inflammasomes to viral infection.* Trends Microbiol, 2015. **23**(1): p. 55-63.

90. Barlan, A.U., et al., *Adenovirus membrane penetration activates the NLRP3 inflammasome.* J Virol, 2011. **85**(1): p. 146-55.

91. Wang, W., et al., *STING promotes NLRP3 localization in ER and facilitates NLRP3 deubiquitination to activate the inflammasome upon HSV-1 infection.* PLoS Pathog, 2020. **16**(3): p. e1008335.

92. Nour, A.M., et al., *Varicella-zoster virus infection triggers formation of an interleukin-1beta (IL-1beta)-processing inflammasome complex.* J Biol Chem, 2011. **286**(20): p. 17921-33.

93. Wang, P., et al., *Nlrp6 regulates intestinal antiviral innate immunity.* Science, 2015. **350**(6262): p. 826-30.

94. Shen, C., et al., *Phase separation drives RNA virus-induced activation of the NLRP6 inflammasome.* Cell, 2021. **184**(23): p. 5759-5774 e20.

95. Zhu, S., et al., *Nlrp9b inflammasome restricts rotavirus infection in intestinal epithelial cells.* Nature, 2017. **546**(7660): p. 667-670.

96. Hornick, E.E., et al., *Dendritic cell NLRC4 regulates influenza A virus-specific CD4(+) T cell responses through FasL expression.* Journal of Clinical Investigation, 2019. **129**(7): p. 2888-2897.

97. Rahman, M.M. and G. McFadden, *Myxoma virus lacking the pyrin-like protein M013 is sensed in human myeloid cells by both NLRP3 and multiple Toll-like receptors, which independently activate the inflammasome and NF-kappaB innate response pathways.* J Virol, 2011. **85**(23): p. 12505-17.

98. Tschopp, J. and K. Schroder, *NLRP3 inflammasome activation: The convergence of multiple signalling pathways on ROS production?* Nat Rev Immunol, 2010. **10**(3): p. 210-5.

99. Hornung, V., et al., *AIM2 recognizes cytosolic dsDNA and forms a caspase-1-activating inflammasome with ASC.* Nature, 2009. **458**(7237): p. 514-8.

100. Sester, D.P., et al., *Deficient NLRP3 and AIM2 Inflammasome Function in Autoimmune NZB Mice.* J Immunol, 2015. **195**(3): p. 1233-41.

101. Rathinam, V.A.K., et al., *The AIM2 inflammasome is essential for host defense against cytosolic bacteria and DNA viruses.* Nat Immunol, 2010. **11**(5): p. 395-403.

References

102. Ekchariyawat, P., et al., *Inflammasome signaling pathways exert antiviral effect against Chikungunya virus in human dermal fibroblasts.* Infect Genet Evol, 2015. **32**: p. 401-8.

103. Hamel, R., et al., *Biology of Zika Virus Infection in Human Skin Cells.* J Virol, 2015. **89**(17): p. 8880-96.

104. Ansari, M.A., et al., *Constitutive interferon-inducible protein 16-inflammasome activation during Epstein-Barr virus latency I, II, and III in B and epithelial cells.* J Virol, 2013. **87**(15): p. 8606-23.

105. Johnson, K.E., L. Chikoti, and B. Chandran, *Herpes simplex virus 1 infection induces activation and subsequent inhibition of the IFI16 and NLRP3 inflammasomes.* J Virol, 2013. **87**(9): p. 5005-18.

106. Gariano, G.R., et al., *The Intracellular DNA Sensor IFI16 Gene Acts as Restriction Factor for Human Cytomegalovirus Replication.* PLoS Pathog, 2012. **8**(1).

107. Rolle, S., et al., *The interferon-inducible 204 gene is transcriptionally activated by mouse cytomegalovirus and is required for its replication.* Virology, 2001. **286**(2): p. 249-55.

108. Hertel, L., et al., *The interferon-inducible 204 gene, a member of the Ifi 200 family, is not involved in the antiviral state induction by IFN-alpha, but is required by the mouse cytomegalovirus for its replication.* Virology, 1999. **262**(1): p. 1-8.

109. Kato, H., et al., *Differential roles of MDA5 and RIG-I helicases in the recognition of RNA viruses.* Nature, 2006. **441**(7089): p. 101-5.

110. Rintahaka, J., et al., *Cytosolic antiviral RNA recognition pathway activates caspases 1 and 3.* J Immunol, 2008. **180**(3): p. 1749-57.

111. Poeck, H., et al., *Recognition of RNA virus by RIG-I results in activation of CARD9 and inflammasome signaling for interleukin 1 beta production.* Nat Immunol, 2010. **11**(1): p. 63-9.

112. Rajan, J.V., et al., *The NLRP3 inflammasome detects encephalomyocarditis virus and vesicular stomatitis virus infection.* J Virol, 2011. **85**(9): p. 4167-72.

113. Chen, X., et al., *Pyroptosis is driven by non-selective gasdermin-D pore and its morphology is different from MLKL channel-mediated necroptosis.* Cell Res, 2016. **26**(9): p. 1007-20.

114. Shen, J. and J. Tower, *Programmed cell death and apoptosis in aging and life span regulation.* Discov Med, 2009. **8**(43): p. 223-6.

115. Elmore, S., *Apoptosis: a review of programmed cell death.* Toxicol Pathol, 2007. **35**(4): p. 495-516.

116. Vanden Berghe, T., et al., *Differential signaling to apoptotic and necrotic cell death by Fas-associated death domain protein FADD.* J Biol Chem, 2004. **279**(9): p. 7925-33.

117. Wang, L., et al., *Caspase-10 is an initiator caspase in death receptor signaling.* Proc Natl Acad Sci U S A, 2001. **98**(24): p. 13884-13888.

118. Irmler, M., et al., *Inhibition of death receptor signals by cellular FLIP.* Nature, 1997. **388**(6638): p. 190-5.

119. Imre, G., *Cell death signalling in virus infection.* Cell Signal, 2020. **76**: p. 109772.

120. Kroemer, G., L. Galluzzi, and C. Brenner, *Mitochondrial membrane permeabilization in cell death.* Physiol Rev, 2007. **87**(1): p. 99-163.

121. Galluzzi, L., et al., *Viral control of mitochondrial apoptosis.* PLoS Pathog, 2008. **4**(5): p. e1000018.

122. Bao, Q. and Y. Shi, *Apoptosome: a platform for the activation of initiator caspases.* Cell Death Differ, 2007. **14**(1): p. 56-65.

123. Carrington, E.M., et al., *Anti-apoptotic proteins BCL-2, MCL-1 and A1 summate collectively to maintain survival of immune cell populations both in vitro and in vivo.* Cell Death Differ, 2017. **24**(5): p. 878-888.

124. Daley-Bauer, L.P., et al., *Mouse cytomegalovirus M36 and M45 death suppressors cooperate to prevent inflammation resulting from antiviral programmed cell death pathways.* Proc Natl Acad Sci U S A, 2017. **114**(13): p. E2786-E2795.

125. Skaletskaya, A., et al., *A cytomegalovirus-encoded inhibitor of apoptosis that suppresses caspase-8 activation.* Proc Natl Acad Sci U S A, 2001. **98**(14): p. 7829-34.

126. Arnoult, D., et al., *Cytomegalovirus cell death suppressor vMIA blocks Bax- but not Bak-mediated apoptosis by binding and sequestering Bax at mitochondria.* Proc Natl Acad Sci U S A, 2004. **101**(21): p. 7988-93.

127. Karbowski, M., et al., *Role of Bax and Bak in mitochondrial morphogenesis.* Nature, 2006. **443**(7112): p. 658-62.

128. Norris, K.L. and R.J. Youle, *Cytomegalovirus proteins vMIA and m38.5 link mitochondrial morphogenesis to Bcl-2 family proteins.* J Virol, 2008. **82**(13): p. 6232-43.

129. Cam, M., et al., *Cytomegaloviruses inhibit Bak- and Bax-mediated apoptosis with two separate viral proteins.* Cell Death Differ, 2010. **17**(4): p. 655-65.

130. Terhune, S., et al., *Human cytomegalovirus UL38 protein blocks apoptosis.* J Virol, 2007. **81**(7): p. 3109-23.

131. Xuan, B., et al., *Human cytomegalovirus protein pUL38 induces ATF4 expression, inhibits persistent JNK phosphorylation, and suppresses endoplasmic reticulum stress-induced cell death.* J Virol, 2009. **83**(8): p. 3463-74.

132. Brune, W. and C.E. Andoniou, *Die Another Day: Inhibition of Cell Death Pathways by Cytomegalovirus.* Viruses-Basel, 2017. **9**(9).

133. Rello, S., et al., *Morphological criteria to distinguish cell death induced by apoptotic and necrotic treatments.* Apoptosis, 2005. **10**(1): p. 201-8.

134. Jeffries, A.M., A.J. Suptela, and I. Marriott, *Z-DNA binding protein 1 mediates necroptotic and apoptotic cell death pathways in murine astrocytes following herpes simplex virus-1 infection.* J Neuroinflammation, 2022. **19**(1): p. 109.

135. Kaiser, W.J., et al., *Toll-like receptor 3-mediated necrosis via TRIF, RIP3, and MLKL.* J Biol Chem, 2013. **288**(43): p. 31268-79.

136. Vanlangenakker, N., et al., *TNF-induced necroptosis in L929 cells is tightly regulated by multiple TNFR1 complex I and II members.* Cell Death Dis, 2011. **2**(11): p. e230.

137. Sun, L., et al., *Mixed lineage kinase domain-like protein mediates necrosis signaling downstream of RIP3 kinase.* Cell, 2012. **148**(1-2): p. 213-27.

138. Micheau, O. and J. Tschopp, *Induction of TNF receptor I-mediated apoptosis via two sequential signaling complexes.* Cell, 2003. **114**(2): p. 181-90.

139. Pasparakis, M. and P. Vandenabeele, *Necroptosis and its role in inflammation.* Nature, 2015. **517**(7534): p. 311-320.

140. Dondelinger, Y., et al., *NF-kappaB-Independent Role of IKKalpha/IKKbeta in Preventing RIPK1 Kinase-Dependent Apoptotic and Necroptotic Cell Death during TNF Signaling.* Mol Cell, 2015. **60**(1): p. 63-76.

141. Feoktistova, M., et al., *cIAPs block Ripoptosome formation, a RIP1/caspase-8 containing intracellular cell death complex differentially regulated by cFLIP isoforms.* Mol Cell, 2011. **43**(3): p. 449-63.

References

142. Sun, X., et al., *Identification of a novel homotypic interaction motif required for the phosphorylation of receptor-interacting protein (RIP) by RIP3.* J Biol Chem, 2002. **277**(11): p. 9505-11.

143. Wang, H.Y., et al., *Mixed Lineage Kinase Domain-like Protein MLKL Causes Necrotic Membrane Disruption upon Phosphorylation by RIP3.* Mol Cell, 2014. **54**(1): p. 133-146.

144. Upton, J.W. and W.J. Kaiser, *DAI Another Way: Necroptotic Control of Viral Infection.* Cell Host Microbe, 2017. **21**(3): p. 290-293.

145. Dhuriya, Y.K. and D. Sharma, *Necroptosis: a regulated inflammatory mode of cell death.* J Neuroinflammation, 2018. **15**(1): p. 199.

146. Weinlich, R., et al., *Necroptosis in development, inflammation and disease.* Nat Rev Mol Cell Biol, 2017. **18**(2): p. 127-136.

147. Upton, J.W., W.J. Kaiser, and E.S. Mocarski, *Virus inhibition of RIP3-dependent necrosis.* Cell Host Microbe, 2010. **7**(4): p. 302-313.

148. Wang, X., et al., *Direct activation of RIP3/MLKL-dependent necrosis by herpes simplex virus 1 (HSV-1) protein ICP6 triggers host antiviral defense.* Proc Natl Acad Sci U S A, 2014. **111**(43): p. 15438-43.

149. Huang, Z., et al., *RIP1/RIP3 binding to HSV-1 ICP6 initiates necroptosis to restrict virus propagation in mice.* Cell Host Microbe, 2015. **17**(2): p. 229-42.

150. Fletcher-Etherington, A., et al., *Human cytomegalovirus protein pUL36: A dual cell death pathway inhibitor.* Proc Natl Acad Sci U S A, 2020. **117**(31): p. 18771-18779.

151. Bergsbaken, T., S.L. Fink, and B.T. Cookson, *Pyroptosis: host cell death and inflammation.* Nat Rev Microbiol, 2009. **7**(2): p. 99-109.

152. de Vasconcelos, N.M. and M. Lamkanfi, *Recent Insights on Inflammasomes, Gasdermin Pores, and Pyroptosis.* Cold Spring Harb Perspect Biol, 2020. **12**(5).

153. Shi, J., et al., *Cleavage of GSDMD by inflammatory caspases determines pyroptotic cell death.* Nature, 2015. **526**(7575): p. 660-5.

154. Shi, J., W. Gao, and F. Shao, *Pyroptosis: Gasdermin-Mediated Programmed Necrotic Cell Death.* Trends Biochem Sci, 2017. **42**(4): p. 245-254.

155. Orning, P., et al., *Pathogen blockade of TAK1 triggers caspase-8-dependent cleavage of gasdermin D and cell death.* Science, 2018. **362**(6418): p. 1064-1069.

156. Sarhan, J., et al., *Caspase-8 induces cleavage of gasdermin D to elicit pyroptosis during Yersinia infection.* Proc Natl Acad Sci U S A, 2018. **115**(46): p. E10888-E10897.

157. Degen, M., et al., *Structural basis of NINJ1-mediated plasma membrane rupture in cell death.* Nature, 2023.

158. Lee, Y.S., et al., *Interleukin-1 (IL-1) signaling in intestinal stromal cells controls KC/ CXCL1 secretion, which correlates with recruitment of IL-22- secreting neutrophils at early stages of Citrobacter rodentium infection.* Infect Immun, 2015. **83**(8): p. 3257-67.

159. Chung, Y., et al., *Critical regulation of early Th17 cell differentiation by interleukin-1 signaling.* Immunity, 2009. **30**(4): p. 576-87.

160. Ichinohe, T., et al., *Inflammasome recognition of influenza virus is essential for adaptive immune responses.* J Exp Med, 2009. **206**(1): p. 79-87.

161. Ramos, H.J., et al., *IL-1beta signaling promotes CNS-intrinsic immune control of West Nile virus infection.* PLoS Pathog, 2012. **8**(11): p. e1003039.

162. Okamura, H., et al., *Cloning of a new cytokine that induces IFN-gamma production by T cells.* Nature, 1995. **378**(6552): p. 88-91.

163. Dao, T., W.Z. Mehal, and I.N. Crispe, *IL-18 augments perforin-dependent cytotoxicity of liver NK-T cells.* J Immunol, 1998. **161**(5): p. 2217-22.
164. Johnston, J.B., et al., *A poxvirus-encoded pyrin domain protein interacts with ASC-1 to inhibit host inflammatory and apoptotic responses to infection.* Immunity, 2005. **23**(6): p. 587-98.
165. Gerlic, M., et al., *Vaccinia virus F1L protein promotes virulence by inhibiting inflammasome activation.* Proc Natl Acad Sci U S A, 2013. **110**(19): p. 7808-13.
166. Gregory, S.M., et al., *Discovery of a viral NLR homolog that inhibits the inflammasome.* Science, 2011. **331**(6015): p. 330-4.
167. Maruzuru, Y., et al., *Herpes Simplex Virus 1 VP22 Inhibits AIM2-Dependent Inflammasome Activation to Enable Efficient Viral Replication.* Cell Host Microbe, 2018. **23**(2): p. 254-265 e7.
168. Orzalli, M.H., N.M. Broekema, and D.M. Knipe, *Relative Contributions of Herpes Simplex Virus 1 ICP0 and vhs to Loss of Cellular IFI16 Vary in Different Human Cell Types.* J Virol, 2016. **90**(18): p. 8351-9.
169. Dell'Oste, V., et al., *Innate Nuclear Sensor IFI16 Translocates into the Cytoplasm during the Early Stage of In Vitro Human Cytomegalovirus Infection and Is Entrapped in the Egressing Virions during the Late Stage.* J Virol, 2014. **88**(12): p. 6970-6982.
170. Lei, X.B., et al., *Enterovirus 71 Inhibits Pyroptosis through Cleavage of Gasdermin D.* J Virol, 2017. **91**(18).
171. Ma, J., et al., *SARS-CoV-2 nucleocapsid suppresses host pyroptosis by blocking Gasdermin D cleavage.* EMBO J, 2021. **40**(18): p. e108249.
172. Schroder, K. and J. Tschopp, *The inflammasomes.* Cell, 2010. **140**(6): p. 821-32.
173. Rathinam, V.A., et al., *The AIM2 inflammasome is essential for host defense against cytosolic bacteria and DNA viruses.* Nat Immunol, 2010. **11**(5): p. 395-402.
174. Spel, L. and F. Martinon, *Detection of viruses by inflammasomes.* Curr Opin Virol, 2021. **46**: p. 59-64.
175. Munks, M.W., et al., *Genome-wide analysis reveals a highly diverse CD8 T cell response to murine cytomegalovirus.* J Immunol, 2006. **176**(6): p. 3760-6.
176. Kattenhorn, L.M., et al., *Identification of proteins associated with murine cytomegalovirus virions.* J Virol, 2004. **78**(20): p. 11187-97.
177. Kalejta, R.F., *Tegument proteins of human cytomegalovirus.* Microbiol Mol Biol Rev, 2008. **72**(2): p. 249-65, table of contents.
178. Nobre, L.V., et al., *Human cytomegalovirus interactome analysis identifies degradation hubs, domain associations and viral protein functions.* Elife, 2019. **8**: p. e49894.
179. Bartok, E., et al., *iGLuc: a luciferase-based inflammasome and protease activity reporter.* Nat Methods, 2013. **10**(2): p. 147-154.
180. Cranmer, L.D., et al., *Identification, analysis, and evolutionary relationships of the putative murine cytomegalovirus homologs of the human cytomegalovirus UL82 (pp71) and UL83 (pp65) matrix phosphoproteins.* J Virol, 1996. **70**(11): p. 7929-39.
181. Huang, Y., et al., *Interaction between HCMV pUL83 and human AIM2 disrupts the activation of the AIM2 inflammasome.* Virol J, 2017. **14**(1): p. 34.
182. Broz, P. and V.M. Dixit, *Inflammasomes: mechanism of assembly, regulation and signalling.* Nat Rev Immunol, 2016. **16**(7): p. 407-20.

References

183. Tzeng, T.C., et al., *A Fluorescent Reporter Mouse for Inflammasome Assembly Demonstrates an Important Role for Cell-Bound and Free ASC Specks during In Vivo Infection.* Cell Rep, 2016. **16**(2): p. 571-582.

184. Madera, S. and J.C. Sun, *Cutting edge: stage-specific requirement of IL-18 for antiviral NK cell expansion.* J Immunol, 2015. **194**(4): p. 1408-12.

185. Schattgen, S.A. and K.A. Fitzgerald, *The PYHIN protein family as mediators of host defenses.* Immunological Reviews, 2011. **243**: p. 109-118.

186. Brune, W. and C.E. Andoniou, *Die Another Day: Inhibition of Cell Death Pathways by Cytomegalovirus.* Viruses, 2017. **9**(9).

187. Botto, S., et al., *Human Cytomegalovirus Immediate Early 86-kDa Protein Blocks Transcription and Induces Degradation of the Immature Interleukin-1beta Protein during Virion-Mediated Activation of the AIM2 Inflammasome.* MBio, 2019. **10**(1).

188. Shi, F., et al., *Coronaviruses Nsp5 Antagonizes Porcine Gasdermin D-Mediated Pyroptosis by Cleaving Pore-Forming p30 Fragment.* MBio, 2022. **13**(1): p. e0273921.

189. Lei, X., et al., *Enterovirus 71 Inhibits Pyroptosis through Cleavage of Gasdermin D.* J Virol, 2017. **91**(18).

190. Dorfleutner, A., et al., *A Shope Fibroma virus PYRIN-only protein modulates the host immune response.* Virus Genes, 2007. **35**(3): p. 685-94.

191. Shi, H., A. Murray, and B. Beutler, *Reconstruction of the Mouse Inflammasome System in HEK293T Cells.* Bio Protoc, 2016. **6**(21).

192. Sergerie, Y., S. Rivest, and G. Boivin, *Tumor necrosis factor-alpha and interleukin-1 beta play a critical role in the resistance against lethal herpes simplex virus encephalitis.* J Infect Dis, 2007. **196**(6): p. 853-60.

193. Sims, J.E. and D.E. Smith, *The IL-1 family: regulators of immunity.* Nat Rev Immunol, 2010. **10**(2): p. 89-102.

194. Mack, C., et al., *Inhibition of proinflammatory and innate immune signaling pathways by a cytomegalovirus RIP1-interacting protein.* Proc Natl Acad Sci U S A, 2008. **105**(8): p. 3094-9.

195. Puren, A.J., G. Fantuzzi, and C.A. Dinarello, *Gene expression, synthesis, and secretion of interleukin 18 and interleukin 1beta are differentially regulated in human blood mononuclear cells and mouse spleen cells.* Proc Natl Acad Sci U S A, 1999. **96**(5): p. 2256-61.

196. Gram, A.M., J. Frenkel, and M.E. Ressing, *Inflammasomes and viruses: cellular defence versus viral offence.* J Gen Virol, 2012. **93**(Pt 10): p. 2063-2075.

197. Pien, G.C., et al., *Cutting edge: selective IL-18 requirements for induction of compartmental IFN-gamma responses during viral infection.* J Immunol, 2000. **165**(9): p. 4787-91.

198. Liu, B., et al., *Interleukin-18 improves the early defence system against influenza virus infection by augmenting natural killer cell-mediated cytotoxicity.* J Gen Virol, 2004. **85**(Pt 2): p. 423-428.

199. Krause, E., et al., *Murine cytomegalovirus virion-associated protein M45 mediates rapid NF-kappaB activation after infection.* J Virol, 2014. **88**(17): p. 9963-75.

200. Fliss, P.M., et al., *Viral mediated redirection of NEMO/IKKγ to autophagosomes curtails the inflammatory cascade.* PLoS Pathog, 2012. **8**(2): p. e1002517.

201. Gaidt, M.M., et al., *The DNA Inflammasome in Human Myeloid Cells Is Initiated by a STING-Cell Death Program Upstream of NLRP3.* Cell, 2017. **171**(5): p. 1110-1124 e18.

202. Azab, W., et al., *How Host Specific Are Herpesviruses? Lessons from Herpesviruses Infecting Wild and Endangered Mammals.* Annu Rev Virol, 2018. **5**(1): p. 53-68.

203. Ding, L., et al., *The regional function of cGAS/STING signal in multiple organs: One of culprit behind systemic lupus erythematosus?* Med Hypotheses, 2015. **85**(6): p. 846-9.

204. Collins, T.M., M.R. Quirk, and M.C. Jordan, *Biphasic viremia and viral gene expression in leukocytes during acute cytomegalovirus infection of mice.* J Virol, 1994. **68**(10): p. 6305-11.

205. Hsu, K.M., et al., *Murine cytomegalovirus displays selective infection of cells within hours after systemic administration.* J Gen Virol, 2009. **90**(Pt 1): p. 33-43.

206. Zhang, S., et al., *MCMV exploits the spleen as a transfer hub for systemic dissemination upon oronasal inoculation.* Virus Res, 2016. **217**: p. 47-54.

207. Katzenstein, D.A., G.S. Yu, and M.C. Jordan, *Lethal infection with murine cytomegalovirus after early viral replication in the spleen.* J Infect Dis, 1983. **148**(3): p. 406-11.

208. Sacher, T., et al., *The role of cell types in cytomegalovirus infection in vivo.* Eur J Cell Biol, 2012. **91**(1): p. 70-7.

209. Fan, X., L. Jiao, and T. Jin, *Activation and Immune Regulation Mechanisms of PYHIN Family During Microbial Infection.* Front Microbiol, 2021. **12**: p. 809412.

210. Li, H., et al., *Structural mechanism of DNA recognition by the p202 HINa domain: insights into the inhibition of Aim2-mediated inflammatory signalling.* Acta Crystallogr F Struct Biol Commun, 2014. **70**(Pt 1): p. 21-9.

211. Ma, X.Y., et al., *The interferon-inducible p202a protein modulates NF-kappaB activity by inhibiting the binding to DNA of p50/p65 heterodimers and p65 homodimers while enhancing the binding of p50 homodimers.* J Biol Chem, 2003. **278**(25): p. 23008-19.

212. Datta, B., et al., *p202, an interferon-inducible modulator of transcription, inhibits transcriptional activation by the p53 tumor suppressor protein, and a segment from the p53-binding protein 1 that binds to p202 overcomes this inhibition.* J Biol Chem, 1996. **271**(44): p. 27544-55.

213. Conrady, C.D., et al., *Resistance to HSV-1 infection in the epithelium resides with the novel innate sensor, IFI-16.* Mucosal Immunol, 2012. **5**(2): p. 173-83.

214. Ryabchenko, B., et al., *Immune sensing of mouse polyomavirus DNA by p204 and cGAS DNA sensors.* FEBS J, 2021. **288**(20): p. 5964-5985.

215. Yu, L., et al., *p204-Mediated innate antiviral responses in mouse adipose cells and their effects on cell functions.* Immunol Cell Biol, 2015. **93**(2): p. 147-57.

216. Bryan, N.B., et al., *Activation of inflammasomes requires intracellular redistribution of the apoptotic speck-like protein containing a caspase recruitment domain.* J Immunol, 2009. **182**(5): p. 3173-82.

217. Diner, B.A., et al., *The functional interactome of PYHIN immune regulators reveals IFIX is a sensor of viral DNA.* Mol Syst Biol, 2015. **11**(1): p. 787.

218. Shen, W., et al., *Nuclear trafficking of the human cytomegalovirus pp71 (ppUL82) tegument protein.* Virology, 2008. **376**(1): p. 42-52.

219. Bresnahan, W.A. and T.E. Shenk, *UL82 virion protein activates expression of immediate early viral genes in human cytomegalovirus-infected cells.* Proc Natl Acad Sci U S A, 2000. **97**(26): p. 14506-11.

220. Baldick, C.J., Jr., et al., *Human cytomegalovirus tegument protein pp71 (ppUL82) enhances the infectivity of viral DNA and accelerates the infectious cycle.* J Virol, 1997. **71**(6): p. 4400-8.

References

221. Trgovcich, J., et al., *Human cytomegalovirus protein pp71 disrupts major histocompatibility complex class I cell surface expression.* J Virol, 2006. **80**(2): p. 951-63.

222. Fu, Y.Z., et al., *Human Cytomegalovirus Tegument Protein UL82 Inhibits STING-Mediated Signaling to Evade Antiviral Immunity.* Cell Host Microbe, 2017. **21**(2): p. 231-243.

223. Varnum, S.M., et al., *Identification of proteins in human cytomegalovirus (HCMV) particles: the HCMV proteome.* J Virol, 2004. **78**(20): p. 10960-6.

224. Odeberg, J., et al., *Human cytomegalovirus protein pp65 mediates accumulation of HLA-DR in lysosomes and destruction of the HLA-DR alpha-chain.* Blood, 2003. **101**(12): p. 4870-7.

225. Arnon, T.I., et al., *Inhibition of the NKp30 activating receptor by pp65 of human cytomegalovirus.* Nat Immunol, 2005. **6**(5): p. 515-23.

226. Abate, D.A., S. Watanabe, and E.S. Mocarski, *Major human cytomegalovirus structural protein pp65 (ppUL83) prevents interferon response factor 3 activation in the interferon response.* J Virol, 2004. **78**(20): p. 10995-1006.

227. Biolatti, M., et al., *Human Cytomegalovirus Tegument Protein pp65 (pUL83) Dampens Type I Interferon Production by Inactivating the DNA Sensor cGAS without Affecting STING.* J Virol, 2018. **92**(6).

228. Biolatti, M., et al., *The Viral Tegument Protein pp65 Impairs Transcriptional Upregulation of IL-1beta by Human Cytomegalovirus through Inhibition of NF-kB Activity.* Viruses, 2018. **10**(10).

229. Xu, X., et al., *Human Cytomegalovirus infection activates NLRP3 inflammasome by releasing mtDNA into cytosol in human THP-1 cells.* Microbiol Immunol, 2023.

230. Huang, Y., et al., *Human cytomegalovirus triggers the assembly of AIM2 inflammasome in THP-1-derived macrophages.* J Med Virol, 2017. **89**(12): p. 2188-2195.

231. He, Y.S., L. Xu, and E.S. Huang, *Characterization of human cytomegalovirus UL84 early gene and identification of its putative protein product.* J Virol, 1992. **66**(2): p. 1098-108.

232. Xu, Y., et al., *Human cytomegalovirus DNA replication requires transcriptional activation via an IE2- and UL84-responsive bidirectional promoter element within oriLyt.* J Virol, 2004. **78**(21): p. 11664-77.

233. Sanders, R.L. and D.H. Spector, *Human cytomegalovirus IE2 86 and IE2 40 proteins differentially regulate UL84 protein expression posttranscriptionally in the absence of other viral gene products.* J Virol, 2010. **84**(10): p. 5158-70.

234. Gao, Y., K. Colletti, and G.S. Pari, *Identification of human cytomegalovirus UL84 virus- and cell-encoded binding partners by using proteomics analysis.* J Virol, 2008. **82**(1): p. 96-104.

235. Swift, S., et al., *Rapid production of retroviruses for efficient gene delivery to mammalian cells using 293T cell-based systems.* Curr Protoc Immunol, 2001. **Chapter 10**: p. Unit 10 17C.

236. Harvey, D.M. and A.J. Levine, *p53 alteration is a common event in the spontaneous immortalization of primary BALB/c murine embryo fibroblasts.* Genes Dev, 1991. **5**(12B): p. 2375-85.

237. Jordan, S., et al., *Virus Progeny of Murine Cytomegalovirus Bacterial Artificial Chromosome pSM3fr Show Reduced Growth in Salivary Glands due to a Fixed Mutation of MCK-2.* J Virol, 2011. **85**(19): p. 10346-10353.

238. Pawletko, K., *The role of the murine cytomegalovirus protein M28 in cross-species infection*, 2020, Staats-und Universitätsbibliothek Hamburg Carl von Ossietzky.

239. Puhach, O., et al., *Murine cytomegaloviruses m139 targets DDX3 to curtail interferon production and promote viral replication.* PLoS Pathog, 2020. **16**(10): p. e1008546.

240. Handke, W., et al., *Viral inhibition of BAK promotes murine cytomegalovirus dissemination to salivary glands.* J Virol, 2013. **87**(6): p. 3592-6.

241. Tischer, B.K., G.A. Smith, and N. Osterrieder, *En passant mutagenesis: a two step markerless red recombination system.* Methods Mol Biol, 2010. **634**: p. 421-30.

242. van Diemen, F.R., et al., *CRISPR/Cas9-Mediated Genome Editing of Herpesviruses Limits Productive and Latent Infections.* PLoS Pathog, 2016. **12**(6): p. e1005701.

243. Ramakrishnan, M.A., *Determination of 50% endpoint titer using a simple formula.* World J Virol, 2016. **5**(2): p. 85-6.

244. Zurbach, K.A., T. Moghbeli, and C.M. Snyder, *Resolving the titer of murine cytomegalovirus by plaque assay using the M2-10B4 cell line and a low viscosity overlay.* Virol J, 2014. **11**: p. 71.

245. Jakobs, C., et al., *Immunoblotting for active caspase-1.* Methods Mol Biol, 2013. **1040**: p. 103-15.

10 Appendix

10.1 Curriculum vitae

<u>Personal Information</u>

Yingqi Deng, born 01 November 1992 in Jilin, China

<u>Education</u>

December 2017-Present	Graduate student (PhD candidate)
	Department of Chemistry, University of Hamburg
	Research Department of Virus-Host-Interaction, Leibniz Institute of Virology (LIV)
	Hamburg, Germany
	Supervisors: Prof. Dr. Wolfram Brune, Prof. Dr. Thomas Dobner.
	Project: Inhibition of the AIM2 inflammasome and pyroptosis by murine cytomegalovirus
September 2014 - June 2017	Master's degree in Animal Medicine
	Jilin University, Department of Animal Medicine
	Changchun, China
	Thesis title: Study on the effects of sites within the receptor-binding domain of H9N2 subtype influenza virus on its receptor affinity.
September 2010 - June 2014	Bachelor's degree in Animal Science
	Jilin University, Department of Animal Science
	Changchun, China
	Thesis title: Phylogenetic analysis of avian H9N2 subtype influenza virus isolated from Jilin Province
September 2007 - June 2010	High school
	Dunhua Experimental High school, Dunhua, China

10.2 List of hazardous substances

Substance	GHS symbol	Hazard statements	Precautionary statements
2-mercaptoethanol		H301 + H331-H310-H315-H317-H318-H373-H410	P261-P280-P301 + P310 + P330-P302 + P352 + P310-P305 + P351 + P338 + P310-P403 + P233
Acetic acid		H226-H314	P280-P305 + P351 + P338-P310
Actinomycin D		H300	P264-P301 + P310
Acrylamide		H301-H312 + H332-H315-H317-H319-H340-H350-H361f-H372	P201-P280-P301 + P310-P305 + P351 + P338-P308 + P313
Ammonium bicarbonate		H302	P301 + P312 + P330
Ammonium persulfate		H272-H302-H315-H317-H319-H334-H335	P220-P261-P280-P305 + P351 + P338-P342 + P311
Ampicillin		H315-H317-H319-H334-H335	P261-P280-P305 + P351 + P338-P342 + P311
Bis-acrylamide		H302 + H332	
Boric acid		H360FD	P201-P308 + P313
Bromophenolblue		H332-H302-H319	P261-P264-P280-P304+340-P312-P301+312-P330-P305+351+338-P337+313
Chloramphenicol		H350	P201-P308 + P313

Chloroform		H302-H331-H315-H319-H351-H361d-H336-H372-H412	P201-P273-P301+P312+P330-P302 + P352-P304+P340+P311-P308+P313
Cycloheximide		H302-H330-H341	P260-P281-P284-P310
EDTA		H319	P305 + P351 + P338
Ethanol		H225-H319	P210-P280-P305 + P351 + P338-P337 + P313-P403 + P235
Ethidium bromide		H302-H330-H341	P260-P281-P284-P310
Guanidine hydrochloride		H302 + H332-H315-H319	P261-P280-P301 + P312 + P330-P304 + P340 + P312-P305 + P351 + P338-P337 + P313
Glycerin		H315-H319-H335	P280-P302+P352-P304+P340-P305+P351+P338
Hydrochloric acid		H290-H314-H335	P261-P280-P305 + P351 + P338-P310
Isopropanol		H225-H319-H336	P210-P261-P305 + P351 + P338
Kanamycin		H360	P201-P308 + P313
Liquid nitrogen		H281	P202-P271 + P403-P282
Methanol		H225-H301 + H311 + H331-H370	P210-P260-P280-P301 + P310-P311
Nonidet-P40		H315-H319-H302	P264-P280-P305 + P351+338- P332 +313-P337+313-P362+364
Penicillin		H317-H334	P261-P280-P342 + P311

Propidium iodide		H315-H319-H335	P264-P280-P362+364-P261
Protein A-agarose		H226	
Protein G-agarose		H226	
Puromycin		H373	
Sodium dodecyl sulfate		H315-H318-H335	P280-P304 + P340 + P312-P305 + P351 + P338 + P310
Sodium hydroxide		H290-H314	P280-P305 + P351 + P338-P310
Streptomycin		H302-H361	P281
Sulfuric acid		H290-314	P280-P301+P330+P331-P303+P361+P353-P305+P351+P338+P310
TEMED		H225-H302-H314-H332	P210-P280-P305 + P351 + P338-P310
Triton X-100		H302-H319-H411	P273-P280-P301 + P312 + P330-P337 + P313-P391-P501
Zeocin		H302-341	P264-P301+P312

10.3 Acknowledgments

Firstly, I would like to thank my supervisor Prof. Dr. Wolfram Brune for giving me the opportunity to be a PhD student in his laboratory and to do research on this interesting and challenging project. I am profoundly grateful to his guidance, expertise, patience and unwavering support. He has not only shaped my research but also enriched my academic and personal growth. I also want to thank my second supervisor Prof. Thomas Dobner who provides me great ideas for this project.

I would like to extend my sincere appreciation to Prof. Dr. Nicole Fischer for reviewing my doctoral thesis and Prof. Dr. Elke Oetjen and Prof. Dr. Marcus Altfeld for their expertise as members of the examination commission for my oral defense.

I would like to thank Chinese Scholarship Council (CSC) for subsidizing me to do research in Germany.

I would like to express my heartfelt gratitude to my colleague Dr. Eléonore Ostermann, whose knowledge-sharing, teachings, valuable insights and suggestions have greatly contributed to the development of this thesis.

I am indebted to Dr. Eléonore Ostermann and Michaela Bockelmann for their collaboration and help to perform the animal experiments.

I would like to express my appreciation to Dr. Eléonore Ostermann, Laura-Marie Luoto for critical proofreading my thesis and Irke Waßmann for the German translation.

I would like to specially thank Dr. Jiajia Tang, Tianyu Zhang and his wife Mingxiao Yang for their support, understanding and encouragement. I am grateful for their presence in my life.

I would like to thank all my colleagues Eléonore, Tianyu, Laura-Marie, Michaela, Irke, Luis, Renke, Ina, Enrico, Giorgia, Jan, Ana, Laura, Vincent for their support and help.

Finally, I would like to express my deepest gratitude to my husband and our parents, who hold the most profound significance in my life. Their unconditional love, unwavering belief and constant support have been pillars of strength throughout this journey.

10.4 Declaration on oath

I hereby declare on oath that this doctoral dissertation is written independently and solely by my own based on the original work of my PhD and has not been used other than the acknowledged resources and aids. The submitted written version corresponds to the version on the electronic storage medium. I hereby declare that I have not previously applied or pursued for a doctorate (Ph.D. studies).

Hamburg, June 2023

Yingqi Deng